Thermo-Mechanical Behavior of Polymer Composites Exposed to Fire

Zhenyu Zhang

Dissertation submitted to the faculty of the Virginia Polytechnic Institute and State University in partial fulfillment of the requirements for the degree of

Doctor of Philosophy
in
Engineering Mechanics

Scott W. Case, Chair
Brian Y. Lattimer
Surot Thangjitham
Scott Hendricks
Carin L. Roberts-Wollmann

June 29, 2010
Blacksburg, Virginia

Keywords: Polymer Composites, Fire, Thermo-Mechanical Behavior, Compressive Failure, Finite Element Analysis

Thermo-Mechanical Behavior of Polymer Composites Exposed to Fire

Zhenyu Zhang

ABSTRACT

One of the most critical issues for Polymer Matrix Composites (PMCs) in naval applications is the structural performance of composites at high temperature such as that experienced in a fire. A three-dimensional model including the effect of orthotropic viscoelasticity and decomposition is developed to predict the thermo-mechanical behavior and compressive failure of polymer matrix composites (PMCs) subjected to heat and compressive load. An overlaid element technique is proposed for incorporating the model into commercial finite element software ABAQUS. The technique is employed with the user subroutines to provide practicing engineers a convenient tool to perform analysis and design studies on composite materials subjected to combined fire exposure and mechanical loading.

The resulting code is verified and validated by comparing its results with other numerical results and experimentally measured data from the one-sided heating of composites at small (coupon) scale and intermediate scale. The good agreement obtained indicates the capability of the model to predict material behavior for different composite material systems with different fiber stacking sequences, different sample sizes, and different combined thermo-mechanical loadings.

In addition, an experimental technique utilizing Vacuum Assisted Resin Transfer Molding (VARTM) is developed to manufacture PMCs with a hypodermic needle inserted for internal pressure measurement. One-sided heating tests are conducted on the glass/vinyl ester composites to measure the pressure at different locations through thickness during the decomposition process. The model is employed to simulate the heating process and predict the internal pressure due to the matrix decomposition. Both predicted and measured results indicate that the range of the internal pressure peak in the designed test is around 1.1-1.3 atmosphere pressure.

Acknowledgements

First of all, I would like to acknowledge Dr. Scott Case for his advice and encouragement since the start of this work. He guided me into the composite material area and provided me many opportunities to improve the research capability. I am lucky to have him as my mentor and have enjoyed the time when I worked with him these years. Dr. Case not only helped me to facilitate the research progress, but also influenced my attitude to face and solve the problem through his integrity and optimism; this attitude will greatly benefit me in future. I would also like to thank Dr. Brian Lattimer for his continuing support and inspiration. Discussions with him provided me a clear understanding of experiment and modeling in this area. I sincerely acknowledge his generous help on the data, the experimental device, and the computer without which the work cannot proceed smoothly. I want to thank Dr. Surot Thangjitham, Dr. Scott Hendricks, Dr. Carin Roberts-Wollmann, and Dr. John Lesko for their academic and research instructions over years. Their courses gave me a solid background of mechanics and their review opinions on this work extended my research scope.

The help from Dr. Jim Lua and Dr. Jay Shi is greatly appreciated. My ABAQUS skill improvement is largely a result of communications with them. Thank you to Patrick Summers and Thomas Goodrich for their hard working on the measured material properties and experimental tests which are very significant to my model validation. Thank you to Dr. Stefanie Feih for the discussion and suggestion about the model comparison and test conditions. Thanks to Dr. Aixi Zhou, Dr. Daniel Peairs, Dr. Nathan Post, Russell Langford, Dr. Theophanis Theophanous, Dr. Jason Cain, and Frederick Cook for introducing me into Materials Response Group and being patient to teach me the operation of experiment machine and the manufacture of composite panel. Thanks to Mac McCord for answering me many questions about the calibration of the loading machine. Thanks to Beverly Williams for making the meeting and conference arrangements. Also Thanks to David Simmons and ESM machine shop for preparing the samples for tests.

Table of Contents

List of Figures

List of Tables

Chapter 1: Introduction and Background

1.1 Introduction

1.1.1 Applications of Polymer Matrix Composites

Polymer matrix composites (PMCs) are an important class of engineering materials used over a wide range of applications in the industrial and military areas because of their high specific strength, long fatigue life, excellent corrosion resistance, and stability against dimensional variation. In the automotive industry, fiber reinforced polymer (FRP) composite materials have been slowly incorporated into cars to enhance efficiency, reliability and customer appeal. Composites are replacing steel in body panels, grills, bumpers and structural members. As manufacturing technologies mature, new composite materials, such as high heat distortion thermoplastics, high glass loaded polyesters, and structural foams, facilitate the use of composites.

The applications of composites in the civil infrastructure include piping systems, storage tanks, commercial ladders, aerial towers, drive shafts, and bridge structures. For example, the use of PMCs for large diameter industrial piping is attractive because handling and corrosion considerations are greatly improved. Filament wound piping can be used at the working temperature up to around 150 °C with a service life of 100 years. Interior surfaces of PMCs are much smoother than steel or concrete reducing frictional losses.

The primary benefits that composite components can offer in the aerospace industry are the reduced weight improving fuel economy, the reduced production and maintenance costs, and the assembly simplification. The long-term durability and the reduction of fabrication costs encourage the use of PMCs in the marine industries.

Various marine structures are made of composite materials, including hulls, bulkheads, deckhouses, masts, and other topside structures. The Navy has been employing composite materials effectively for many years and has an increasing number of projects and investigations under way for further exploring the use of composites. In one of the naval research and development programs, composite propulsion shafts of glass and carbon reinforcing fibers in an epoxy matrix are projected to weigh 75% less than the traditional steel shafts and offer the advantages of corrosion resistance, low bearing loads, reduced magnetic signature, higher fatigue resistance, greater flexibility, excellent vibration damping and improved life-cycle cost. Figure 1.1 shows the profile and hull lay-up configuration for a 0.35 scale boat model in another Navy project named Advanced Material Transporter (AMT) [1].

As PMCs are further explored in the engineering areas, challenges are presented because of the low rigidity, poor impact resistance, and difficulties in joining of PMCs. For example, joined composites are needed to form variously shaped structures in the wind turbine manufacture. Adhesives that can withstand the centrifugal forces applied to each blade are required to bond very large composite components. In addition, one of the most critical issues is the fire performance of composites. Unlike other structural materials, composites are reactive at high temperature because of the organic matrix and fibers. Although PMCs have lower thermal conductivity than conventional metals, thus slowing the spread of fire from the heat source, they have worse overall fire performance because of the chemical and mechanical response changes that occur in PMCs exposed to fire. The dense smoke, soot, and toxic gases generated from the decomposition reaction for PMCs in fire increase health risk and decrease survivability for any-one remaining in

the area. The reduction in strength of heated composites, especially compression strength, causes the decreased structural integrity and eventually component failure. The recently released military standard for performance of composites during fires outlines rigorous test and evaluation procedures for qualification. Figure 1.2 shows French La Fayette class frigate making use of glass/polyester resin/balsa core composite panels for both deckhouse and deck structure (shaded areas) to reduce weight and improve fire performance as compared to aluminum [1].

1.1.2 Fire Process of Polymer Matrix Composites

There are various chemical and physical phenomena involved in the fire process of PMCs as Mouritz et al. [2] summarized in Figure 1.3. Prior to the onset of thermal decomposition, heat transfer in composite materials is a result of pure conduction. When the temperature increases to the vicinity of the glass transition temperature, the composites first undergo reversible mechanical changes, such as thermal softening, and viscoelasticity dominates the mechanical behavior. PMCs may exceed failure criteria leading to global failure or local damage, such as fiber kinking and matrix cracks.

When the composite materials reach sufficiently high temperatures above the decomposition temperature, the chemical reaction occurs and the organic matrix degrades to form carbonaceous char releasing combustible gaseous products and radiating heat energy. At the beginning of the decomposition, the gases are trapped in the solid because of the low porosity and permeability of the composites. As the reaction proceeds, more resin matrix degrades to char with increasing porosity and permeability. Some decomposition gases carrying heat flow out of the solid and the heat transfer is influenced by gas diffusion besides thermal conduction. Other gases are held and accumulated inside

the pores building up the internal pressure. Meanwhile, a layer of carbonaceous char can propagate through the composites on continued heating, insulating the exposed surface and impeding further fire damage because of its low thermal conductivity. The mechanical behavior of composites in this phase is dominated by the decomposition effect.

Eventually, the composites reach flaming combustion. If the energy released by the combustion process is sufficient, the fire will grow and spread instead of self extinguishing. The composite structure with various types of damage accumulated inside the solid and propagated during the process fails when the loading condition is beyond the residual strength. Other possible phenomena occurring in the process include moisture vapors from the composite into the fire, ignition of flammable reaction gases, internal pressure build-up due to the formation of volatile gases and vaporization of moisture, matrix cracking, fiber-matrix interfacial debonding, and delamination damage.

A great deal of research has been conducted to characterize the flammability properties of composites and to develop fire resistant composites. Some studies have investigated the thermo-mechanical properties of PMCs in fire and post fire. Several recent works focus on the evaluation of the reducing mechanical properties, the residual strength, and the failure time of PMCs during combined heating and compressive loading. Failure under compressive loading is important when considering the performance of structural columns and wall panel assemblies during fire. There are different compressive failure modes depending on different fire scenarios and applied loadings, including local kinking, delamination, global buckling, debonding between components, and mixed failure mode, as shown in Figure 1.4. The objective of this work

is to investigate the thermo-mechanical behavior and compressive failure of polymer composites over temperature ranges from temperatures below the glass transition temperature to temperatures above the decomposition temperature. A three-dimensional coupled thermo-mechanical model is developed and incorporated into the commercial finite element software for predicting the fire structure response of PMCs. In addition, an experimental technique based on Vacuum Assisted Resin Transfer Molding (VARTM) is developed to manufacture PMCs with inserted hypodermic needle for examining the internal pressure of composites after decomposition. The model is verified and validated by comparing its results with other numerical results and experimentally measured data of the one-sided heating test for composites at coupon, intermediate-scale and large-scale level.

1.2 Background

1.2.1 Flammability Characteristics of Composites

At very high temperatures exceeding the polymer matrix decomposition temperature, combustible gases are produced and the fire-exposed surface of composites ignites. The fire, the gas toxicity, and the smoke density are issues to human health and survivability. The high temperature caused by the burning of composites is an obvious threat. If the smoke is toxic, it presents an additional risk. If the smoke is too dense, it will hinder the people in the vicinity of the fire escaping and become an obstruction to firefighter.

ASTM E 162 provides a laboratory test procedure for measuring the flame spread index and comparing the surface flammability of composites exposed to a prescribed

level of radiant heat energy. ASTM E 662 is a common test method to characterize the degree of smoke generation or smoke obscuration by determining the specific optical density of the smoke. The test is conducted in a closed chamber and the light attenuation is recorded. The sample is subjected to a radiant heat flux under both piloted ignition and smothering conditions. The resulting light transmissions provide the specific optical density. The heat release rate (HRR) defined as the amount of heat generated in a fire due to the combustion of a material and the peak heat release rate are primary parameters to determine the size and growth characteristics of a fire. Ignitability defined as the time required for a material to reach flaming combustion is another parameter to characterize the flammability of composites. ASTM E 1354 is used primarily to determine the HRR, also the effective heat of combustion, mass loss rate, the time to sustained flaming, and smoke production. These properties are determined on small size specimens that are representative of those in the intended end use. ASTM E 1321 consists of constructing a vertical 90º corner of the material and placing it in a large scale cone calorimeter. An ignition source, usually a gas burner, of specified heat flux output is used to ignite the material at the bottom of the corner. Wall temperatures and flame spread speeds are recorded along with usual cone calorimeter data. The use of composites inside naval submarines is covered by MIL-STD-2031, *Fire and Toxicity Test Methods and Qualification Procedure for Composite Material Systems Used in Hull, Machinery, and Structural Applications inside Naval Submarines*. This military standard contains test methods, requirements, and the qualification procedure for flammability characteristics such as the flame-spread index, the specific optical density of smoke, the combustion gas oxygen-temperature index, and the long-term outgassing.

Sorathia and co-workers [3-4], and Sevart et al. [5] investigated and compared the flammability of conventional and advanced fiber reinforced thermoset and thermoplastic composite materials suitable for surface ship and submarine applications. Polymers with a high aromatic content, such as phenolic polymers and epoxy, tend to form char insulating the exposed surface and impeding further fire damage. Phenolic laminates, as studied by Scudamore [6], Egglestone and Turley [7], Brown and Mathys [8], show a long ignition time, low heat release rate, and low smoke yields compared to other polymer matrix, such as vinyl ester and polyester. However, their mechanical properties are not considered adequate, without modification, for structural applications. It is found that different fire retardant additives and reinforcements have a significant effect on composite combustion. Halogenated polymers and polymers modified with halogenated additives are highly resistant to ignition. But the combustion of halogenated materials produces toxic acid gases (HCl, HF, HBr) which cause respiratory and eye irritation in people.

Since styrenated vinyl ester systems are presently used by the United States Navy in experimental applications for top-side structures, Sorathia and co-workers [9-11] characterized the fire performance of brominated vinyl ester based solid and sandwich (balsa core) composites, evaluated various vinyl ester resins with and without additives, and improved the fire safety of composite materials for naval applications. Other fire resistant polymers, such as potassium aluminosilicate and phthalonitrile polymers, were also examined for their flammability characteristics in [12-15]. Another approach to facilitate the application of composites in fire is to protect the core of composite structure by thermal barriers. Studies [16-18] evaluated the fire retardant performance of fire

barriers, such as ceramic fabric, hybrid of ceramic and intumescent coatings, silicone foam, and so forth.

1.2.2 Thermo-Mechanical Properties of Composites

Composites with high flammability and low fire resistance are being used increasingly in structural applications where fire is an ever present risk, such as aircraft, ships and offshore oil drilling platforms. The fire structural response is as significant to safety as the fire reaction behavior that has been more widely studied.

One important aspect to the understanding of the thermo-mechanical behavior of composites exposed to fire is the measurement of composite properties. In order to investigate the thermally-induced behavior of the glass-filled polymer composite, Henderson and co-workers [19-21], and Florio et al. [22-23] measured the kinetics of decomposition for both the pyrolysis and carbon-silica reactions, thermo-chemical expansion, specific heat, heat of decomposition, thermal conductivity, mass loss, volumetric heat transfer coefficient, porosity, and permeability, also monitored the morphology and the material damage by scanning electron microscopy. The thermal properties were found to be strong functions of temperature and heating rate. Lattimer, Ouellette, and Trelles [24-25] measured the decomposition and the specific heat capacity of glass reinforced vinyl ester composites at coupon size from room temperature to 800°C using a thermogravimetric analyzer (TGA) and a differential scanning calorimeter (DSC). Goodrich [26] developed the experimental techniques for quantitative specific heat measurement based on ASTM standards, recorded micro-structural changes of composites during decomposition and cooling following decomposition using an environmental scanning electron microscope (ESEM), devised a gas infusion technique

to measure the porosity, and measured the permeability of glass vinyl ester composites and balsa wood using the standard pressure differential gas flow technique. A temperature and mass dependent heat diffusion model was developed by Lua et al. [27] to determine the thermal properties of a woven fabric composite based on the temperature dependent thermal properties of the fiber and the resin. The accuracy of the model was demonstrated by comparing its prediction with available experimental data for a composite plate subjected to a hydrocarbon fire. Regarding the large-scale fire tests, Welch, Jowsey and co-workers [28] demonstrated a method for post-processing thermocouple data in order to establish a well characterized dataset of physical parameter values which can be used with confidence in model validation.

The internal pressure caused by the decomposition gases trapped inside the composites has influence on the thermo-mechanical response of composites and may contribute to the structure failure. One important property directly related to the internal pressure is permeability of decomposed composites. A small value of permeability at the start of decomposition can hold gases in pores building up pressure. More gases are generated by the continuous heating and contribute to the increasing pressure; however, the permeability also becomes larger with more material decomposition leading more gases to flow out of the solid and release the pressure eventually. Besides the research conducted by Goodrich [26] mentioned above, Wiecek [29], Ramamurthy et al. [30-31], and Doherty [32] examined the permeability of glass/phenolic composites, while Ahn et al. [33] used embedded fiber optic sensors to measure simultaneously the three principal permeabilities of fiber preforms made of continuous or short fibers. In order to predict the internal pressure accurately, Dimitrienko [34] determined the permeability by an

expression in terms of porosity and Sullivan [35] defined permeability as a logarithmic function of the degree of char, based on the measured virgin and char values. Ramamurthy [36] measured the internal pressure of glass/phenolic composites at different locations by drilling holes and inserting the hypodermic tubes into the sample to carry gases to the pressure transducers. There are other methods of pressure measurement presented in [37-38] which are concerned about the gas pressure in wood.

Since the non-linear viscoelastic effects dominate the mechanical behavior and delayed failure of polymer matrix composites at lower temperatures in the vicinity of the glass transition temperature, Case, Lesko, and co-workers [39-42] examined the compression creep rupture behavior of the glass/vinyl ester composite material system subject to combined load and one-sided heating simulating fire exposure and extended a compression strength model to include viscoelasticity for predicting the failure time. Ha and Springer [43-44] conducted tensile, compressive, shear, and four point bend tests for graphite epoxy composites over the range 24°C to 177°C to determine constants in their developed model, calculated the stresses and strains in loaded multidirectional laminates, and compared the predicted results with the measured data. Pering et al. [45], Shen and Springer [46] investigated the effects of moisture on the tensile strength of graphite epoxy composites using laminates with different lay-ups and the decrease in ultimate tensile and shear properties of composites exposed to high temperature. Tensile coupons and single lap-splice coupons of glass fiber reinforced polymer (GFRP) composites at a range of temperatures between room temperature and 200°C were tested by Chowdhury et al. [47] to study the mechanical properties under steady-state and transient thermal conditions. Mouritz, Mathys, and Gardinera [48-54] explored the post-fire mechanical

properties of various fiber reinforced polymer composites, including glass, carbon or Kevlar fibers with polyester, epoxy or phenolic resin matrix. The tension, compression, flexure, and interlaminar shear properties were measured after the composites had been exposed to intense radiant heat. It is found that the post-fire properties decrease rapidly with increasing heat flux and duration of a fire due to the thermal degradation of the polymer matrix. A model combining the properties of the fire-damaged and undamaged regions of composites was used to evaluate the post-fire mechanical properties and compared to the measured data for validation. Based on the model, Gibson et al. [55] developed a thermo-mechanical model composed of a thermal model for predicting the extent of thermal decomposition and a two layer model for predicting the residual properties of composites damaged by fire. Since woods are also significant components in composite structures, such as wood core in sandwich composites to improve the bending resistance, the decrease in mechanical properties of wood exposed to fire was studied by Springer and Dastin et al. [56-57].

In the perspective of micro-structure, Lua [58] proposed a four-cell micro-mechanics model to establish a mapping relation between the global and constituent thermo-mechanical response parameters and to quantify the composite properties at a given state of constituent damage. Deng and Chawla [59] used a unit cell model to capture the geometry of the woven glass fiber reinforced composites and evaluated the Young's modulus and coefficient of thermal expansion based on the properties of fiber and resin using finite element method. The damage induced in graphite epoxy laminates by fire was inspected by visual observation, scanning electron microscope (SEM),

planimetric measurements of the area of matrix loss on the sample face exposed to fire, and micro-hardness tester in [60].

Lee and Springer et al. [61-62] performed tests to measure the longitudinal and transverse tensile and compressive moduli and strengths, and the longitudinal shear moduli and strengths of composite laminates with different degrees of cure for evaluating the effects of cure on the mechanical properties of composite laminates. The post-curing effects on properties of composites manufactured by the vacuum-assisted resin transfer molding (VARTM) method were studied in [63]. The strength, stiffness, creep, and fatigue performance of composites were tracked at various points in the time after varying levels of post cure. In addition, other researchers [64-70] focused on the properties of different composite material systems and composite components, and failure for different structural geometries.

1.2.3 Modeling for Thermo-Mechanical Behavior of Composites

Until recently, models to analyze the structural behavior of composites in fire were not available. In most situations, fire tests have been conducted on composite components that are representative of the structural application for accessing the structural integrity of composites in fire. However, the tests are expensive and the accuracy of measured results depends on complicated experimental conditions. The most troublesome issue is the generality of the measured data. There is little possibility to extrapolate the information from these tests to predict the structural behavior of composite components in other fire scenarios without efficient fire structural models.

Accurate modeling of heat transfer through the composites is the critical first step in fire structural analysis. In order to predict the thermal response of the decomposing

polymer composites exposed to high temperature, various models were developed with specific assumptions based on the observed chemical and physical phenomena during the heating process. In 1984, Henderson et al. [71] presented a one-dimensional transient thermal model considering the decomposition reaction and measured the temperature dependent thermal properties as inputs into the model to predict the temperature profile through a sample. The model was further developed to include the combined effects of thermo-chemical expansion and storage of the decomposition gases in [29, 72-73]. The assumption of local thermal equilibrium existing between the solid matrix and decomposition gases within the tortuous pore network of the material was released in a later model presented in [74]. When the Henderson model is extended to three-dimensional case, it is not easy to determine the direction of gas flow and the permeability has to be considered in the gas convection term increasing computational burden. In order to improve the utility of the Henderson model in finite difference and finite element implementation, Miano and Gibson [75] modified the model by using a simple temperature dependent decomposition model, ignoring the volatile convection in heat transfer equation, and using a thermal diffusivity related to the thermal conductivity, specific heat and density. Looyeh, Gibson, Dodds, and co-workers [76-78] investigated the thermal response of laminated glass fiber reinforced panels with several different matrix materials by furnace fire testing and thermal modeling. A three-dimensional heat transfer model permitting temperature dependent material properties, arbitrary locations of heat sources and sinks, and a wide variety of realistic boundary conditions was formulated by Milke and Vizzini [79] to examine the thermal response of an anisotropic composite laminate. The study conducted by Looyeh et al. [80] analyzed the behavior of

sandwich panels in fire by developing a model accounting for decomposition in skins, transient heat conduction in core, and the effect of thermal contact resistance at interfaces. A model for determining the heat fluxes imposed on all surfaces of structural members was presented in [81] to improve the treatment of the heat input provided by a fire to the structural elements. Boyer and Thomas [82] developed an analytical model to assess the effects of thermal expansion on heat transfer, surface recession, and pyrolysis for a new rubber-modified composite materials which can expand up to 125 percent when heated. Xie and Des Jardin [83] examined the heat transfer between fire and solid using a level set based embedded interface method for further analysis of coupled response of composites structures and the local flow environment.

When the polymer composites are heated, the increasing temperature has an influence on the viscoelastic properties of polymer matrix in accord with the time-temperature superposition principle (TTSP) (before the materials start to decompose). The mechanical properties of composites continue to degrade and the char is formed as the temperature increases to the decomposition temperature. On the other hand, the thermo-chemical expansion of composites and the decomposition gas diffusion contribute to the temperature distribution through the composite materials. The coupled thermo-mechanical model is necessary for a better understanding of thermo-structural response of composites exposed to fire.

There is a great deal of research working on numerical methods for thermo-viscoelastic analysis of composite materials. Lin and Hwang [84], and Zocher et al. [85] endeavored to develop the numerical algorithm based on the finite element method for the efficient three-dimensional analysis of stress and deformation histories in composites.

Studies [86-88] developed various numerical methods to analyze and predict temperature and time dependent properties. An algorithm to predict long-term laminate properties of fiber reinforced composites considering the influence of water and temperature is presented in [89]. Case, Lesko and co-workers [39-42] included a characterization of the non-linear thermo-viscoelasticity and a compression strength failure criterion for the prediction of local compression failure due to micro-buckling into their model, also conducted experiments on the E-glass/vinyl ester composite laminates subjected to combined compression and one-sided simulated fire exposure for model validation. Burdette [90] assembled a series of models consisting of a fire model, a thermal response model, a stiffness-temperature model, a mechanical response model, and a material failure model to describe the fire growth and structural response processes for the loaded and fire-exposed composite structures. For the heating with temperature above the decomposition temperature, a model assuming the composite laminate in fire to comprise an unaffected layer with virgin properties and a heat-affected layer with zero properties was proposed and used to estimate the reductions in failure load of composites in [49-50, 91]. Feih, Gibson, Mouritz, Mathys, and co-workers [92-97] developed a thermo-mechanical model based on Henderson equations, temperature-dependent strength, and laminate theory to predict the time-to-failure of polymer laminates loaded in tension or compression and exposed to one-sided radiant heating by fire. The model was applied on sandwich composite materials with combustible glass vinyl ester skins and balsa core for estimating the residual compressive strength and the time-to-failure in [98]. The accuracy of the model was evaluated by comparing the predicted mass loss, temperature, and time-to-failure to the measured data. Asaro, Lattimer, and Ramroth [99] monitored the

collapse of glass vinyl ester laminates and cored sandwich samples at intermediate scale subjected to various levels of heat fluxes and applied loads. A temperature and time dependent model considering thermally induced material degradation was proposed to analyze the observation of collapse. Liu et al. [100] also concerned about the response of composite columns under axial compressive loading and in a non-uniform temperature distribution through the thickness The modulus was described as a polynomial function of temperature using experimental data. The eccentric loading resulting from the movement of the neutral axis away from the centroid of the cross-section and the out-of-plane deflections versus the applied heat flux were calculated. Bai et al. [101-103] included temperature dependent stiffness, viscosity, and effective coefficient of thermal expansion into a thermo-mechanical model. The model is employed with the beam theory to predict the deflections of cellular glass fiber-reinforced polymer slabs using finite difference method. Flanagan et al. [104] devised a facesheet push-off test for quantifying the delamination failure mode observed in fire tests of sandwich composite structures and an approach based on the existing fracture mechanics was applied to analyze the test. Lua and colleagues developed an ABAQUS Fire Interface Simulator Toolkit [105] for fire simulation and structural response and failure prediction via a two-way coupling between Fire Dynamics Simulator (FDS) and ABAQUS. From the perspective of designing, Gu and Asaro [106-109] investigated different failure modes of PMC and sandwich panels under transverse thermal gradients and compressive or transverse mechanical loads, such as buckling, deflection induced by the shift of the neutral axis, thermal distortion. Key and Lua [110] expanded isothermal multi-continuum theory (MCT) based on the two-constituent decomposition to include thermal effects related to large temperature

gradients caused by fires. Fire condition and progressive failure were simulated using the thermo-mechanical MCT algorithm. It was indicated that the thermal residual stresses resulting from the fiber and matrix coefficient of thermal expansion mismatch are significant to structural softening, damage initiation, and damage progress for composites subjected to extreme thermal conditions.

A porous network in the formerly solid material is formed with the continuing decomposition. The decomposition gases are held in the pores and an internal pressure develops when the permeability is small. As the heating processes, the porosity and permeability become larger and the gases start to flow out of the solid. The internal pressure built up to a high level resulting from the expansion of hot gases may cause the delamination failure of composites. Therefore, some coupled thermo-mechanical models include the internal pressure effect into material constitutive equation. Biot and Willis [111] established the theory of the deformation of a porous elastic solid containing a compressible fluid in 1957 and Carroll [112] derived an effective stress law for anisotropic elastic deformation. Dimitrienko [113-114] developed a method for porous media with phase transformations, which can determine not only the macroscopic characteristics of processes in porous media but also the microscopic characteristics in each of the phases. Furthermore, a model taking account of the pore pressure effect on thermo-mechanical response of composite materials and the shrinkage of composites heated up to the pyrolise temperature was developed in [34, 115-117]. Looyeh et al. [118], Sullivan, Salamon, and co-workers [35, 119-121] introduced the concept of Carroll's effective stress into the governing equations based on previous models so that the chemical decomposition, internal heat and mass transfer, gas pressure, and

deformation were accounted for in their models. Another model considering the contribution of moisture vapors, besides decomposed volatiles, to pressure in pores and progressive failure was developed by McManus and Springer [122-123] to describe the high temperature behavior of composites. From a micro-mechanical point of view, Wu and Katsube [124] proposed a constitutive model to couple the thermo-chemical decomposition and thermo-mechanical deformation. Another model using homogenization methods to formulate the damaged composites in terms of the volume fractions associated with fiber, resin and char was developed by Luo, Xie, and Des Jardin [125-127].

Given that the dominant loading mode for a structure composed of fiber reinforced polymer matrix composites subject to fire exposure is often compressive, a model accounting for a state of compression loading through a compression mechanics analysis is needed. The Budiansky and Fleck model [128] is a post micro-buckling, mechanistic model which combines the plasticity of the matrix material (through shear deformation) with the effects of kinking kinematics in the buckled region in order to estimate the residual compressive strength of unidirectional fiber reinforced composites. A detailed derivation of the theoretical results and expressions for static kinking strength and matrix plasticity can be found in Budiansky and Fleck [128]. Jensen and Christoffersen [129] analyzed the compressive failure by fiber kinking of unidirectional fiber composites. Bausano [130] used thermally modified micromechanics together with classical lamination theory and ANSYS to predict the rupture times which were found to be controlled by the glass transition temperature of the matrix, and also demonstrated that the basic Budiansky and Fleck model can be extended to successfully predict

compression failures in polymer matrix composites with a woven reinforcing phase. Boyd [131] further extended the compression strength model to include the non-linear viscoelasticity and applied it to the woven roving reinforced composites.

Major advances in the fire and structural modeling of polymer composites have been achieved in recent years; however, further investigation and development are needed in the research areas listed below.

- Capability of thermal models to analyze the temperature of composites containing reactive fibers. The influence of decomposition and oxidation of the reactive fibers on the temperature has not been adequately addressed.
- Thermal models considering the influence of damage, such as delamination and debonding, on the heat transfer in composites.
- Investigation of structural behavior of composites in fire under loading conditions other than tension and compression, such as shear, torsion, and fatigue.
- Thermo-mechanical models to include various types of damage, such as pore formation, decomposition, thermal softening of mechanical properties, delamination, kinking, buckling, matrix cracking, and fiber damage.
- Analysis of fire process in the level of material points, but not the ply level. Previous models used mostly took advantage of the concept of average strength. Failure prediction is based on the comparison of residual average strength to the applied load.
- A convenient method to implement models to engineering application

1.3 Research Objectives

In the previous literature, the models can be roughly divided into two classes. One is concerned about the thermo-mechanical behavior of composites at temperatures in the vicinity of glass transition temperature where the viscoelastic properties make a significant contribution to the composite structural response. The other focuses on the composite behavior in intense heating when the decomposition and gas diffusion occur in composite materials. To our knowledge, there are no models considering both viscoelasticity and decomposition, as well as pore formation during the heating process.

The purpose of the study is to develop a three-dimensional coupled thermo-mechanical model for predicting the material behavior of polymer composites exposed to fire. Various types of damage, such as thermal softening, decomposition, pores formation, and compression kinking, are included. The model can predict temperature, deflection, time-to-failure of composites over a wide temperature range from temperatures below the glass transition temperature to temperatures above the decomposition temperature. The model is incorporated into the commercial software ABAQUS by user subroutine named UMAT [132] and UMATHT [133] for the convenience of engineering application. The material behavior of composites subjected to combined thermo-mechanical loading is analyzed by the model and the code. A number of one-sided heating tests conducted on different material systems with different stack sequences of fiber orientation and different sample sizes are simulated and the model is verified and validated by comparing its results with other numerical results and experimentally measured data.

In addition, both experimental and numerical approaches are employed to investigate the internal pressure during the heating process. The thermal part of the model is used to predict the temperature and the pressure, and examine the effect of porosity and permeability. An experimental technique based on Vacuum Assisted Resin Transfer Molding (VARTM) is developed to manufacture PMCs with inserted hypodermic needle for internal pressure measurement and one-sided heating tests are conducted on the glass/vinyl ester composites to measure the pressure at different locations through thickness after decomposition.

Chapter 2 develops the model and shows the process of finite element implementation. The verification of heat transfer model and orthotropic viscoelasticity is performed. The model is also validated by comparing the predicted temperature, compression strain, in-plane and out-of-plane displacements, and failure times with the measured data from one-sided heating tests for composites at coupon level. Chapter 3 extends the analysis to different composite material systems at intermediate scale for validation of the model generality. Chapter 4 focuses on the investigation of internal pressure of the decomposition gases.

1.4 Figures

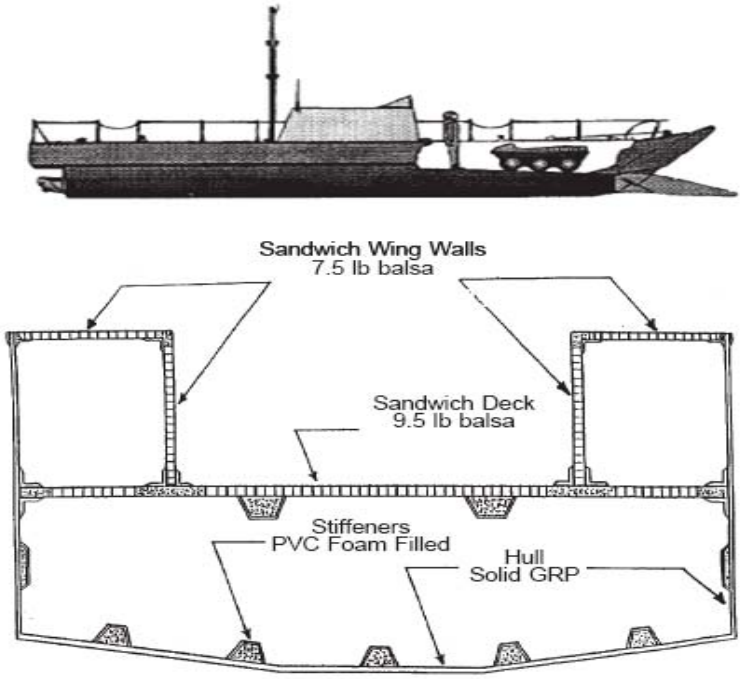

Figure 1.1: Profile and hull lay-up configuration of a 0.35 scale boat model (used with permission of Eric Greene [1])

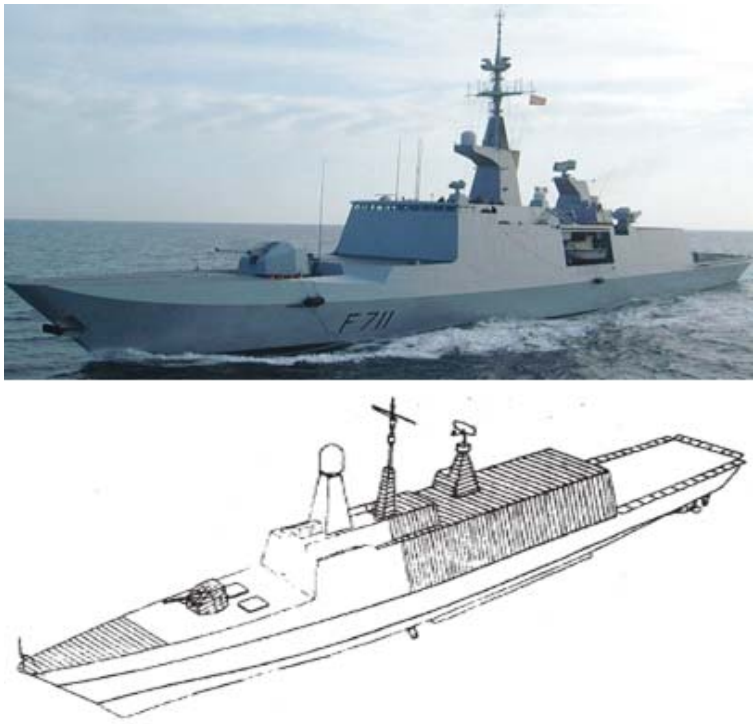

Figure 1.2: French LA FAYETTE class frigate using sandwich composites for both deckhouse and deck structure (used with permission of Eric Greene [1])

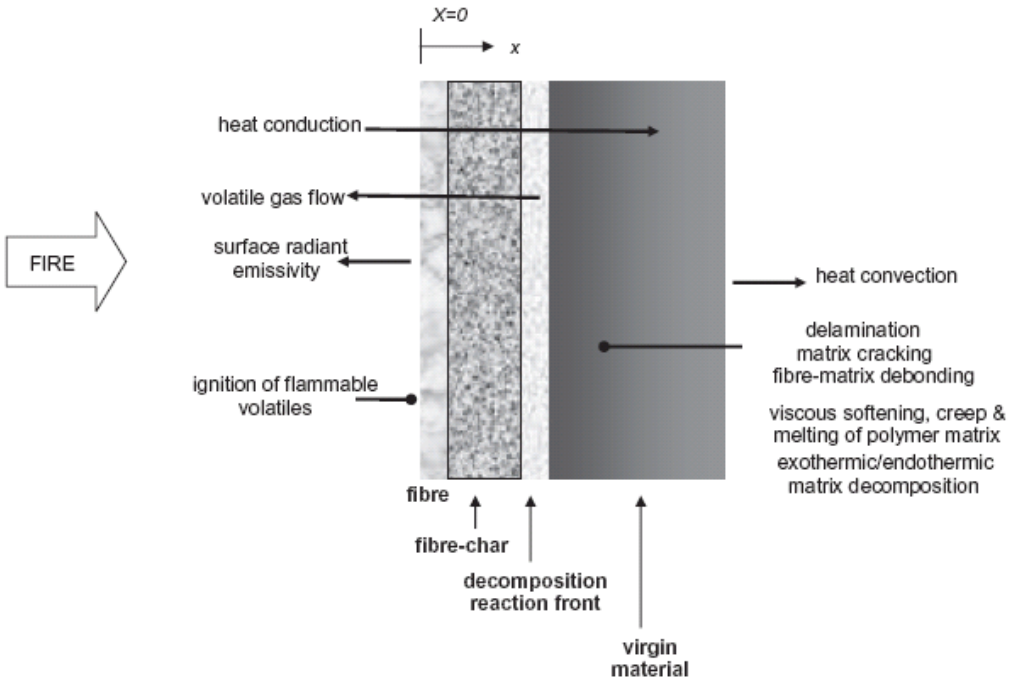

Figure 1.3: Schematic of various chemical and physical phenomena in the through-thickness direction of composites exposed to fire (used with permission of Adrian P. Mouritz [2])

Figure 1.4: Compressive failure modes of PMCs exposed to fire (used with permission of Patrick Summers [134])

Chapter 2: A Model and Finite Element Implementation for Structural Response of Polymer Composites Exposed to Fire

2.1 Abstract

A three-dimensional model is developed to predict the thermo-mechanical behavior and compressive failure of polymer composites with a wide temperature range from temperatures below the glass transition temperature to temperatures above the decomposition temperature. Both the effects of viscoelasticity and decomposition are included in this model. The model is incorporated into the commercial software ABAQUS for the convenience of engineering application. The resulting code is verified and validated by comparing its results with other numerical results and experimentally measured data of the one-sided heating test for composites at coupon level. The good agreement indicates the capability of the model to predict behavior for different stacking sequences and different combined thermo-mechanical loadings.

Keywords: Thermo-mechanical behavior; Viscoelsaticity; Decomposition; Finite element analysis; Fire

2.2 Introduction

Composite materials are used over a wide range of applications in marine, aerospace, civil infrastructure, and automobiles. Increased utilization of composite materials in situations where fire is a concern requires the ability to predict the structural-mechanical response of composites subjected to different fire scenarios. Although the lower thermal conductivity of PMCs compared to conventional metals can prevent the

spread of fire from the heat source, PMCs have worse overall fire performance because of the chemical and mechanical changes that occur in PMCs exposed to fire. The toxic gases and dense smoke generated from the decomposition reaction for PMCs in fire increase the health risk and threaten public safety. Also, the reduction in strength of heated composites especially compression strength causes decreased structural integrity and eventually component failure. In order to improve the performance of PMCs under combined thermo-mechanical loadings, it is important to understand the structural response of PMCs in fire.

Accurate heat transfer modeling is a significant component in the fire structural analysis. Various models have been developed to predict the thermal response of the decomposing polymer composites exposed to high temperature with specific assumptions based on the observed physical phenomena during the heating process. Henderson et al. [71] presented a one-dimensional transient thermal model considering the decomposition reaction and the measured temperature dependent thermal properties were used as inputs into the model to predict the temperature profile through a sample composed of glass and talc filler, and phenol-formaldehyde resin. The model was subsequently further developed to include the combined effects of thermo-chemical expansion and storage of the decomposition gases [72]. The assumption of local thermal equilibrium existing between the solid matrix and decomposition gases within the tortuous pore network of the material was released in a later model [74]. Looyeh et al. [78] derived the finite element formulation for a simplified Henderson's model, while Dodds, Gibson, and co-workers [76] investigated the thermal response of laminated glass fiber reinforced panels with several different matrix materials by furnace fire testing for the model validation.

Another study conducted by Looyeh et al. [80] analyzed the behavior of sandwich panels in fire by developing a model accounting for decomposition in skins, transient heat conduction in core, and the effect of thermal contact resistance at interfaces. Lattimer and Ouellette [24] measured the thermal and physical properties of glass/vinyl ester composites for the application of Henderson's model on this type of composite material system.

When the polymer composites are heated, the increasing temperature has an influence on the viscoelastic response of the polymer matrix. The mechanical properties of composites continue to degrade and char is formed once the temperature increases to the decomposition temperature. A coupled thermo-mechanical model is necessary to describe the thermo-structural response of composites exposed to fire. Lin and Hwang [84], and Zocher et al. [85] developed the numerical algorithm based on the finite element method for the efficient three-dimensional mechanical analysis of anisotropic composite materials. Case, Lesko and co-workers [39-42, 130-131] characterized the non-linear viscoelasticity of glass/vinyl ester composites in temperature around the glass transition temperature and conducted the one-sided heating test on composite coupon samples under compression loading. They proposed a thermo-viscoelastic model including a compression strength failure criterion for the kinking failure mode, analyzed the structure response of composites based on classical lamination theory, and predicted the time-to-failure for the model validation. Burdette [90] assembled a series of models consisting of a fire model, a thermal response model, a stiffness-temperature model, a mechanical response model, and a material failure model to describe the fire growth and structural response processes for the loaded and fire-exposed composite structures. For

the heating with temperature above the decomposition temperature, a model assuming that the composite laminate in fire is composed of a virgin layer and a heat-affected layer was proposed and used to estimate the reductions in failure load of composites in [49-50, 91]. Feih, Gibson, Mouritz, Mathys, and co-workers [92-94, 96] developed a model based on Henderson equations, temperature-dependent strength, and lamination theory to predict the time-to-failure of polymer laminates loaded in tension or compression and exposed to one-sided radiant heating by fire. The accuracy of the model was evaluated by comparing the predicted mass loss, temperature, and time-to-failure to the measured data.

Pores inside composites resulting from the polymer decomposition connect to form a porous network with continuing heating. When the permeability is small, most of the decomposition gases are held in the pores and an internal pressure develops. As the heating processes, more gases are generated and the porosity and permeability become larger reducing the difficulty for gases flowing out of the solid. The internal pressure is built up to a high level at some point because of the increase of trapped gases and the expansion of hot gases. The pressure has influence on the mechanical response of composites and may cause the delamination failure. Therefore, some coupled thermo-mechanical models [34-35, 115, 118, 121-123, 125] include the internal pressure effect into the constitutive equations governing the material behavior of composites.

The previous models can be roughly divided into two cases. One case is concerned with the thermo-mechanical behavior of composites at temperatures in the vicinity of glass transition temperature where the viscoelastic properties make a significant contribution to composite structural response. The other case focuses on the composite behavior in intense heating when the decomposition and gas diffusion occur in

composite materials. To our knowledge, there are no models considering both viscoelasticity and decomposition during the heating process. The study will develop a three-dimensional model to predict the thermo-mechanical behavior of polymer composites over temperature ranges from temperatures below the glass transition temperature to temperatures above the decomposition temperature. The decomposition reaction and the storage of decomposition gases in the solid are considered in the heat transfer equation and the gas diffusion equation. The effects of viscoelasticity and decomposition are included in the material constitutive equation. A time/temperature dependent compression strength failure criterion developed in [40-41] is used to predict the failure time for the kinking failure mode.

The model is incorporated into the commercial software ABAQUS by the UMAT and UMATHT subroutines for the convenience of engineering application. The numerical method provides a framework for the implementation of more complicated models in further development, such as models considering multi-phase decomposition and multi-stage softening of mechanical properties. The analysis using finite element method can predict thermo-mechanical response and residual strength at each material point, but not in ply level. After the material properties and progressive failure behavior are assigned to the simulated sample, the analysis can calculate the distribution and history of thermo-mechanical variables at the measured points in experiment for complete validation. The code is verified and validated by comparing its results with other numerical results and experimentally measured data of the one-sided heating test for composites at coupon level. The tests from [40, 92, 130] for different stacking sequences and different combined thermo-mechanical loadings are simulated to valdate

the generality of the model. This validated viscoelastic solution module has been integrated with GEM's AFIST, an ABAQUS Fire Interface Simulator Toolkit [105], for fire simulation and structural response and failure prediction via a two-way coupling between Fire Dynamics Simulator (FDS) and ABAQUS.

2.3 Model and Finite Element Implementation

2.3.1 Thermo-Mechanical Model

There are four governing equations in the model: the heat transfer equation, the decomposition equation, the gas diffusion equation, and the material constitutive equation.

The thermal part of the model is based on [72, 118, 121] and is described by Eq. (2.1-2.3)

$$\frac{1}{V}\left(mC_p + m_g C_{pg}\right)\frac{\partial T}{\partial t} - \nabla \bullet \left(k_1 \frac{\partial T}{\partial x}\mathbf{i} + k_2 \frac{\partial T}{\partial y}\mathbf{j} + k_3 \frac{\partial T}{\partial z}\mathbf{k} \right) - \frac{PM}{RT} C_{pg} \left(\frac{\gamma_1}{\mu}\frac{\partial P}{\partial x}\mathbf{i} + \frac{\gamma_2}{\mu}\frac{\partial P}{\partial y}\mathbf{j} + \frac{\gamma_3}{\mu}\frac{\partial P}{\partial z}\mathbf{k} \right) \bullet \nabla T + \frac{1}{V}\left(h - h_g\right)\frac{\partial m}{\partial t} = 0 \tag{2.1}$$

$$\frac{1}{m_0 - m_f}\frac{\partial m}{\partial t} = -A\left(\frac{m - m_f}{m_0 - m_f}\right)^n e^{(-E/RT)} \tag{2.2}$$

$$-\nabla \bullet \left[\rho_g \left(\frac{\gamma_1}{\mu}\frac{\partial P}{\partial x}\mathbf{i} + \frac{\gamma_2}{\mu}\frac{\partial P}{\partial y}\mathbf{j} + \frac{\gamma_3}{\mu}\frac{\partial P}{\partial z}\mathbf{k} \right) \right] + \frac{1}{V}\left(\frac{\partial m}{\partial t} + \frac{\partial m_g}{\partial t} \right) = 0 \tag{2.3}$$

where m is the remaining solid mass, m_g is the mass of gas related to internal pressure P by the equation of state of ideal gas $m_g = (PM\phi V)/(RT)$, V is the control volume, C_p is the specific heat of solid, C_{pg} is the specific heat of gas, γ_i and $k_i = k_{ig}\phi + k_{is}(1-\phi)$ (i=1,2,3) are the permeability and thermal conductivity of composites in three coordinate directions, k_{ig}, k_{is}, and ϕ are the thermal conductivity of gases, the thermal conductivity

of solids, and the porosity of composites, μ is the viscosity of decomposition gas, $h = Q + \int_{T_r}^{T} C_p dT$ is enthalpy of solid, Q is heat of decomposition, $h_g = \int_{T_r}^{T} C_{pg} dT$ is enthalpy of gas, A is pre-exponential factor, E is activation energy, R is gas constant, n is order of reaction, m_0 is initial mass, and m_f is final mass. The thermal properties of the solid material, the porosity, and the permeability are assumed to be functions of temperature and decomposition factor. The decomposition factor F is defined by $F = \left(m - m_f\right) / \left(m_0 - m_f\right)$.

The heat transfer equation Eq. (2.1) is based on the energy conservation principle, considering the energy stored in the gas and the solid components, the heat conduction, the convection energy due to the decomposition gases flowing out of the solid, and the heat generated or consumed by the decomposition reaction. The remaining solid mass is calculated by the decomposition equation Eq. (2.2) which has a form of the n^{th} order Arrhenius equation. The gas diffusion equation Eq. (2.3) is derived from the mass conservation equation. The total mass change of remaining solid, the gas trapped inside the solid, and the gas flowing out of the solid should be zero in the control volume. Eq. (2.3) combined with Darcy's law can be used to predict the gas pressure. The derivation of these equations from one-dimension to three-dimension can be referred to Appendix A.

For the stress analysis, the material is assumed to be composed of virgin material and char material. The material constitutive equation is given by Eq. (2.4). The viscoelasticity of virgin material is described by the first term on the right hand side of Eq. (2.4) where $\varepsilon_j^m\left(\xi'\right)$ is the mechanical strain given by Eq. (2.5) in which ε_j^t is total strain, ε_j^{th} is thermal strain, α_j is the coefficient of thermal expansion, T is the

temperature, and T_r is the reference temperature. Further, each of the stiffness quantities of virgin material is expanded in a Prony series Eq. (2.6) where M is the number of Prony series terms and ξ is the temperature-reduced time defined by Eq. (2.7) in which a_T is temperature shift factor. The second term on the right hand side of Eq. (2.4) represents the contribution of char material. Since the stiffness of char material is assumed to be very small, this term is neglected.

$$\sigma_i(\xi) = F\int_0^{\xi} C_{ij}^{v}(\xi-\xi')\frac{\partial \varepsilon_j^m(\xi')}{\partial \xi'}d\xi' + (1-F)C_{ij}^{c}\varepsilon_j^m(\xi) \tag{2.4}$$

$$\varepsilon_j^m = \varepsilon_j^t - \varepsilon_j^{th} = \varepsilon_j^t - \alpha_j(T-T_r) \tag{2.5}$$

$$C_{ij}^{v}(\xi) = C_{ij\infty} + \sum_{m=1}^{M} C_{ijm}e^{-\xi/\tau_{ijm}} \tag{2.6}$$

$$\xi = \xi(t) = \int_0^t \frac{1}{a_T}d\tau \tag{2.7}$$

The time-temperature dependent compression strength model developed in [40-41] is used to calculate the compression strength for the local kinking failure mode of the fiber reinforced polymer composites, given by

$$\sigma_c(t,T) = G(t,T)\left[1+n\left(\frac{3}{7}\right)^{\frac{1}{n}}\left(\frac{\bar{\phi}/\gamma_Y}{n-1}\right)^{\frac{n-1}{n}}\right]^{-1} \tag{2.8}$$

where G is the shear relaxation modulus, n is the strain hardening parameter, γ_Y is the shear strain at the yield point, and $\bar{\phi}$ is the initial fiber misalignment angle. The model considers the local shear yielding due to the initial fiber misalignment angle as the mechanism of kinking failure, and includes the viscoelastic effect represented by the

shear relaxation modulus. Although the parameters n and γ_Y are dependent on the temperature around the glass transition temperature, they do not have a strong influence on the predicted compression strength. They can be fixed at a constant value at the room temperature and the compression strength is dominated by the initial misalignment angle $\bar{\phi}$ and the shear relaxation modulus G depending on time and temperature. To further improve the compression model, this study considers the decomposition effect on the compression kinking failure by including the decomposition factor as a scale factor into the expression of the composite compression strength.

$$\sigma_c(t,T) = F(t,T)G(t,T)\left[1+n\left(\frac{3}{7}\right)^{\frac{1}{n}}\left(\frac{\bar{\phi}/\gamma_Y}{n-1}\right)^{\frac{n-1}{n}}\right]^{-1} \tag{2.9}$$

2.3.2 Finite element implementation

In solving the governing equations (Eq. 2.1-2.4), we must determine strains, temperature, remaining solid mass, and gas pressure. There are two user subroutines provided by ABAQUS for more flexible and wider engineering application. The first subroutine is UMAT, which is used to define the material constitutive equation. The other subroutine is UMATHT, which is used to define the heat transfer equation. Since the gas diffusion equation has the same form as heat transfer equation, it can also be defined in UMATHT. However, only one UMATHT user subroutine can be assigned to one layer of elements. As a result, in order to implement the model into ABAQUS, two overlaid layers of elements are employed. These overlaid elements have their displacement degrees of freedom fixed to each other at the nodes. The solution procedure employs one UMAT subroutine and one UMATHT subroutine applied to the first overlaid layer to define the constitutive, decomposition, and heat transfer equations.

Another UMATHT subroutine is applied to the second overlaid layer to solve the gas diffusion equation. In practice, the four equations are not solved simultaneously in each time increment. The constitutive equation is solved first based on the decomposition factor at the end of last time increment. Then the heat transfer equation and decomposition equation are solved and the temperature is transferred to the other layer for calculating the gas diffusion equation. Variables in these equations, such as temperature, decomposition factor, and pressure, are exchanged between user subroutines by common blocks in the code.

Variables to be defined in UMATHT for solving the heat transfer and gas diffusion equation include the internal thermal energy per unit mass U, the variation of internal thermal energy per unit mass with respect to temperature $\frac{\partial U}{\partial T}$, the variation of internal thermal energy per unit mass with respect to the spatial gradients of temperature $\frac{\partial U}{\partial(\partial T / \partial x_i)}$ (i=1,2,3), the heat flux vector $\mathbf{f}$, the variation of the heat flux vector with respect to temperature $\frac{\partial \mathbf{f}}{\partial T}$, and the variation of the heat flux vector with respect to the spatial gradients of temperature $\frac{\partial \mathbf{f}}{\partial(\partial T / \partial x_i)}$ (i=1,2,3). These terms need to be evaluated at the end of each time increment. The decomposition equation is implemented into heat transfer UMATHT using finite forward difference to update the remaining solid mass. Details of UMATHT implementation for thermal model can be referred to Appendix A.

For the purpose of the numerical implementation, Eq. (2.4) is recast in the incremental form which is modified from the corresponding equation in [85] and further developed to include the decomposition effect.

$$\Delta\sigma_i = F_{n+1}\left(C'_{ij}\Delta\varepsilon_j^m + \Delta\sigma_i^R\right) + \frac{F_{n+1}-F_n}{F_n}\sigma_i\left(t_n\right) \tag{2.10}$$

where

$$C'_{ij} = C_{ij\infty} + \frac{1}{\Delta\xi}\sum_{m=1}^{M}\eta_{ijm}(1-e^{-\Delta\xi/\tau_{ijm}}) \tag{2.11}$$

$$\Delta\sigma_i^R = -\sum_{j=1}^{J}\sum_{m=1}^{M}(1-e^{-\Delta\xi/\tau_{ijm}})S_{ijm}(\xi_n) \tag{2.12}$$

in which F_n and F_{n+1} are the decomposition factors at the start and the end of the current time increment, $\eta_{ijm} = C_{ijm}\tau_{ijm}$, $\Delta\xi = \xi_{n+1} - \xi_n$ (the current increment of the temperature-reduced time corresponding to the current time increment), $\sigma_i\left(t_n\right)$ is the stress component at the start of the current time increment, $\Delta\sigma_i$ is the current increment of stress component, $\Delta\varepsilon_j$ is the current increment of strain component, J is number of strain components ($J = 6$ for three-dimensional strain array in ABAQUS), and $C_{ij\infty}$, τ_{ijm} , C_{ijm} are Prony series parameters related to material properties. $S_{ijm}(\xi_n)$ are given by

$$S_{ijm}(\xi_n) = e^{-\Delta\xi/\tau_{ijm}}S_{ijm}(\xi_{n-1}) + \eta_{ijm}(1-e^{-\Delta\xi/\tau_{ijm}})\frac{\Delta\varepsilon_j^m}{\Delta\xi} \tag{2.13}$$

in which $\Delta\xi = \xi_n - \xi_{n-1}$ is the previous increment of the temperature-reduced time, and $\Delta\varepsilon_j$ is the previous strain increment. The recursion relation is initiated with $S_{ijm}(\xi_1) = 0$ for $n = 1$. The incremental form of the constitutive equation Eq. (2.10) is used to update stress status and evaluate Jacobian matrix of the constitutive model in UMAT subroutine of ABAQUS. The derivation of incremental form of material constitutive equation can be referred to Appendix B.

2.4 Model Verification

2.4.1 Temperature Verification

A verification exercise for thermal analysis is conducted before the prediction of the thermal response of the actual composite structures. As a start, it is assumed that there is no accumulation of decomposition gases in the solid material. Based on this assumption, the thermal part of the model is reduced to the model in [71]. In order to compare with numerical results from the one-dimensional model, all gases are assumed to flow in only one direction for the three-dimensional verification examples. The reduced heat transfer equation is given by

$$\frac{1}{V}mC_p\frac{\partial T}{\partial t}-\nabla\bullet\left(k_1\frac{\partial T}{\partial x}\mathbf{i}+k_2\frac{\partial T}{\partial y}\mathbf{j}+k_3\frac{\partial T}{\partial z}\mathbf{k}\right)+\dot{m}_g C_{pg}\frac{\partial T}{\partial x}+\frac{1}{V}\left(h-h_g\right)\frac{\partial m}{\partial t}=0 \qquad (2.14)$$

in which mass flux $\dot{m}_g=-A\int_0^x\frac{\partial\rho}{\partial t}dx$, and A is the cross section area. Variables related to internal energy for implementing the heat transfer equation into UMATHT are also simplified.

$$\Delta U=\frac{1}{V}mC_p\Delta T+\frac{1}{V}(h-h_g)\Delta m+\dot{m}_g C_{pg}\frac{\partial T}{\partial x}\Delta t \qquad (2.15)$$

$$\frac{\partial U}{\partial T}=\frac{1}{V}mC_p \qquad (2.16)$$

$$\frac{\partial U}{\partial(\partial T/\partial x_i)}=0 \quad i=1,2,3 \quad x_1=x,x_2=y,x_3=z \qquad (2.17)$$

The verification example considered is illustrated in Figure 2.1 and consists of a sample with a heat flux applied to one side. The thickness of the sample is 0.0127m. Thermal conductivities in three directions are set to the same value and the boundary conditions on the surfaces parallel to the thickness direction are set to be thermal

insulated for comparing with results from the one-dimensional model. The boundary condition on the exposed surface is

$$q''_{s,o} = \left(q''_{rad} - \varepsilon_s \sigma T_s^4\right) + h_{conv}\left(T_{\infty,o} - T_s\right) \tag{2.18}$$

where the radiant heat flux $q''_{rad} = 25$ kW/m^2, the emissivity of the exposed surface $\varepsilon_s = 1$, the Stefan-Boltzman constant $\sigma = 5.67\times10^{-11}$ kw/m^2-K^4, the convection heat flux coefficient $h_{conv} = 0.01$ kW/m^2-K, and the temperature in infinity $T_{\infty,o} = 300$ K. The boundary condition on the unexposed surface is assumed to be thermal insulated $q''_{s,L} = 0$. The initial temperature is assumed as constant through thickness, $T_{Ini} = 300$K. The material properties used in this example are organized in Table 2.1.

Table 2.1: Thermal properties for the temperature verification problem

Property	Value or function
Virgin density $\rho_0=m_0/V$ (kg/m^3)	1700
Final density $\rho_f=m_f/V$ (kg/m^3)	1255
Solid specific heat C_p (J/kg-K)	1100
Gas specific heat C_g (J/kg-K)	3000
Solid thermal conductivity k (W/m-K)	0.30
Heat of decomposition Q (J/kg)	-2×10^5
Pre-exponential factor A (s^{-1})	5.0×10^{28}
Activation energy E (J/mol)	3.62×10^5
Order of reaction n	4.6

The transient heat transfer procedure in ABAQUS and the UMATHT subroutine based on the three-dimensional thermal model are used to execute the analysis. There are 20 three-dimensional solid elements. In addition, a one-dimensional heat transfer element is developed from the same model using another user subroutine named UEL. A MATLAB FEM code developed by Summers [134] has already been verified by

comparing with the results obtained from HEATING 7.3 which is used widely commercially. These three codes are used to solve the same problem. The temperature history curves at the exposed surface, the middle surface, and the unexposed surface resulting from these codes are compared at Figure 2.2 and the curves of mass loss per unit area at the exposed surface versus time are compared at Figure 2.3. It is found that both the temperature and the mass loss curves obtained from UMATHT agree well with the results obtained from UEL and MATLAB code. The good agreement verifies the UMATHT implementation of the three-dimensional thermal model.

2.4.2 Verification for FE Implementation of Orthotropic Viscoelasticity

A pure shear creep test with unit shear stress applied is simulated using UMAT routine to implement the orthotropic viscoelastic model with degenerate isotropic properties. The shear modulus is given by

$$G(t) = 2\times10^8 + 4\times10^8 \times e^{-t/0.1} \text{ Pa} \tag{2.19}$$

The result of shear strain calculated by UMAT is compared with the theoretical solution in Figure 2.4. The numerical results agree well with the theoretical results.

For further verification, the calculated results from the UMAT routine with degenerate isotropic properties are compared to the results from the built-in ABAQUS isotropic viscoelastic routine for a simple problem considering temperature effect on the viscoelastic properties. The geometric model for this problem is shown in Figure 2.5. The dimension of the model is 10 m in length, 4 m in width, and 1 m in thickness. The fixed constraint is applied on one end of the model. This model has a combination of normal and shear stresses resulting from the combination of a pressure denoted as “1” and a

concentrated force denoted as "2" applied initially, and another concentrated force denoted as "3" applied after one minute. The simulated temperature profile of

$$T(x,y,z,t) = 383 - (x-6)^2 - y^2 - (z-2.5)^2 + t^2 \text{ K} \tag{2.20}$$

is applied along with material properties of

$$G_{12}(\xi) = G_{13}(\xi) = G_{23}(\xi) = G_\infty + \sum_{i=1}^{12} G_i e^{-\xi/\tau_i} \tag{2.21}$$

$$\nu_{12} = \nu_{13} = \nu_{23} = 0.3 \tag{2.22}$$

$$E_1(\xi) = E_2(\xi) = E_3(\xi) = 2G(\xi)(1+\nu) \tag{2.23}$$

where $\xi(t) = \int_0^t \frac{1}{a_T} d\tau$. In general, any reasonable temperature shift factor a_T may be employed. However, in order to compare with the built-in ABAQUS isotropic viscoelastic routine, the WLF form is chosen,

$$\log_{10}(a_T) = \frac{-C_1(T-T_r)}{C_2 + T - T_r} \tag{2.24}$$

where $T_r = 383K$, $C_1 = 48.62$, and $C_2 = 156.87$. The parameters in the Prony series of shear modulus can be referred to Table 2.2. Results of normal and shear strains at one node whose coordinate is $(4.667, 0.8, 2.121)$ from the UMAT routine are compared with the built-in ABAQUS isotropic viscoelatic model with excellent agreement, as shown in Figure 2.6.

Table 2.2: Parameters of G_{12} Prony series for the viscoelasticity verification problem

i	G_i (GPa)	τ_i (s)
1	-0.18797	6×10^{-10}
2	0.11799	6×10^{-9}
3	0.18147	6×10^{-7}
4	0.30442	1.897×10^{-4}
5	0.26655	6×10^{-2}
6	0.081069	6×10^{-1}
7	0.63234	6×10^{0}
8	0.76585	6×10^{1}
9	1.3851	6×10^{2}
10	1.1578	6×10^{3}
11	0.42281	6×10^{4}
12	0.16437	1.897×10^{6}
∞	0.11050	

2.5 Model Validation for One-sided Heating Test at Coupon Level

2.5.1 Thermo-Mechanical Analysis with Viscoelasticity

In order to validate the viscoelasticity part of the model and the code, the one-sided heating tests under compression loading conducted by Bausano [130] and Boyd et al. [40] are simulated and the predicted results from the model are compared to the measured data shown in the paper. The schematic of the compression creep rupture test subject to one-sided heat flux is shown in Figure 2.7. The compression load is ramped to a set point and is kept being constant during the test. Then a heat flux is applied to one side of the composite sample until the in-plane displacement in the loading direction reaches the upper limit and the kinking failure occurs.

The composite material system is composed of Vetrotex 324 E-glass woven fiber and Ashland Derakane 510A-40 vinyl ester resin. Material properties, such as density, thermal conductivity, specific heat capacity, coefficient of thermal expansion, as well as

the compression and shear relaxation moduli (with temperature shift factor) in the coordinates based on the principal material orientation consistent with the woven fiber orientation, are collected from references [39-42, 130-131]. The experimental compression and shear relaxation moduli can be fitted into Prony series form,

$$E_1(\xi) = E_\infty + \sum_{i=1}^{12} E_i e^{-\xi/\tau_i} \tag{2.25}$$

$$G_{12}(\xi) = G_\infty + \sum_{i=1}^{12} G_i e^{-\xi/\tau_i} \tag{2.26}$$

where subscripts 1 and 2 denote warp and weft direction respectively. The parameters in the Prony series are organized in the Table 2.3 and Table 2.4. Based on the typical modulus ratio in the elastic situation, other moduli and Possion's ratio are set as following,

$$E_2(\xi) = 0.899E_1(\xi),\ E_3(\xi) = 0.443E_1(\xi) \tag{2.27}$$

$$G_{13}(\xi) = 0.864G_{12}(\xi),\ G_{23}(\xi) = 0.834G_{12}(\xi) \tag{2.28}$$

$$\nu_{12} = 0.11,\ \nu_{13}=0.21,\ \nu_{23}=0.22 \tag{2.29}$$

Table 2.3: Parameters of E_1 Prony series for validation of model with viscoelasticity

i	E_i (GPa)	τ_i (s)
1	0.6751	6×10^{-3}
2	1.0206	6×10^{-2}
3	0.8996	6×10^{-1}
4	0.9070	6×10^{0}
5	1.8357	6×10^{1}
6	1.7820	6×10^{2}
7	2.5111	6×10^{3}
8	1.3335	6×10^{4}
9	2.4931	6×10^{5}
10	1.6366	6×10^{6}
11	0.9783	6×10^{7}
12	2.6812	6×10^{8}
∞	10.8937	

Table 2.4: Parameters of G_{12} Prony series for validation of model with viscoelasticity

i	G_i (GPa)	τ_i (s)
1	0.1269	6×10^{-9}
2	0.1797	6×10^{-7}
3	0.3079	1.897×10^{-4}
4	0.2569	6×10^{-2}
5	0.0963	6×10^{-1}
6	0.6315	6×10^{0}
7	0.7569	6×10^{1}
8	1.3900	6×10^{2}
9	1.1533	6×10^{3}
10	0.4287	6×10^{4}
11	0.1290	1.897×10^{6}
12	0.0339	6×10^{7}
∞	0.1090	

The test samples in [130] have 10 layers of woven fabric with the warp directions stacked as $[0/+45/90/45/0]_s$, while the samples in [40] have the warp directions aligned with the direction of loading. The dimension of all samples is normally 25 mm wide and

6.1 mm thick with gage length of 50 mm exposed to the applied heat flux. In these tests, the temperature is not high enough to cause significant decomposition, so that viscoelasticity dominates the mechanical behavior, and any decomposition that results can be neglected. Therefore, the basic heat transfer equation only considering the heat conduction is accurate enough to predict temperature distribution and the material constitutive equation can be reduced to

$$\sigma_i(\xi) = \int_0^{\xi} C_{ij}^{v}(\xi - \xi') \frac{\partial \varepsilon_j^m(\xi')}{\partial \xi'} d\xi' \tag{2.30}$$

The time and temperature dependent compression strength model is used to calculate the compression strength and determine if the material points fail. Considering the material is the woven glass fiber composite, the failure condition at each integration point is defined as

$$\sigma_c < \max(|\sigma_1|, |\sigma_2|) \tag{2.31}$$

where σ_c is the calculated compression strength, σ_1 and σ_2 are the normal stresses in the warp and weft directions. Once the failure condition is satisfied, the stiffness at the point is decreased to a very small value and there is no stress at the point. The time-to-failure of the sample is determined by the time when the in-plane displacement in the loading direction increases suddenly to a large value, reflecting that the sample no longer has capacity to resist the compression load.

Since the heat flux applied to the front surface of the sample is controlled in tests of [130], the thermal boundary condition on the exposed surface in the analysis has the same expression as Eq. (2.18) in which q''_{rad} is the radiant heat flux of 5 kW/m^2, 10 kW/m^2, or 15 kW/m^2, the emissivity of the exposed surface $\varepsilon_s = 0.95$, the Stefan-

Boltzman constant $\sigma = 5.67 \times 10^{-11}$ kW/m^2-K^4, the convection heat flux coefficient $h_{conv} = 0.015$ kW/m^2-K, and $T_{\infty,o} = 298$ K . The thermal boundary conditions on the back surface and side surfaces includes the radiation to the environment and the heat convection, given by

$$q''_{s,o} = \varepsilon_s \sigma \left(T^4_{\infty,o} - T^4_s \right) + h_{conv} \left(T_{\infty,o} - T_s \right) \tag{2.32}$$

Tests in [40] control the temperature on the front surface of the sample, so the measured temperature on the front and back surface is applied as the thermal boundary condition. The initial temperature for all tests is assumed as constant through thickness, $T_{Ini} = 298$K . Constraints to compel all nodes on the loading surface to have the same displacement in the loading direction and to fix displacements on the other two directions are applied on the loading end of the sample, while constraints to fix all displacement degrees of freedom are applied on the other end to simulate the clamped-clamped constraint.

Figure 2.8 shows the temperature contour for one of the tests with heat flux of 5 kW/m^2 and compression stress of 53.2 MPa at 1300 seconds. Figure 2.9 compares the predicted temperatures at the hot and cold surface with experimentally measured data for the heat flux of 5kW/m^2, 10kW/m^2, and 15kW/m^2. The predicted compression strain on the cold surface is compared with the measured data for the different loading levels and the same heat flux as shown in Figure 2.10. Initially, the strain drops to a negative value under the compression loading. Then the strain starts to increase because of thermal expansion of the heated composite sample. As the material softens and fails, the strain decreases. Since the progressive failure analysis is included in the code, the compression strain decreases dramatically at the predicted end of the test. As observed from the

figures, the calculated results accurately predict the initial strain value and capture the features of measured data.

The measured and predicted times-to-failure are organized in Table 2.5 and plotted in Figure 2.11. Black symbols represent the results of the quasi-isotropic samples, while red symbols represent the results of the warp-aligned samples. The maximum relative difference between the measured and predicted failure times in log-log plot is 14.3%, which indicates that the model can predict well the thermo-mechanical behavior of composites heated to the temperature around the glass transition temperature with little decomposition. Also, the consistent results of two types of composite coupon samples indicate that the prediction of the model is good for composites with different stacking sequences.

Table 2.5: Comparison of the measured and predicted failure times for small scale tests conducted at Virginia Tech
Quasi-isotropic samples

Heat Flux (kW/m^2)	Compression Stress (MPa)	Measured Failure Time (s)	Predicted Failure Time (s)
5	53.2	2957	1300
	56.0	1430	1220
	63.6	821	1200
	81.8	490	670
	109.2	360	430
10	8.6	563	470
	15.2	259	400
	30.0	190	345
	43.5	168	305
	120.9	120	160
15	7.9	568	230
	29.7	120	185
	57.8	95	148
	57.8	132	148
	88.1	87	124

Warp-aligned laminates

Test No.	Set point of the front-face temperature (°C)	Compression Stress (MPa)	Measured Failure Time (s)	Predicted Failure Time (s)
1	120, 130, 135[a]	35.9	13206	5100
2	130	33.8	10823	5400
3	130	32.4	3957	2600
4	135	33.1	295	520
5	135	33.1	669	440
6	135	35.9	686	640
7	135	34.5	923	750
8	135	35.2	900	1080
9	135	27.6	3300	1300
10	135	26.2	5012	2800

[a]Test 1: the set point of front-face tempearture is 120 °C at the beginning, stepped up to 130 °C, then 135°C later.
[*]Although the set points of the front-face temperature are the same for tests 2-3 and tests 4-10, the actual measured tempeatures on the back face have some variability.

2.5.2 Thermo-Mechanical Analysis with Decomposition

The model considering decomposition is used to predict the thermo-mechanical behavior of composite sample in the one-sided heating tests conducted by Feih [92]. The material system is composed of Colan E-glass woven fiber and Ashland Derakane 411-350 vinyl ester resin. The samples are nominally 560 mm in gage length, 50 mm in width, 9 mm in thickness with 10 layers of warp-aligned fibers. The mechanical boundary condition is clamped-clamped and a compressive load is applied on one end of the sample. The sample is insulated on the back surface and part of front surface to expose a window region with 100 mm exposed length to the applied heat flux as shown in Figure 2.12.

Thermal properties provided in [92], such as conductivity and specific heat, are used as inputs for the coupled thermo-mechanical analysis in ABAQUS. The permeability value of completely decomposed material is assumed very large so that the

calculated internal pressure inside the solid is always equal to the atmosphere pressure. The thermal boundary condition is similar to Eq. (2.18) except that the radiant heat flux applied on the exposed window region is 25 kW/m^2, 50 kW/m^2, and 75 kW/m^2 to cause significant decomposition in composites. Since the compression and shear moduli of this material system were fitted to hyperbolic tangent functions of temperature only (rather than time and temperature), the constitutive equation with the assumption that the char material cannot hold any stress becomes

$$\sigma_i = FC_{ij}(T)\varepsilon_j^m \tag{2.33}$$

The corresponding incremental form of the constitutive equation is given by

$$\Delta\sigma_i = F_{n+1}C_{ij}(T_{n+1})\Delta\varepsilon_j^m + F_{n+1}\left(C_{ij}(T_{n+1}) - C_{ij}(T_n)\right)\varepsilon_j^m(t_n) + \frac{F_{n+1}-F_n}{F_n}\sigma_i(t_n) \tag{2.34}$$

The Jacobian matrix denoted by DDSDDE in the UMAT is calculated by

$$DDSDDE = \frac{\partial\Delta\sigma_i}{\partial\Delta\varepsilon_j^m} = F_{n+1}C_{ij}(T_{n+1}) \tag{2.35}$$

The simulated mechanical boundary condition is still clamped-clamped as same as the testing condition.

Figure 2.13 shows the measured and calculated temperature time history in [92], as well as the temperature predicted by subroutine UMATHT at the exposed surface, the middle surface, and the unexposed surface. It is found that temperature curves resulting from the UMATHT and the measured data are in good agreement. Both predicted and measured temperatures eventually reach over the decomposition temperature which is around 300 °C, so that the decomposition occurs and takes effect on the mechanical response. Figure 2.14 compares the predicted and measured in-plane elongations for tests with various loading levels from 10% to 60% of compression strength at room

temperature and heat fluxes of 25 kW/m^2 and 50 kW/m^2. The increasing elongations at the beginning are because of the thermal expansion of heated sample. The elongation curves reach the peak and start to decrease at some point when the failure effect becomes dominant over the thermal expansion effect. As shown in Figure 2.15, both measured and calculated out-of-plane deflections indicate that the panel moves towards the heating source (positive value) at the beginning of the test because of the thermal bending and moves away from the heating source (negative value) later till the end of the test. Figure 2.16 organizes the times-to-failure for tests with various loading levels from 10% to 90% of compression strength at the room temperature by the same heat flux. The model over-predicts all the time-to-failure for heat flux of 25 kW/m^2, and over-predicts at high loading levels and under-predicts at low loading levels for other two heat fluxes. However, the model captures the major features of both measured elongations and failure times. The summary of failure time comparison for tests presented in [40, 92, 130], as shown in Figure 2.17, validates the model again for different stacking sequences and different combined thermo-mechanical loadings.

2.6 Conclusion

A three-dimensional coupled thermo-mechanical model for the prediction of material behavior of composites exposed to fire is developed. The model is composed of four governing equations: the heat transfer equation, the decomposition equation, the gas diffusion equation, and the material constitutive equation. A time-temperature dependent compression strength model for the local kinking failure mode is improved by including the decomposition factor into the expression of the composite compression strength. The

model can predict temperature, deflection, time-to-failure over a wide temperature range from temperatures below the glass transition temperature to temperatures above the decomposition temperature. Various types of damage, such as thermal softening, decomposition, pores and compression kinking, are included. The technique of two layers of elements is employed to incorporate the model into the commercial software ABAQUS by the UMAT and UMATHT subroutines for the convenience of engineering application.

The three-dimensional thermal model is reduced to one-dimensional case using simplified assumption for temperature verification with an existing one-dimensional model. Orthotropic viscoelasicity model is used to solve isotropic viscoelasticity problem with degenerate property inputs and the predicted mechanical behavior is compared with the results from ABAQUS built-in isotropic viscoelasticity for verification of the mechanical part of the model. Three sets of one-sided heating tests conducted for samples with different thickness and stack sequences of fiber orientation subjected to different combined thermo-mechanical loading are simulated. The model is validated by comparing the predicted temperature, compression strain, in-plane displacements, and the time-to-failure with the measured data.

2.7 Acknowledgements

The authors would like to acknowledge the financial support of the Office of Naval Research under the Naval International Cooperative Opportunities in Science and Technology Program (N00014-07-1-0514) and through the Small Business Innovation Research Program (N00014-08-C-0591).

2.8 Figures

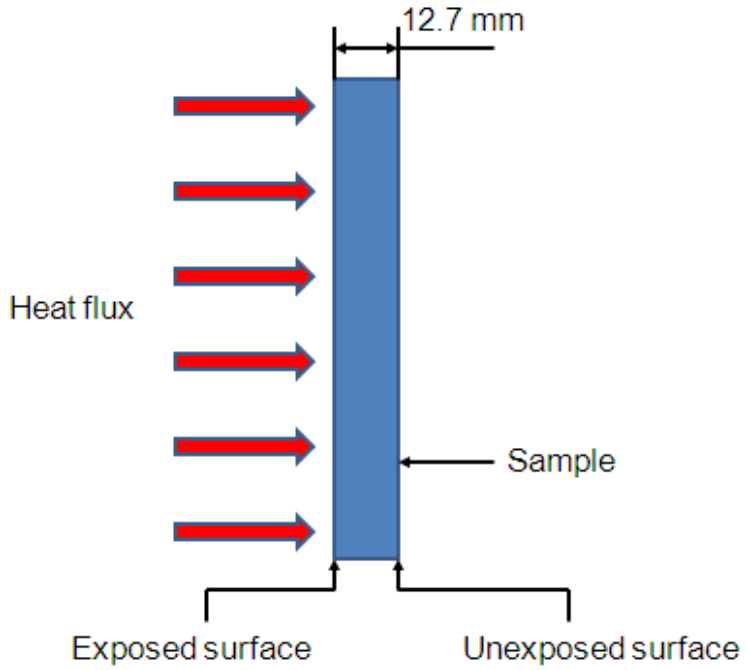

Figure 2.1: Temperature verification study: one-sided heat flux analysis with decomposition

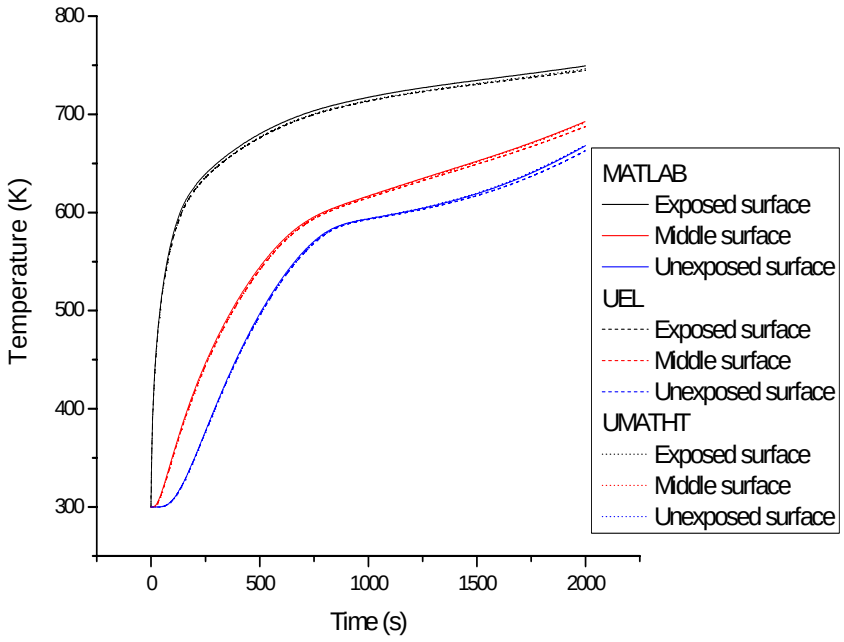

Figure 2.2: Comparison of temperature history curves at the exposed surface, the middle surface, and the unexposed surface for the temperature verification

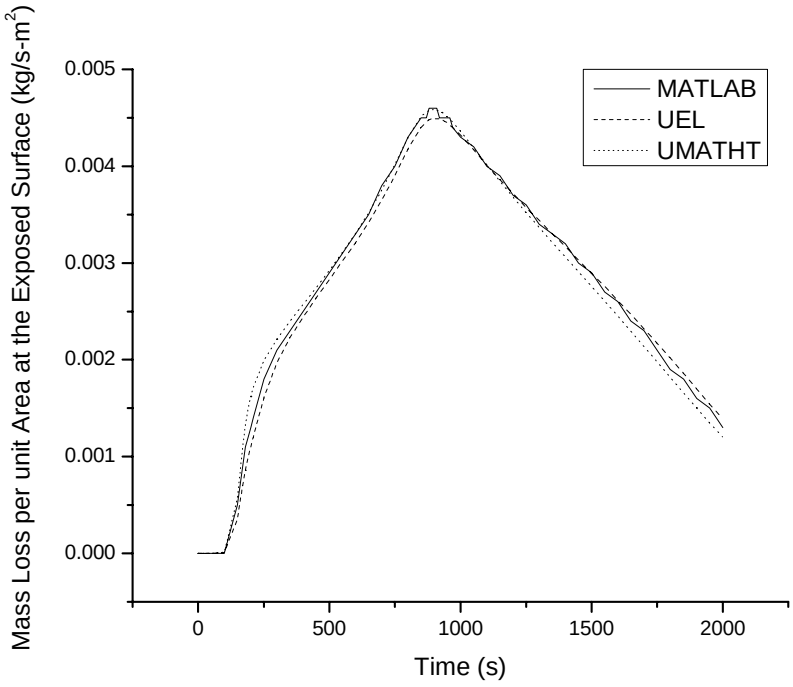

Figure 2.3: Comparison of mass loss at the exposed surface for the verification of thermal model

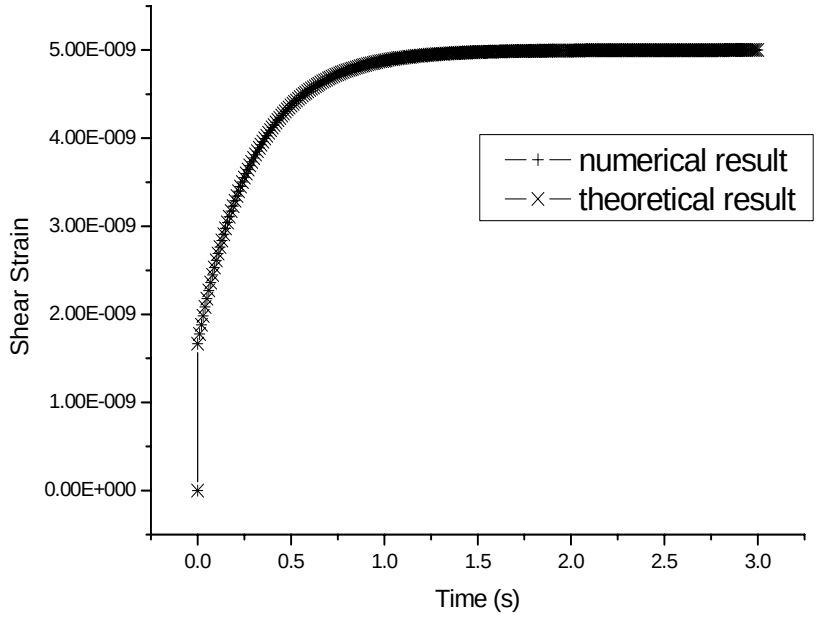

Figure 2.4: Comparison of shear-time curve for three-dimensional isotropic viscoelasticity without temperature effect

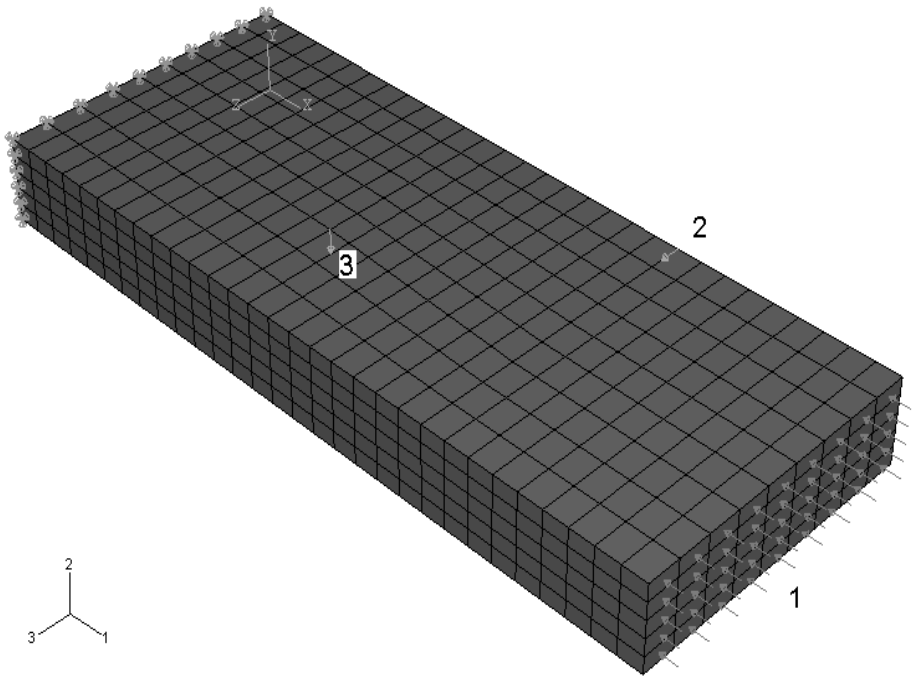

Figure 2.5: Verification problem for three-dimensional isotropic viscoelasticity with temperature effect

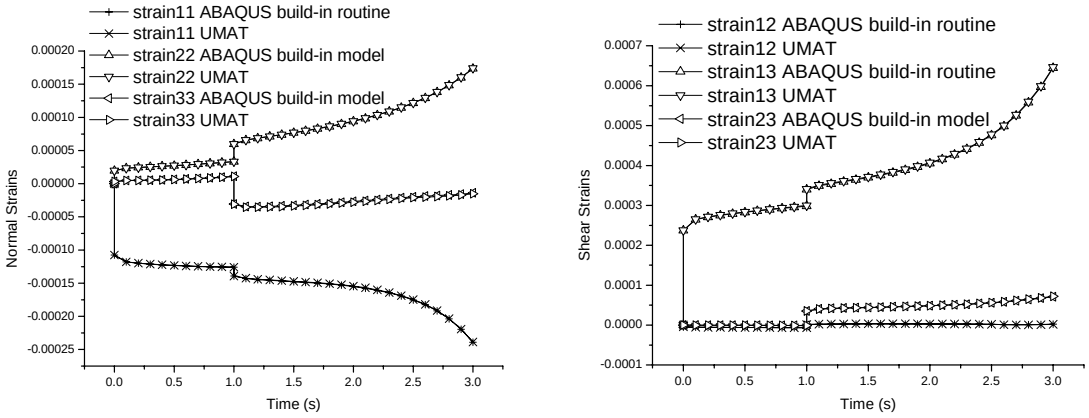

(a) (b)

Figure 2.6: Comparison of (a) normal strains and (b) Shear strains versus time for three-dimensional isotropic viscoelasticity with temperature effect

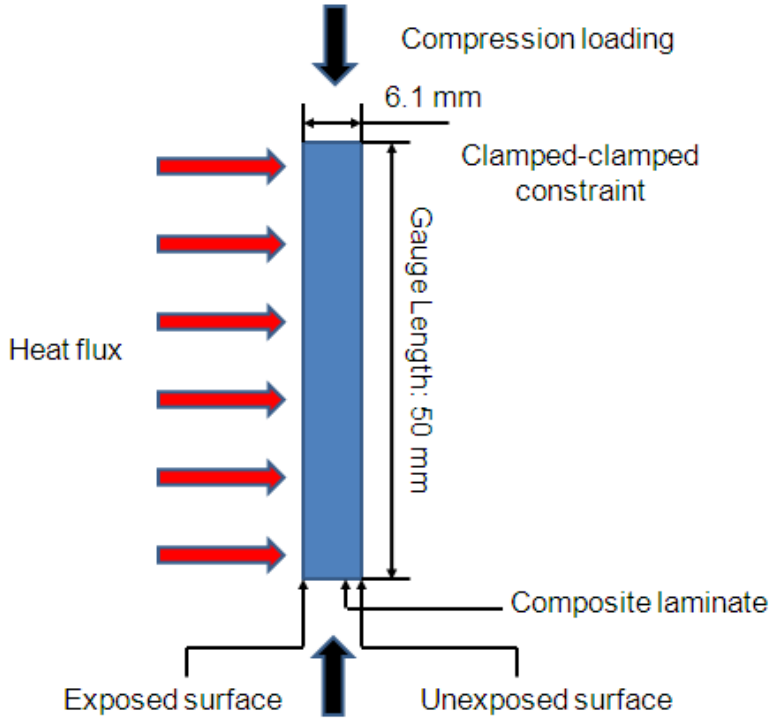

Figure 2.7: The schematic side view of compression creep rupture test conducted at Virginia Tech for coupon composite laminate subject to one-sided heat flux

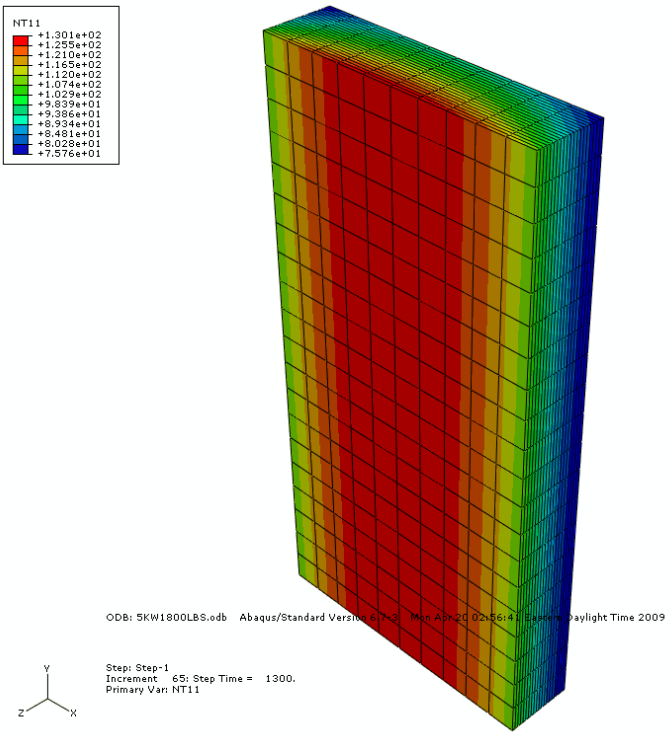

Figure 2.8: Temperature contour of the small scale test with heat flux of 5 kW/m^2 and compression stress of 53.2 MPa

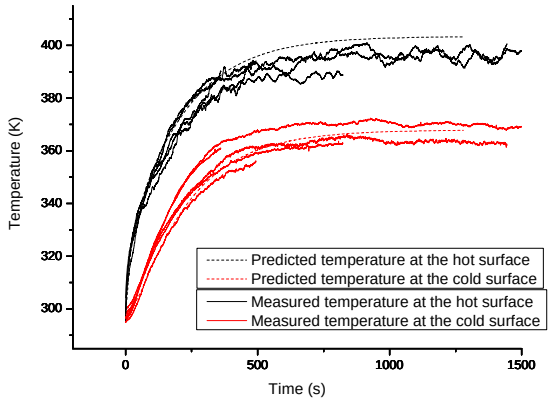

(a)

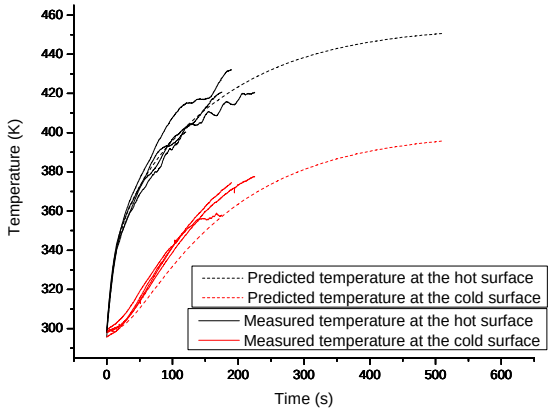

(b)

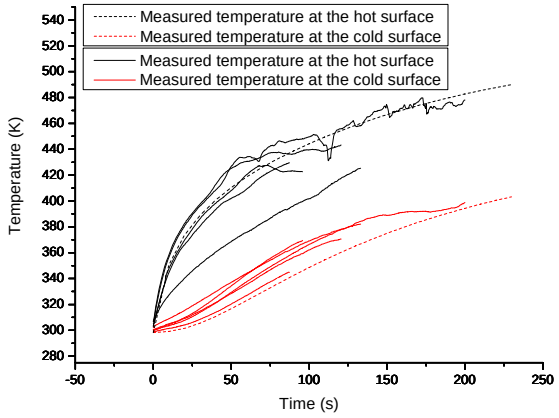

(c)

Figure 2.9: Comparison of temperatures at the hot and cold surfaces for the thermo-mechanical analysis with viscoelasticity of coupon samples subjected to the heat flux of (a) 5 kW/m^2, (b) 10 kW/m^2, and (c) 15 kW/m^2

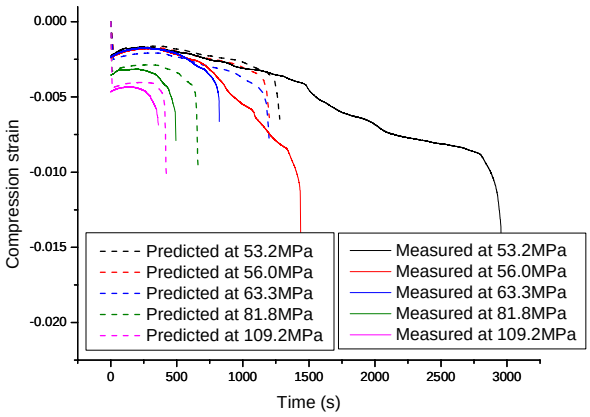

(a)

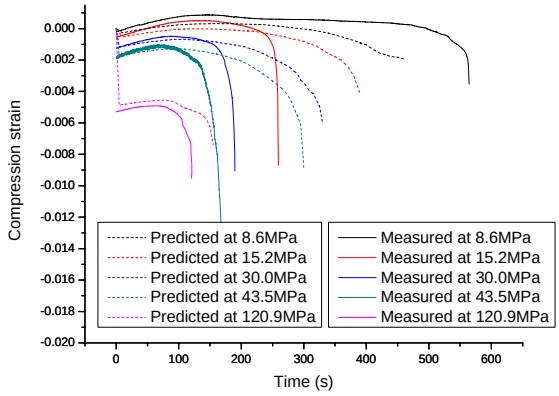

(b)

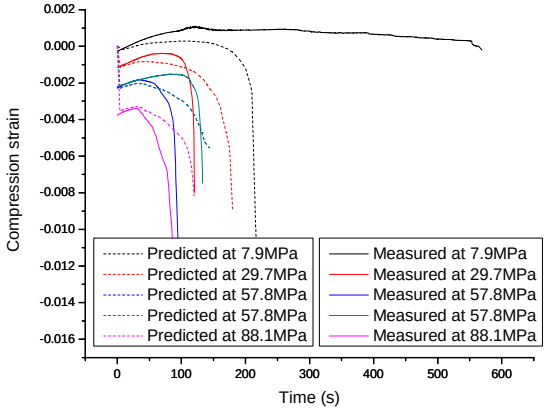

(c)

Figure 2.10: Comparison of compression strain on the cold surface for the thermo-mechanical analysis with viscoelasticy of coupon samples subjected to the heat flux of (a) 5 kW/m^2, (b) 10 kW/m^2, and (c) 15 kW/m^2

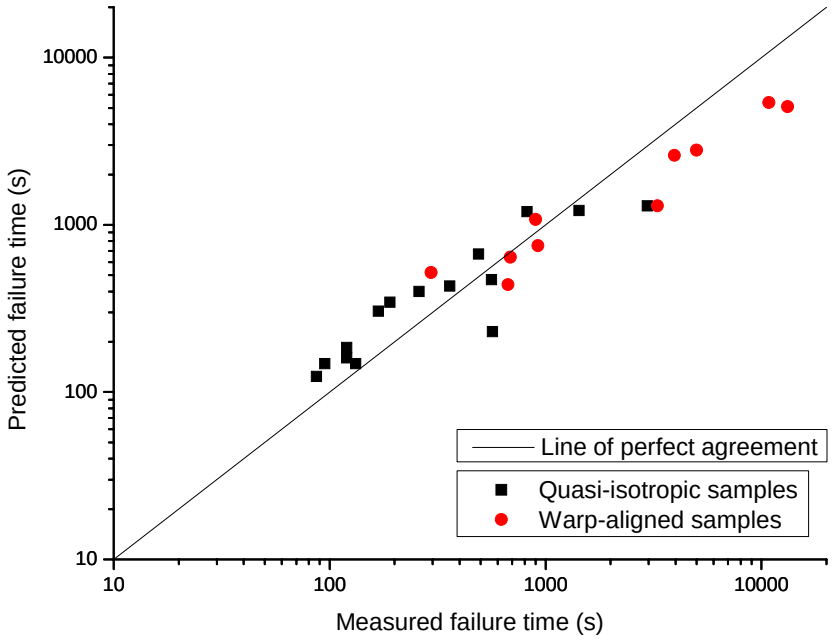

Figure 2.11: Comparison of the measured and predicted failure times for small scale tests with temperature in the vincinity of the glass transition temperature

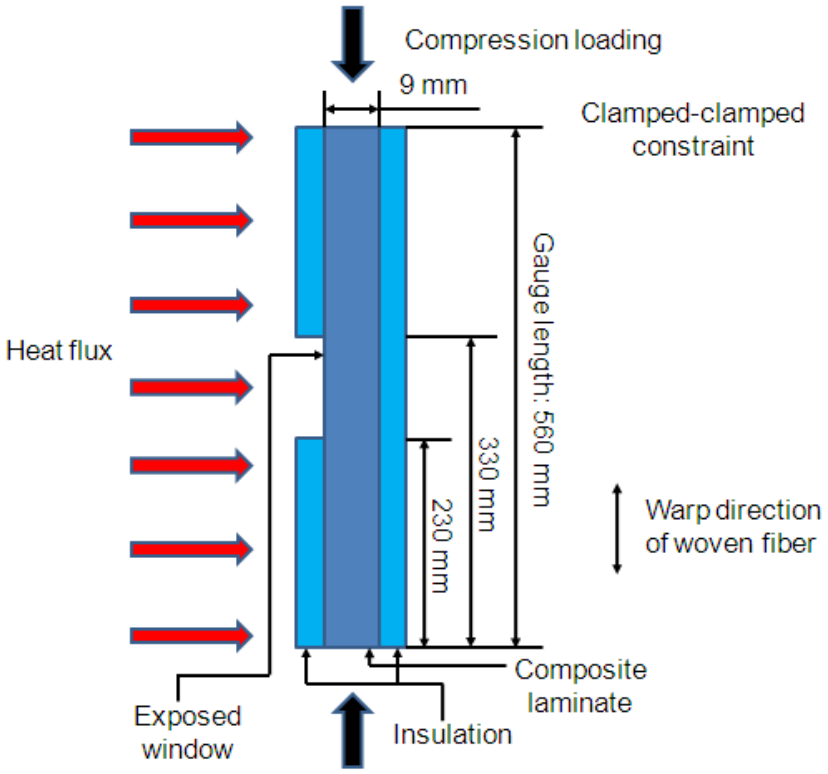

Figure 2.12: The schematic side view of one-sided heating test conducted at RMIT for coupon composite laminate with an exposed window

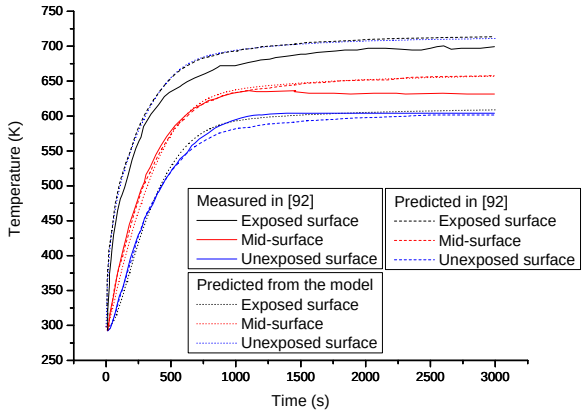

(a)

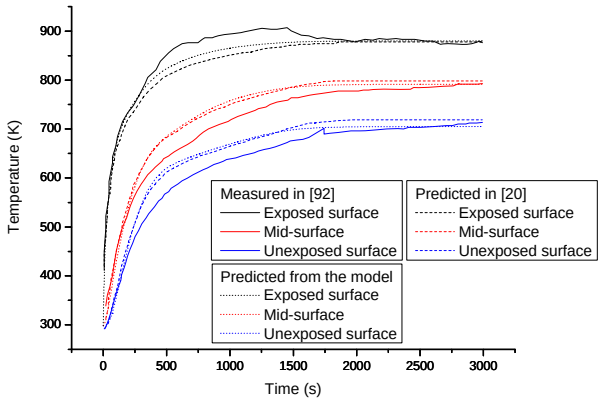

(b)

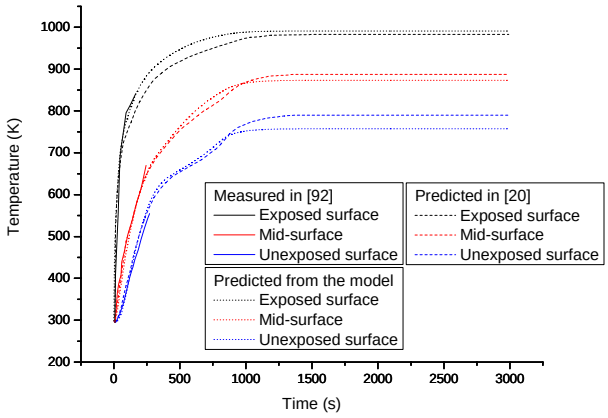

(c)

Figure 2.13: Comparison of temperature history curves for the thermo-mechanical analysis with decomposition of coupon samples subjected to the heat flux of (a) 25 kW/m^2, (b) 50 kW/m^2, and (c) 75 kW/m^2

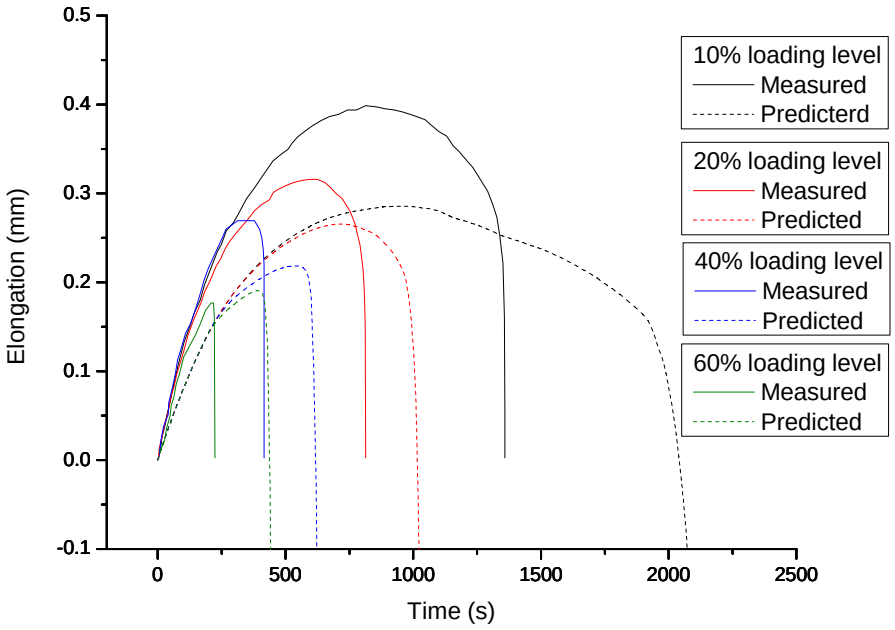

(a)

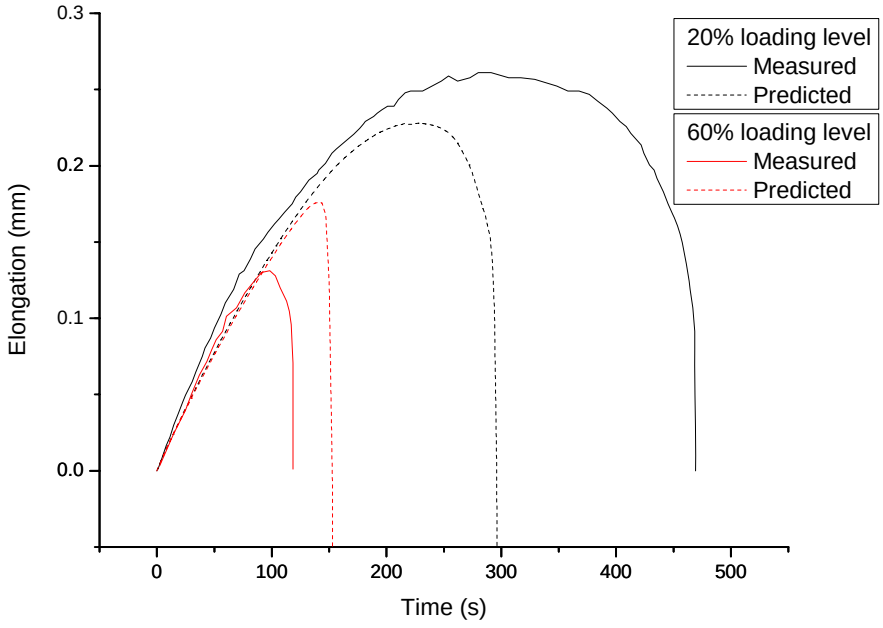

(b)

Figure 2.14: Comparison of elongation for the thermo-mechanical analysis with decomposition of coupon samples subjected to compressive loads at different levels and the heat flux of (a) 25 kW/m^2 and (b) 50 kW/m^2

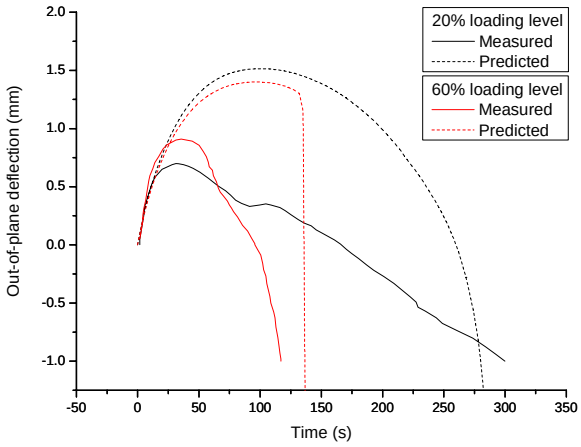

Figure 2.15: Comparison of out-of-plane deflections for the thermo-mechanical analysis with decomposition of coupon samples subjected to compressive loads at different levels and the heat flux of 50 kW/m^2

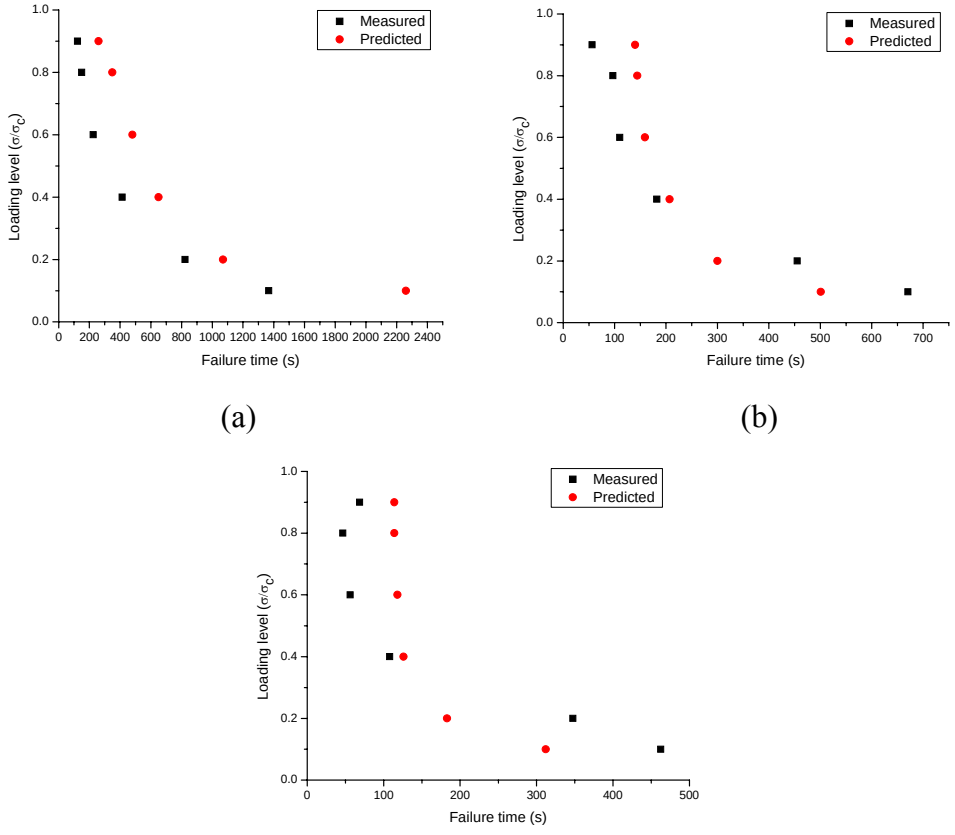

Figure 2.16: Comparison of times-to-failure for the thermo-mechanical analysis with decomposition of coupon samples subjected to compressive loads at different levels and the heat flux of (a) 25 kW/m^2, (b) 50 kW/m^2, and (c) 75 kW/m^2

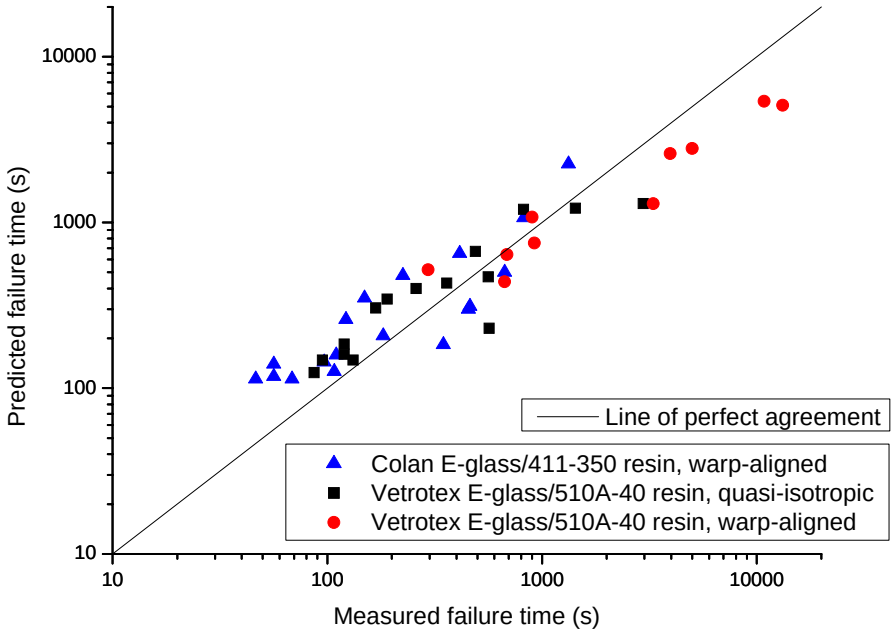

Figure 2.17: Summary of the failure times for all simulated tests at coupon level

Chapter 3: Finite Element Modeling for Thermo-Mechanical Analysis of Polymer Composites at High Temperature

3.1 Abstract

A three-dimensional model including the effect of viscoelasticity and decomposition is developed to predict the thermo-mechanical behavior of polymer matrix composites subjected to the heat and the compressive load. An overlaid element technique is proposed for incorporating the model into commercial finite element software ABAQUS and the technique is employed with the user subroutines for providing practicing engineers a convenient tool to perform analysis and design studies on composite materials subjected to combined fire exposure and mechanical loading. The resulting code is validated by comparing its results with experimentally measured data of the one-sided heating test conducted on the laminate and sandwich samples at intermediate scale. The good agreement indicates the capability of the model to predict structural response of different composite material systems subjected to different combined thermo-mechanical loadings.

Keywords: Thermo-mechanical behavior; Viscoelsaticity; Decomposition; Finite element analysis; Fire

3.2 Introduction

Polymer matrix composites (PMCs) are widely used in contemporary industrial and military areas, such as vehicle body panel in automotive industry, bridge and piping systems in civil infrastructure, and topside structures in marine ships. The advantages of

high specific strength, long fatigue life, excellent corrosion resistance, long-term durability, and the reduction of fabrication costs facilitate the composite application, however, challenging issues, such as the low rigidity, poor impact resistance, and difficulties in joining, are presented with further exploration of PMCs. One of the most critical issues is the thermo-mechanical behavior of PMCs in a high-temperature environment. The thermal softening of composite materials with increasing temperature reduces the structural load capacity and raises the safety risk. The polymer matrix is decomposed with continuous heating and the dense smoke consisting of soot and toxic gases is generated, which threatens the public health, increases the obscurity, impedes the rescue action, and decreases the survivability. The mechanical properties are significantly degraded with further decomposition causing the structural failure eventually. In order to improve the composite fire performance and enhance the reliability of composite application, it is necessary to study and understand the structural response of PMCs subjected to combined thermo-mechanical loadings.

The fire structural process of PMCs is inherently complicated and involves various thermo-chemical and physical phenomena. At the start of the heating, the heat transfer inside the composites is mainly attributed to the thermal conduction. Thermal softening occurs with increasing temperature and viscoelasticity dominates the mechanical behavior of composites at temperatures in the vicinity of the glass transition temperature. Thermal properties, such as conductivity and specific heat, also vary with temperature. When the temperature increases to the decomposition temperature, the chemical reaction is initiated and the polymer matrix begins to decompose. The char material and gases produced by the decomposition hampers the heat transfer because of

the low conductivity. The strength and stiffness of PMCs proceed to decrease with continuous mass loss. Meanwhile, a porous network in the solid is formed and the decomposed gases are held inside the pores initially. The internal pressure built up by the accumulated gases influences the local stress and deformation. Both the number and the size of pores increase with further decomposition and thermal expansion. Connectivity of pores improves the permeability and benefits the gas flow. More and more gases originally trapped inside the pores are forced to flow through the solid by the pressure difference. Since the gases carry the heat, the thermal convection takes effect in the heat transfer. In addition, the heat absorbed or generated by the decomposition reaction and moisture vaporization also influences the temperature distribution of heated composites. Various types of progressive and local failures depending on the combined thermo-mechanical loading, such as kinking, matrix crack, delamination, and debonding between fiber and matrix, have been proceeding in the whole fire process. The material damages reduce the structural integrity and lead to the global failure eventually.

A great deal of research has been conducted to characterize the flammability, thermal, and mechanical properties of composites and perform the heating tests for studying the strength and failure of composites in fire. However, the experimental tests need large expenditure of labor and time. The composite failure in particular tests depends on the sample geometry, material system, boundary condition, heating condition, and loading level. For better design and application of PMCs, various models have been proposed and developed to investigate the thermo-mechanical behavior of composites. Since the thermo-mechanical behavior of PMCs is largely dependent on temperature, accurate thermal analysis is very important. Henderson et al. [71] presented a one-

dimensional transient thermal model considering the heat generated by the decomposition reaction, the heat convection attributed to the gas flow through composites, and the thermal properties dependent on the temperature and decomposition degree. The model was subsequently further developed to include the combined effects of thermo-chemical expansion and storage of the decomposition gases in pores [72], and to examine the effect of the assumption of local thermal equilibrium between the solid matrix and decomposition gases [74]. When the Henderson model is extended to three-dimensional case, it is not easy to determine the direction of gas flow and the permeability has to be considered in the gas convection term increasing computational burden. In order to improve the utility of the Henderson model in finite difference and finite element implementation, Miano and Gibson [75] modified the model by using a simple temperature dependent decomposition model, ignoring the volatile convection in heat transfer equation, and using a thermal diffusivity related to the thermal conductivity, specific heat and density. Looyeh et al. employed a simplified Henderson's model to simulate furnace tests by finite element method [78] and analyzed the behavior of sandwich panels in fire by developing a model accounting for decomposition in skins, transient heat conduction in core, and the effect of thermal contact resistance at interfaces [80]. Dodds, Gibson, and co-workers [76] investigated the thermal response of laminated glass fiber reinforced panels with several different matrix materials by furnace fire testing for the model validation. A three-dimensional heat transfer model was formulated by Milke and Vizzini [79] to examine the thermal response of an anisotropic composite laminate with temperature dependent material properties, arbitrary locations of heat sources and sinks, and a wide variety of realistic boundary conditions. Jowsey [81]

presented a model to determine the heat fluxes imposed on all surfaces of structural members for improving the treatment of the heat input provided by a fire to the structural elements. Xie and Des Jardin [83] examined the heat transfer between fire and solid using a level set based embedded interface method for further analysis of coupled response of composites structures and the local flow environment.

A significant factor dominating the structural response of composites at high temperature is the mechanical stiffness. The degradation of mechanical stiffness of PMCs in the fire process can be divided into two phases based on the temperature range. The first phase is the thermal softening before decomposition, such as viscoelasticity, in which the properties are reduced with increasing temperature and time. The second phase is the decomposition when the polymer matrix is heated to form chars and gases causing the mass loss and material degradation. Case, Lesko and co-workers [39-42] characterized the non-linear thermo-viscoelasticity of glass/vinyl ester composites, proposed a model including a compression strength failure criterion for the prediction of kinking failure, and conducted experiments on the composite laminates subjected to combined compression and one-sided simulated fire exposure for model validation. Zocher et al. [85] endeavored to develop the numerical algorithm based on the finite element method for the efficient three-dimensional thermo-viscoelastic analysis of PMCs. In order to describe the composite material behavior after decomposition, a model assuming that the composite laminate in fire is composed of a virgin layer and a heat-affected layer was proposed and used to estimate the reductions in failure load of composites in [49, 91]. Feih, Gibson, Mouritz, Mathys, and co-workers [92-94, 96] developed a model based on Henderson equations, temperature-dependent strength, and

lamination theory to predict the time-to-failure of polymer laminates loaded in tension or compression and exposed to one-sided radiant heating by fire. The model was applied on sandwich composite materials with combustible glass vinyl ester skins and balsa core for estimating the residual compressive strength and the time-to-failure in [98]. Asaro et al. [99] monitored the collapse of glass vinyl ester laminates and cored sandwich samples at intermediate scale subjected to various levels of heat fluxes and compressive loads. Furthermore, Gu and Asaro [106-107] investigated multiple failure modes for composites under transverse thermal gradients and compressive loads, such as buckling, bending by the shift of the neutral axis, and thermal distortion, and analyzed the thermo-mechanical field from a design perspective. The effects of thermal moment and moment due to eccentric loading on bending deformation of composite columns under axial compressive loads with non-uniform temperature distribution through thickness were discussed by Liu et al. [100] using the beam theory. Looyeh et al. [118] developed a one-dimensional finite element thermo-mechanical model and used the model to analyze an experimental test. Bai et al. [101-103] included temperature dependent stiffness, viscosity, and effective coefficient of thermal expansion into a thermo-mechanical model and employed the model to predict the deflections of cellular glass fiber-reinforced polymer slabs using finite difference method. Considering that the modeling of thermal response is one-dimensional; deflections are calculated based on the beam theory; and the progressive failure of materials is not included, Bai's model lacks the generality to solve a three-dimensional problem with various thermal and mechanical boundary conditions. McManus and Springer [122-123], Dimitrienko [34, 115], Sullivan and Salamon [35, 121] developed the three-dimensional models to analyze the thermo-mechanical behavior

of different carbon fiber and glass fiber composites. These models do not consider viscoelasticity for mechanical properties. There is only comparison of predicted and measured damage depth of delamination for mechanical model validation in [34, 115, 122-123] and the progressive failure is not included in Sullivan's model [35, 121]. Since the models are complex, most of codes for the model implementation are developed by particular person or lab and they are not convenient enough for other practicing engineers to perform analysis.

The study will develop a three-dimensional model to predict the thermo-mechanical behavior of polymer composites over temperature ranges from temperatures below the glass transition temperature to temperatures above the decomposition temperature. The decomposition reaction and the storage of decomposition gases in the solid are considered in the heat transfer equation and the gas diffusion equation. The effects of viscoelasticity and decomposition, as well as the progressive failure, are taken into account in the material constitutive equation. Two major failure modes observed in tests with combined thermal and compression mechanical loading, kinking and bending, are included in the model using a time/temperature dependent compression strength failure criterion and nonlinear geometrical analysis.

In order to provide tools for practicing engineers to perform analysis and design studies, the model is implemented into the commercial finite element software ABAQUS. Since the commercial software has not provided a particular element for PMCs with degrees of freedom of temperature, pressure, and displacements to implement the three-dimensional thermo-mechanical model, an overlaid element technique and a strategy of solution procedure are explored with UMAT and UMATHT subroutines to include the

governing equations and failure criterion into the analysis. The numerical method provides a framework for the convenient implementation of more complicated models, such as models considering multi-phase decomposition and multi-stage softening of mechanical properties. The model and the code are verified and validated by comparing the calculated results with other numerical results and experimentally measured data of the one-sided heating test for composites. The parameters for comparison are not only the temperature and failure times, but also the in-plane and out-of-plane deflections at the specific locations for accurate model validation. Tests conducted on different material systems with various combined thermo-mechanical loadings are simulated to validate the generality of the model.

3.3 Finite Element Modeling

There are four governing equations in the model: the heat transfer equation Eq. (2.1), the decomposition equation Eq. (2.2), the gas diffusion equation Eq. (2.3), and the material constitutive equation Eq. (2.4). The first three equations based on the Henderson's model [72] are extended to three-dimension and used to calculate thermal variables, such as temperature, decomposition factor, and internal pressure, while the last equation is used to analyze the mechanical response of composites, such as stress, strain, and deflections. It is assumed that the composite materials after decomposition consist of materials in two statuses: virgin and char. The stress is correspondingly divided into two parts: contribution from virgin material and char material. Both parts are combined together by the decomposition factor F using the linear mix rule. Since the stiffness of char material is assumed to be very small, the stress contribution from the char material

can be neglected and the constitutive equation is reduced to Eq. (3.1). When the temperature is below the decomposition temperature, the decomposition factor is one and the stress is determined by the viscoelatic properties of virgin material. When material is completely decomposed, the decomposition factor is zero and the material cannot bear any stress.

$$\sigma_i(\xi) = F\int_0^{\xi} C_{ij}^{v}(\xi-\xi')\frac{\partial \varepsilon_j^{m}(\xi')}{\partial \xi'}d\xi' \tag{3.1}$$

The time-temperature dependent compression strength model developed in [40-41] is further advanced to include the decomposition influence on strength, given by Eq. (2.9). The strength model considers the mechanism of the kinking failure as the local shear yielding because of the natural fiber misalignment.

The model is implemented into commercial finite element software ABAQUS for providing practical tools to engineers. Since the model is complicated, there is no built-in model or element for direct implementation. A technique of overlaid elements is developed to compensate the disadvantage of lack of element having temperature, pressure, and displacements together as degrees of freedom. There are two user subroutines provided by ABAQUS for more flexible and wider engineering application: UMAT and UMATHT. UMAT is used to define the material constitutive equation and UMATHT is used to define the heat transfer equation. Since the gas diffusion equation is the same class of partial differential equation as heat transfer equation, it can also be defined in UMATHT. However, only one UMATHT user subroutine can be assigned to one layer of elements. In order to implement the model into ABAQUS, two overlaid layers of elements are employed as shown in Figure 3.1. One UMATHT subroutine and the UMAT subroutine are applied to the first layer of elements to define the heat transfer

and constitutive equations. The decomposition equation is solved in the first layer UMATHT using finite difference method. Another UMATHT subroutine is applied to the second overlaid layer to solve the gas diffusion equation. The mechanical response of the second layer is described as simple elasticity and the stiffness is set to be very small compared to the actual material stiffness assigned to the first layer. The displacement degrees of freedom for two overlaid elements are tied together. Since the stiffness of the second layer can be neglected, the constitutive equation of the first layer determines the mechanical behavior of the overlaid elements. In practice, the four equations are not solved simultaneously in each time increment. The constitutive equation is solved first to determine the deformation and stress distribution based on the material status at the end of last time increment. Then the heat transfer equation and decomposition equation are solved in the first layer UMATHT. The temperature and the decomposition factor are transferred to the second layer UMATHT for calculating the gas diffusion equation. The gas pressure obtained in the second layer UMATHT is stored in common blocks of Fortran code for calling of the first layer subroutines at next step.

3.4 Model Validation for Intermediate Scale One-sided Heating Tests

3.4.1 One-sided Heating Tests Conducted on Intermediate Scale Laminate Composites Subjected to Compression Loading

The one-sided heating tests conducted by Summers [134] are simulated using the developed model and the calculated results are compared with the measured data for model validation. The composite sample is clamped on the top and bottom ends and the compressive load is applied on the top of sample. After the load is ramped to a constant

value, a controlled heat flux is applied on the exposed surface of the sample during the test. Since both stiffness and strength are reduced with the increasing temperature, the failure occurs at some point when the material cannot bear the applied force. It is observed that there are two failure modes in these tests depending on the particular heat flux and stress: kinking and forced-response deflection.

The tested sample is 863.6 mm in length, 203.2 mm in width, and 9 mm (15 plies of fiber) or 12 mm (20 plies of fiber) in thickness. The compressive load varies from 10% to 75% of buckling load at room temperature and the applied heat flux varies from 8 kW/m^2 to 38 kW/m^2. The temperature at different locations through the thickness and the length, the heat flux on the exposed surface, the in-plane deflection on the top surface where the compressive load is applied, and the out-of-plane deflections through the length on the unexposed surface are measured. Figure 3.2 shows the measurement locations of heat flux on the exposed surface, out-of-plane deflection on the unexposed surface, and temperature on the unexposed surface. It is found that the applied heat flux is not uniform across the exposed surface. The exposed surface is divided into several sub-regions in simulation corresponding to the locations of heat flux gages in experiment and the uniform heat flux is applied on each sub-region for an accurate simulated thermal condition. If the material surface is assumed to behaves as a gray body and the absorptivity is assumed to be same as the emissivity, the measured heat flux is given by

$$q''_{measured} = \left(\varepsilon_s q''_{rad} - \varepsilon_s \sigma T_{hfg}^4\right) + h_{conv}\left(T_\infty - T_{hfg}\right) \tag{3.2}$$

where q''_{rad} is the radiant heat flux, ε_s is the emissivity of the front surface, σ is the Stefan-Boltzman constant, h_{conv} is the convection heat flux coefficient, T_{hfg} is the

temperature of the heat flux gage, and T_∞ is the environmental temperature. The actual heat flux absorbed by the sample on the front surface is given by

$$q'' = \left(\varepsilon_s q''_{rad} - \varepsilon_s \sigma T_s^4\right) + h_{conv}\left(T_\infty - T_s\right) \tag{3.3}$$

where T_s is the temperature on the front surface. Eq. (3.3) can be recast for the expression of actual heat flux in terms of the measured heat flux.

$$q'' = q''_{measured} + \varepsilon_s \sigma\left(T_{hfg}^4 - T_s^4\right) + h_{conv}\left(T_{hfg} - T_s\right) \tag{3.4}$$

The thermal boundary condition on the back surface has the same form as Eq. (3.4) and the measured heat flux is set to be zero. Regarding to the simulation of the clamped-clamped mechanical boundary condition, constraints to compel all nodes on the top loading surface to have the same displacement in the loading direction and to fix displacements on the other two directions are applied on the loading end of the sample, while constraints to fix all displacement degrees of freedom are applied on the other end.

The composite material system is Colan A105 E-glass woven fiber and Derakane 411-350 vinyl ester resin. The panels were manufactured via VARTM with warp-aligned fibers and post-cured at 80°C for two hours to assure the consistent material properties as the sample in [92, 135]. The stiffness of the sample is fitted as a tanh function of temperature, given by

$$P(T) = \left(\frac{P_0 + P_R}{2} - \frac{P_0 - P_R}{2}\tanh(k(T - T'_g))\right) \tag{3.5}$$

where P_0 and P_R are the initial and residual stiffness respectively, T'_g is the glass transition temperature, and k is a fitting parameter. The expression is modified by incorporating the decomposition factor as a multiplier to extend the applicable range for materials at high temperature above the decomposition temperature.

$$P(T) = F(T)\left(\frac{P_0 + P_R}{2} - \frac{P_0 - P_R}{2}\tanh(k(T - T'_g))\right) \tag{3.6}$$

The mechanical properties, such as Young's modulus in warp direction E_1 and in-plane shear modulus G_{12}, are collected from [135] as inputs to model. The thermal properties, such as thermal conductivity, specific heat, and decomposition parameters, are collected from [24-25, 134]. Both mechanical and thermal properties of the composite material system are organized in Table 3.1.

Table 3.1: Thermal and mechanical properties of composites consisting of Colan A105 E-glass woven fiber and Derakane 411-350 vinyl ester resin

Property	Value or function
Virgin density $\rho_0=m_0/V$ (kg/m^3)	1683
Final density $\rho_f=m_f/V$ (kg/m^3)	1235
Virgin specific heat C_v (J/kg-K)	$-523.96 + 5.9114T - 4.666\times10^{-3}T^2$
Final specific heat C_f (J/kg-K)	$2.8065\times10^4 - 64.679T + 3.8502\times10^{-2}T^2$
Gas specific heat C_g (J/kg-K)	$-105.08 + 4.38421T - 1.76612\times10^{-3}T^2$
Virgin thermal conductivity k_v (W/m-K)	$0.3889 - 2.592\times10^{-4}T$
Final thermal conductivity k_f (W/m-K)	$0.017641 + 2.830\times10^{-4}T$
Heat of decomposition Q (J/kg)	-8.7×10^{-5}
Pre-exponential factor A (s^{-1})	10×10^{14}
Activation energy E (J/mol)	2.165×10^5
Order of reaction n	0.9
Young's modulus in warp direction E_1 (GPa)	$\frac{26.8+18.2}{2} - \frac{26.8-18.2}{2}\tanh(0.0266(T-361.8))$
In-plane shear modulus G_{12} (GPa)	$\frac{5.041+0.156}{2} - \frac{5.041-0.156}{2}\tanh(0.035(T-356))$
In-plane thermal expansion coefficient (10^{-6}/K)	$-0.0094T + 11.024,\ T \le 627.5$ K $-0.0404T + 22.013,\ 627.5$ K$< T \le 694.1$ K $5.0,\ T > 694.1$ K
Out-of-plane thermal expansion coefficient (10^{-6}/K)	$34.5,\ T \le 374.4$ K $44 + 74\tanh(0.015(T-110)),\ 374.4$ K$< T \le 627.5$ K $-1.6952T + 718.85,\ 627.5$ K$< T \le 694.1$ K $5.0,\ T > 694.1$ K

Since the observed failure modes in the test are kinking and forced-response bending, the time-temperature dependent compression strength model Eq. (2.9) is used to calculate the compression strength and determine if the material points fail. Considering the fiber layers of the sample are all warp-aligned in the loading direction, the failure condition at each integration point is defined as

$$\sigma_c < |\sigma_1| \tag{3.7}$$

where σ_c is the calculated compression strength and σ_1 is stress in the fiber warp direction. Once the failure condition is satisfied, the Young's modulus in warp direction E_1 at the point is decreased to 10% of the value before failure. The time-to-failure of the test is determined by the time when the out-of-plane deflection of sample increases suddenly to a large value, reflecting that the sample no longer has capacity to resist the compression load.

Figure 3.3 shows the contour of the heat flux absorbed by the sample at 120 seconds after heating for one of the tests in which the sample is 12 mm thick, the measured heat flux is 38 kW/m^2, and the compressive load is 6.3 kN (10% of buckling load). Only one half geometry of the sample is modelled because of the symmetry and there are two overlaid elements. The temperature degree of freedom for the second layer is interpreted as pressure. Thus, only the contour of the first layer elements represents the distribution of the heat flux. The maximum of the heat flux is at the centre and the heat flux decreases with the distance away from the centre, which is consistent to the experimental condition. The heat flux absorbed by the sample is smaller than the measured heat flux because of the heat convection and reradiation. The rise of temperature on the front surface enlarges the convection and the reradiation, as well as

the difference between the absorbed and measured heat flux. Figure 3.4 compares the measured and predicted temperature through the length on the unexposed surface. The good agreement confirms that the effect of nonuniform thermal boundary condition is taken account into the simulation. Figure 3.5 and Figure 3.6 compare the temperature at the exposed surface, the unexposed surface, and one third of thickness from the unexposed surface for tests with different nominal levels of heat fluxes applied on the sample of 9 mm and 12 mm thickness. There is little decomposition for the tests with the heat flux below 19.3 kW/m^2, because the temperature is not high enough to cause the decomposition reaction. There is apparent decomposition for the tests with the heat flux of 38 kW/m^2. For example, there is only 8% mass left at the hottest point on the front surface after 150 seconds. It is found that the calculated temperature from the model can match the measured data very well for all tests with and without decomposition. In addition, the model is applicable for samples with different thickness.

Figure 3.7 compares the predicted and measured results of the out-of-plane deflections on different locations through the length on the back surface and the in-plane deflections at the loading end for one test. The positive value in Figure 3.7(a) represents the out-of-plane deflection towards the heating source and the negative value represents the movement away from the heating source. In this test, the out-of-plane deformation is toward the heater at the beginning and turns to the other direction after some point. The eventual failure direction is away from the heater. The finite element analysis predicts the same trend as observed in the test. Both the predicted and measured data indicate that the maximum out-of-plane deflection is located at the centre and the minimum is at the edge. Because the applied heat flux is highest at the centre and the mechanical boundary

condition is symmetrically clamped-clamped. The positive value in Figure 3.7(b) indicates the in-plane compression and the negative value indicates the expansion of the sample. The sample is expanded first after it is exposed to the heating source and the expansion continues till the compressive collapse. The predicted in-plane deflection matches the measured data very well till the failure time when the calculated deformation turns to the compressive direction and increases too faster to cause the convergence issue.

Predicted and measured deflections for all tests with samples of 12 mm thickness subjected to the same heat flux of 38 kW/m^2 and the compressive load at different levels are compared as shown in Figure 3.8. It is found that the failure direction of out-of-plane deflection is from moving towards the heater to moving away from the heater with the decreasing loading level. Since the thermal expansion on the exposed surface is larger than the thermal expansion on the unexposed surface because of the higher temperature, the generated thermal moment forces the panel to deform towards the heater. So both predicted and measured out-of-plane deflections indicate that the panel deforms towards the heater at the beginning of the test. As the heating proceeds, the degradation of polymer composite materials attributed to the thermal softening and decomposition occurs. The reduction of mechanical properties on the exposed surface is faster than the reduction on the unexposed surface causing the neutral axis of the panel to move away from the heater and producing the eccentric moment driving the panel to deform away from the heater. The final failure direction of out-of-plane deflection depends on the balance between the thermal moment and the eccentric moment. The predicted out-of-plane deflection from the model can capture the trend of failure direction with respect to the varying loading level and the predicted range of loading level corresponding to the

switch of the failure direction is between 25% and 50% of buckling load which is consistent to the measured data.

However, there is discrepancy between the predicted and measured deflections and the predicted loading level to switch the failure direction is not always the same as the measured data. Figure 3.9 shows the deflection comparison for the samples of 9 mm thickness subjected to the heat flux of 38 kW/m^2 and compressive load at different levels. In this set of tests, the measured loading level to switch the failure direction is between 25% and 50% of buckling load, which is higher than the predicted loading level between 15% and 25% of buckling load. The peak of predicted out-of-plane deflection for the test with load of 15% buckling load is much delayed compared to the peak of measured deflection. Since the test is a complicated fire structural process, there are several factors leading to the result discrepancy, such as the difference between the ideal simulated test conditions and the actual experimental conditions. In addition, the stiffness inputs to the model are considered as being dependent on only temperature and there is no viscoelasticity included. The lack of time effect for mechanical properties is another possible reason for the discrepancy between the predicted and measured out-of-plane deflections. The predicted in-plane deflections match the measured data well for most of tests. Figure 3.10 and Table 3.2 organize the failure time for all tests. It is found that the composites subjected to lower heat flux and compressive load have longer failure time. The model can generate a good prediction of failure time for composites with different thicknesses and tests with different combined thermo-mechanical loadings.

Table 3.2: Comparison of the measured and predicted failure times for intermediate scale tests conducted on lamiante composites
Samples of 9 mm thickness

Heat Flux (kW/m^2)	Compressive load (% of buckling load)	Measured Failure Time (s)	Predicted Failure Time (s)
38.0	75	36	26
	50	82	57
	25	222	162
	15	312	372
19.3	75	95	66
	50	137	120
	25	695	360
8.0	75	273	288
	50	546	516
	25	>3600	>3600

Samples of 12 mm thickness

Heat Flux (kW/m^2)	Compressive load (% of buckling load)	Measured Failure Time (s)	Predicted Failure Time (s)
38.0	50	48	60
	25	197	168
	15	232	306
	10	531	306
19.3	50	132	108
	25	306	288
	15	891	1428
11.8	50	256	228
	25	334	480
	15	>3600	>3600
8.0	50	316	348
	35	741	516
	25	1975	1060

3.4.2 One-sided Heating Tests Conducted on Intermediate Scale Sandwich Composites Subjected to Compression Loading

One-sided heating tests conducted on sandwich composites by Asoro, Lattimer, and Ramroth [99] are simulated for further validation of the developed three-dimensional

thermo-mechanical model. The sample is the sandwich composites consisting of the balsa wood core and the laminate facesheets on each side with fiber orientation sequence [0/45/90/-45/0]. The material system of the laminate is Derakane 510A vinyl ester resin and plain woven E-glass fiber. The sandwich panel is 910 mm in length, 710 mm in width, 18 mm in thickness, and insulated with a 25 mm thick Superwool 607 blanket. Two types of fire scenario, ISO 834 and UL 1709, and compressive loads at different levels were applied on the sample. Temperatures at six different locations through thickness and out-of-plane displacements at three locations on the unexposed surface were measured during each test as shown in Figure 3.11. The thermal boundary condition on the exposed surface in the simulation is given by

$$q'' = \varepsilon_s \sigma \left(T_f^4 - T_s^4 \right) + h_{conv} \left(T_f - T_s \right) \tag{3.8}$$

where the emissivity of the exposed surface $\varepsilon_s = 0.9$, σ is the Stefan-Boltzman constant, the convection heat flux coefficient $h_{conv} = 0.025$ kW/m^2-K for ISO 834 and $h_{conv} = 0.040$ kW/m^2-K for UL 1709, T_s is the temperature on the exposed surface, and T_f is the furnace temperature corresponding to the particular fire scenario as listed in Table 3.3. Mechanical and thermal properties of wood and laminates are collected from [24, 104, 131] and viscoelasticity is included in the property inputs to the analysis. Considering the fiber stack sequence of the laminate facesheets is quasi-isotropic, the failure condition is modified as

$$\sigma_c < \max(|\sigma_1|, |\sigma_2|) \tag{3.9}$$

where σ_c is the calculated compression strength, σ_1 is stress in the fiber warp direction, and σ_2 is stress in the fiber weft direction.

Table 3.3: Furnace temperature for intermediate scale tests conducted on sandwich composites

Fire scenario	Furnace temperature T_f(K)
ISO 834	$1140t + 293,\ 0 \le t \le 0.5$ min $863,\ 0.5 \le t \le 6.0$ min $345\log(8t+1) + 293,\ t > 6.0$ min
UL 1709	$5300t + 293,\ 0 \le t \le 0.1$ min $110.816t + 811.918,\ 0.1 \le t \le 5.0$ min $1366,\ t > 5.0$ min

Figure 3.12 and Figure 3.13 compare the predicted and measured temperatures at six different locations through thickness and out-of-plane deflections at three different locations on the unexposed surface for sandwich samples subjected to two different thermo-mechanical loadings. In both tests, the predicted temperatures match the measured temperatures well on the exposed surface, the interface between insulation and sample, and the back laminate. The temperature discrepancy in the wood is possibly resulted from the difference between the thermal property inputs of pure dried wood and the actual thermal properties of sandwich core consisting of wood and resin filling the pores in the wood. There is very good agreement for predicted and measured out-of-plane deflections by comparison. The positive value in Figure 3.12(b) and Figure 3.13(b) indicates the out-of-plane deflection towards the heater and the negative value represents the deformation in the other direction. As shown in Figure 3.12(b), the sample deforms towards the heating source at the beginning of the test and moves back after the failure occurs on the front laminate facesheet of sandwich at around 500 seconds. The deflection continues to move away from the heater as more and more elements of the front laminate fail. The back laminate starts to fail at around 1500 seconds causing the sample to deform towards the heater again. The eventual failure direction is away from the heater when a

large number of elements fail. The predicted time-to-failure of the sandwich sample is defined as the time when the panel can no longer resist the applied load. The failure times of four sandwich tests are summarized with the failure times of tests on laminate sample in Figure 3.14. Results for different sets of tests fall into the same curve validating the finite element model is applicable to different material systems, samples with different sizes, and tests with different thermo-mechanical loadings.

3.5 Parameter Study

Since there is a large amount of parameters for inputs to the model and finite element analysis, it is necessary to investigate the influence of parameter variability on the thermo-mechanical behavior of composites in fire. The Young's modulus in the warp direction of the woven fiber is a significant factor to the mechanical behavior of composites. Two different property inputs of Young's modulus with varying the residual modulus E_R and the glass transition temperature T_g' in the temperature dependent expression Eq. (3.5) are examined, as shown in Figure 3.15. The fitting function of the measured data is used as the baseline in Case 1; the residual modulus is reduced by 25% in Case 2; and the glass transition temperature is shifted by 20 K higher in Case 3. Three intermediate scale tests on laminate composites subjected to the compressive load of 25% of buckling load and heat flux of 8 kW/m^2, 19.3 kW/m^2, and 38 kW/m^2 are simulated with different inputs of Young's modulus and the calculated out-of-plane and in-plane deflections are compared in Figure 3.16. The decrease of residual stiffness shortens the failure time, while the increase of glass transition temperature elongates the sample life. The mechanical response of composites exposed to lower heat flux is more sensitive to

the variability of stiffness than the composites at higher temperature. Because more decomposition occurs and the stiffness of virgin material has less influence on the deformation of composites when the temperature is higher. The failure direction of out-of-plane deflection can be switched with further decrease of residual stiffness for some intermediate scale tests as shown in Figure 3.17. The comparison indicates that the accurate measurement and inputs of composite stiffness before the decomposition are significant to a good prediction of the model, especially for the tests at lower temperature.

The variability of thermal properties, such as thermal conductivity and specific heat of the virgin material, is also examined by reducing 25% of the original inputs fitted from the measured data. Figure 3.18(a) compares the calculated temperature through the thickness for tests on laminate composites subjected to compressive load of 25% of buckling load and heat flux of 19 kW/m^2 with different inputs of thermal properties. The change of thermal properties has stronger influence on the temperature at the unexposed surface than at the exposed surface for the same thermal boundary condition. The 25% reduction of thermal conductivity increases the temperature gradient through the thickness and elongates the failure time by 12.5% subsequently, while the 25% reduction of specific heat decreases the temperature gradient and shortens the failure time by 25% as shown in Figure 3.18(b) and Figure 3.18(c). The reasonable inputs of thermal properties are also the required condition to the accurate prediction of thermo-mechanical response of composites at high temperature.

3.6 Conclusion

A three-dimensional model for the analysis of thermo-mechanical behavior of PMCs at high temperature is developed. The model captures the major chemical and physical phenomena during the fire process of PMCs, such as thermal conduction, thermal convection because of the gas flow, decomposition, thermal softening, material degradation, and kinking failure. The overlaid element technique and the strategy for solution procedure of governing equations are explored with user subroutines of ABAQUS for implementing the model into the commercial finite element software and providing the practicing engineers a convenient tool to perform design and analysis. The tool is employed to simulate the one-sided heating tests conducted on intermediate scale laminate and sandwich composites and to predict the thermo-mechanical response of composites subjected to different heating conditions and compressive load at different levels. The calculated results are compared to the experimental data, such as temperatures through the thickness, in-plane deflections, out-of-plane deflections along the length on the unexposed surface, and the failure times. In addition, the failure direction of out-of-plane deflections is discussed. The eventual failure direction is from moving towards the heater to moving away from the heater with the decreasing loading level for the same heating condition. Although an accurate property inputs is needed to improve the predicted results for some tests, the good agreement between the predicted and measured results for most of tests, especially the good match of the failure time, validates that the model can be applied to different material systems with different thermo-mechanical loadings.

3.7 Acknowledgements

The authors would like to acknowledge the financial support of the Office of Naval Research under the Naval International Cooperative Opportunities in Science and Technology Program (N00014-07-1-0514) and through the Small Business Innovation Research Program (N00014-08-C-0591).

3.8 Figures

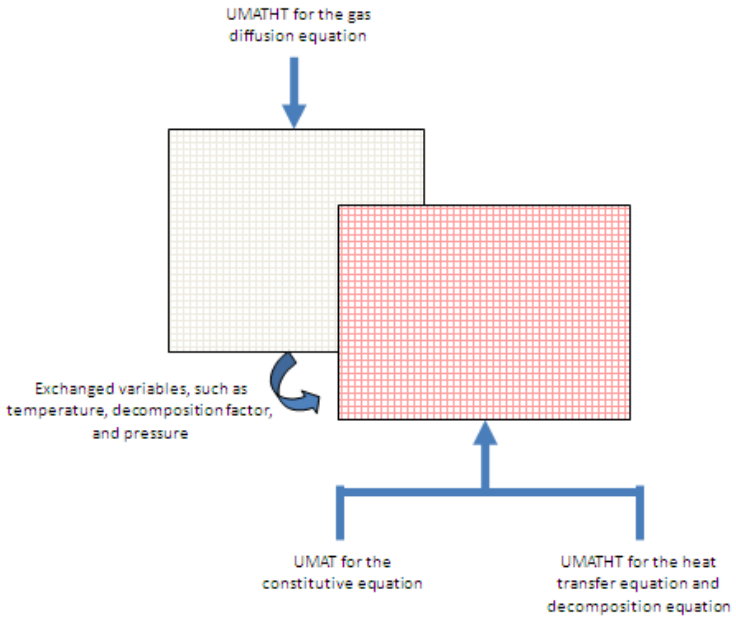

Figure 3.1: Schematic for the technique of two overlaid layers of elements

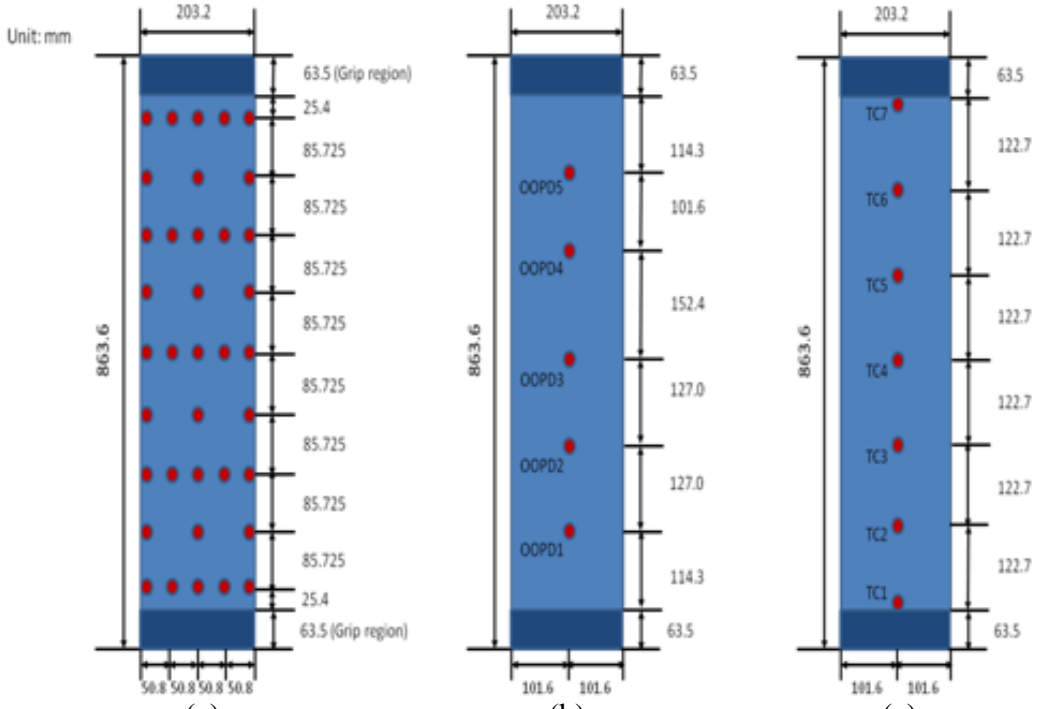

(a) (b) (c)

Figure 3.2: The sensor locations of (a) measured heat flux on the exposed surface, (b) out-of-plane deflection on the unexposed surface, and (c) temperature on the unexposed surface for intermediate scale tests conducted on laminate composites

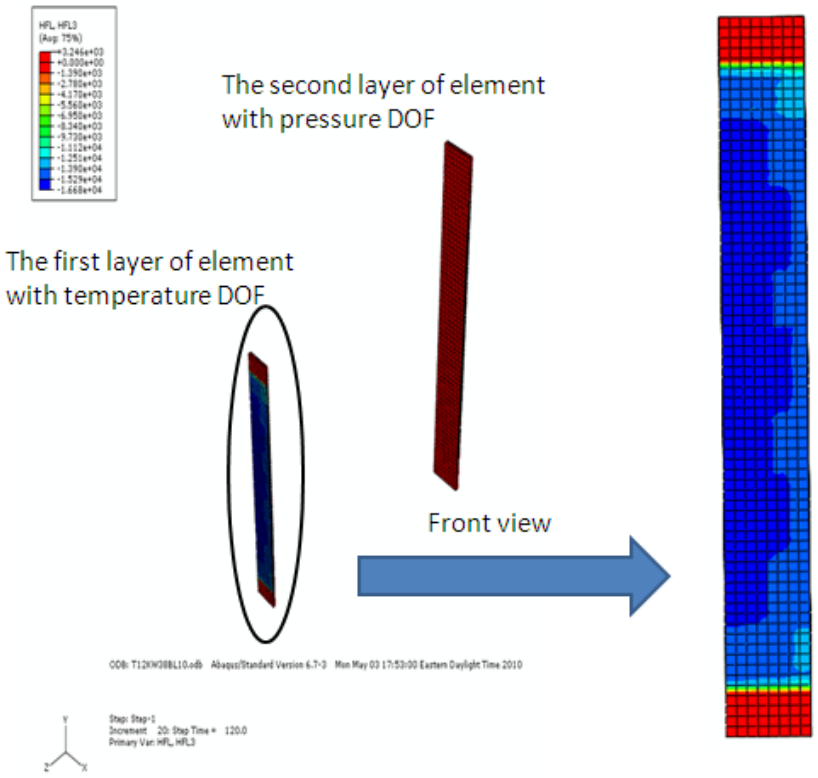

Figure 3.3: Heat flux contour at 120 seconds after heating for one of the intermediate scale tests conducted on laminate composites

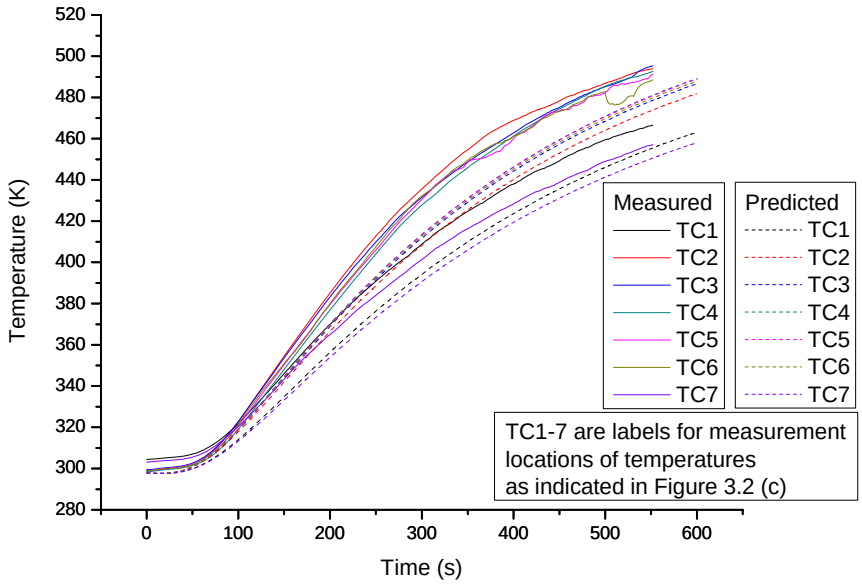

Figure 3.4: Comparison of temperature through the length on the unexposed surface for one of the intermediate scale tests conducted on laminate composites

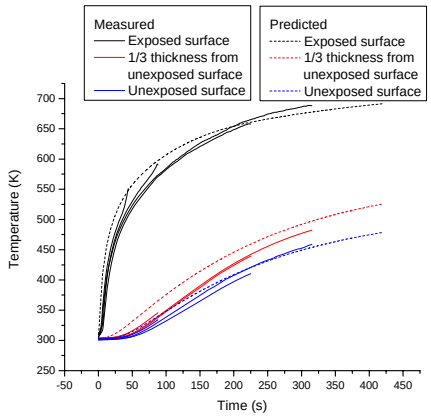

(a)

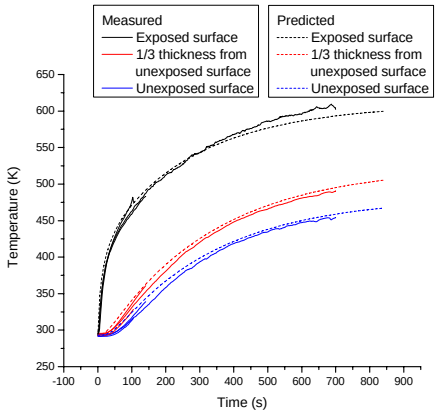

(b)

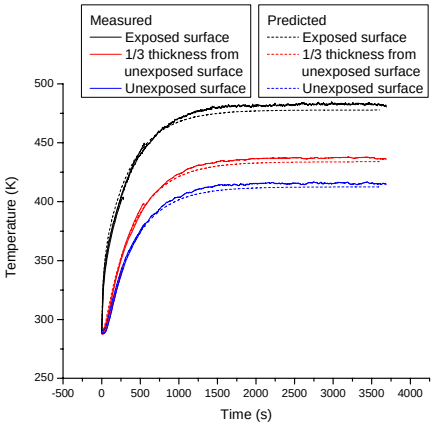

(c)

Figure 3.5: Comparison of temperature history curves for the intermediate scale tests conducted on the laminate samples of 9 mm thickness subjected to the heat flux of (a) 38kW/m^2, (b) 19.3 kW/m^2, and (c) 8 kW/m^2

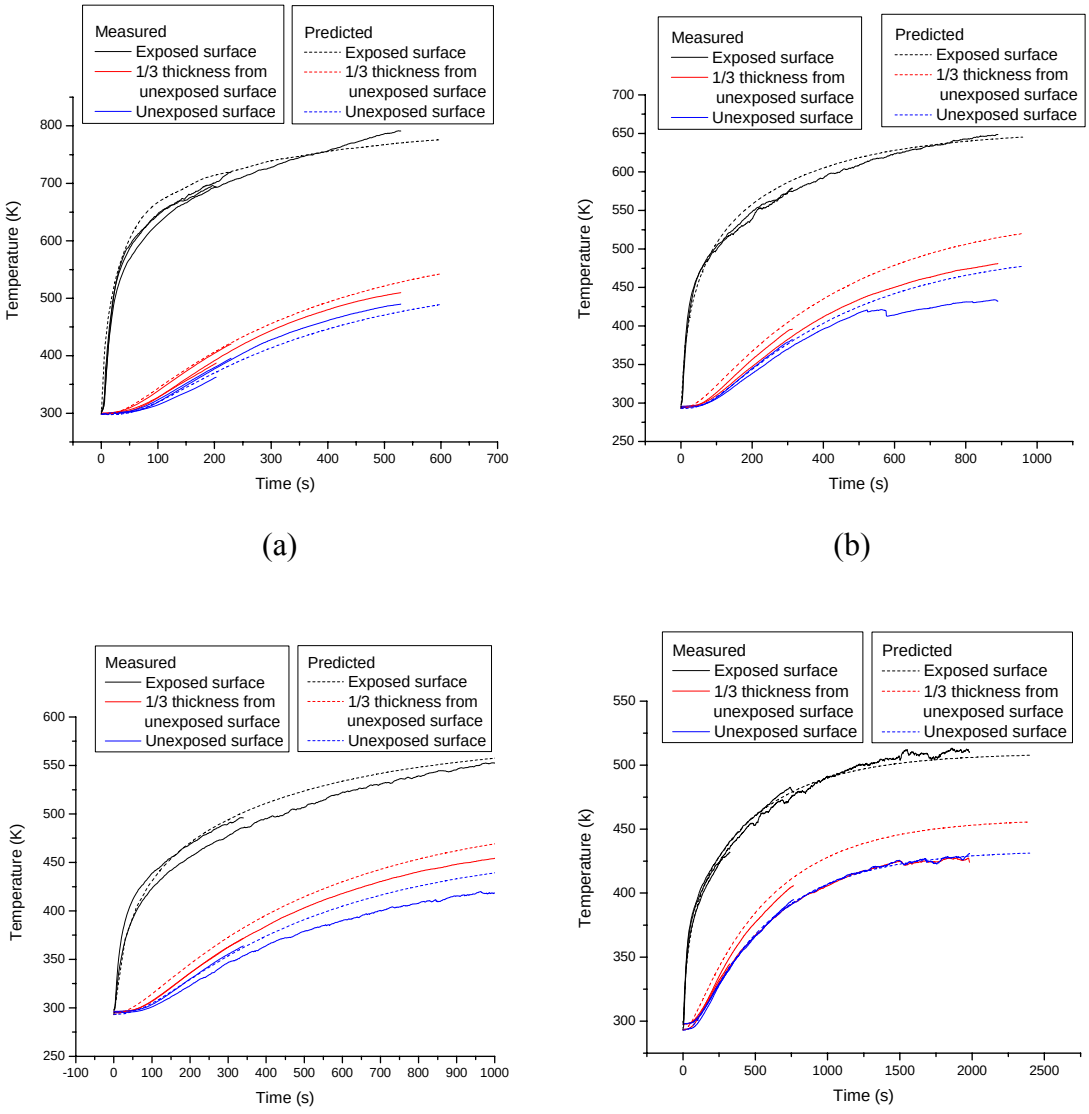

Figure 3.6: Comparison of temperature history curves for the intermediate scale tests conducted on the laminate samples of 12 mm thickness subjected to the heat flux of (a) 38kW/m^2, (b) 19.3 kW/m^2, (c) 11.8 kW/m^2, and (d) 8 kW/m^2

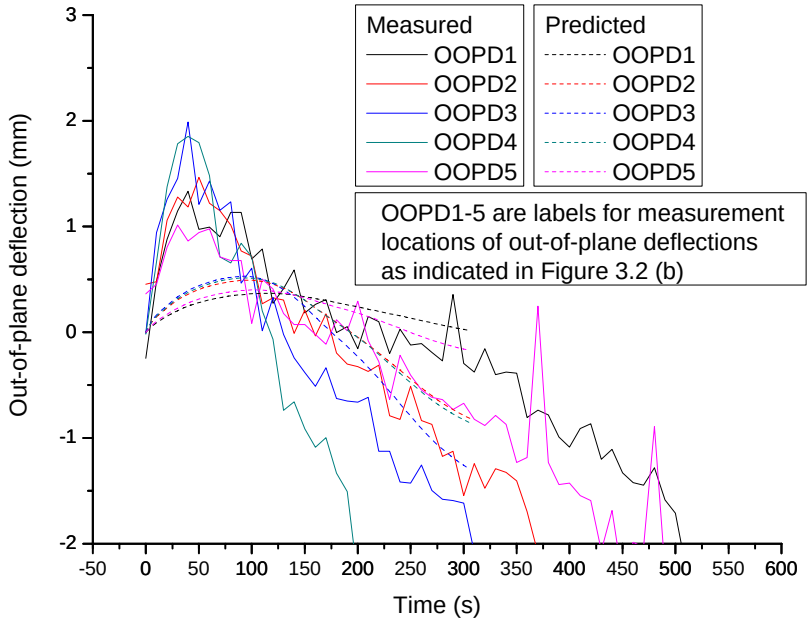

(a)

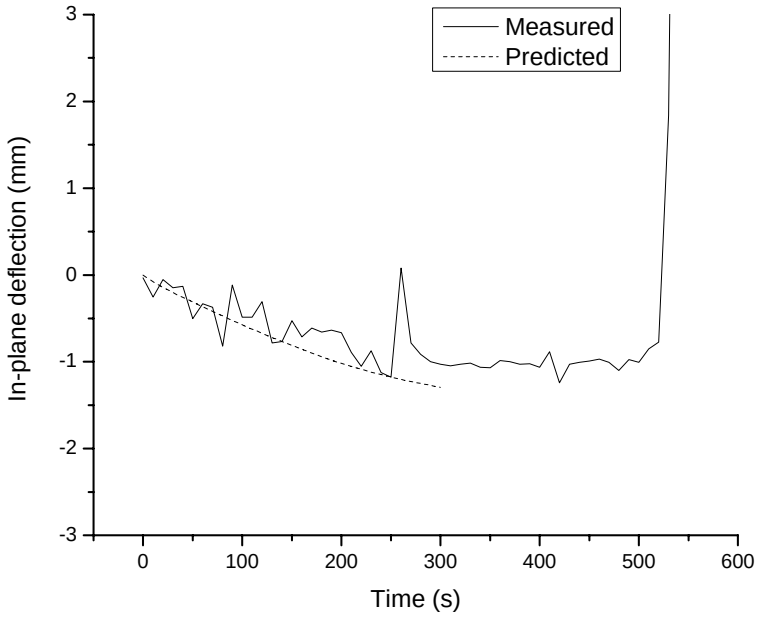

(b)

Figure 3.7: Comparison of (a) out-of-plane deflections at different locations through the length on the back surface and (b) in-plane deflections at the loading end of sample for the intermediate scale tests in which the 12 mm thick sample is subjected to heat flux of 38kW/m^2 and compressive load of 6.3 KN (10% of buckling load)

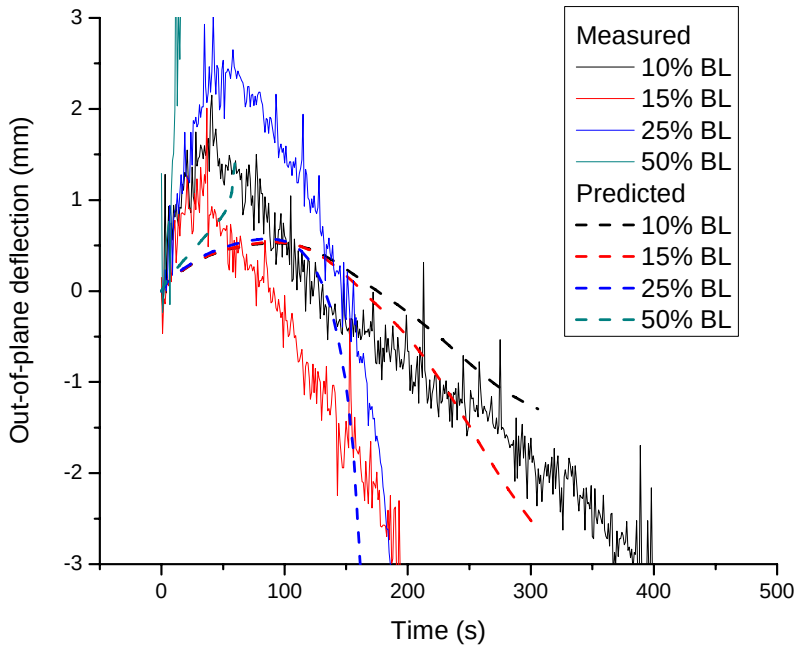

(a)

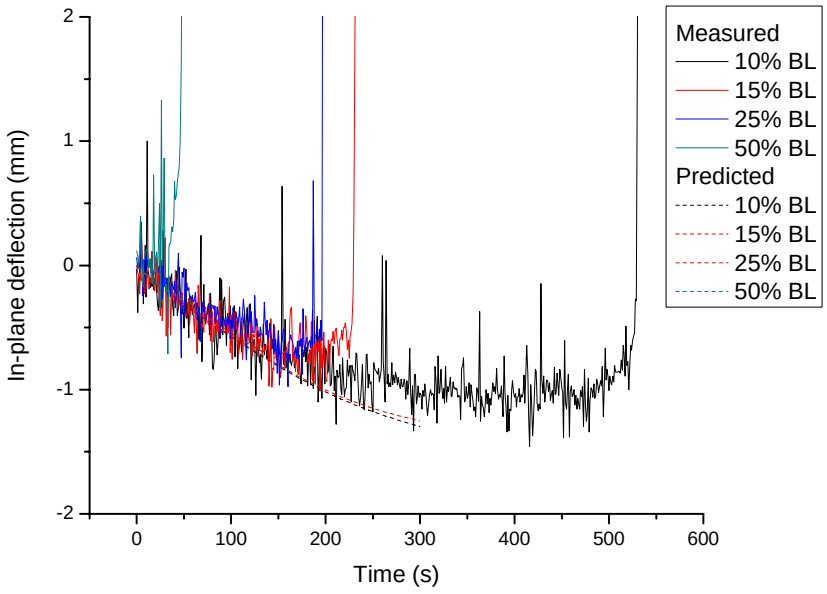

(b)

Figure 3.8: Comparison of (a) out-of-plane deflections at the center of unexposed surface and (b) in-plane deflections at the loading end of sample for the intermediate scale tests in which the 12 mm thick sample is subjected to compressive loads at different levels and the heat flux of 38 kW/m^2

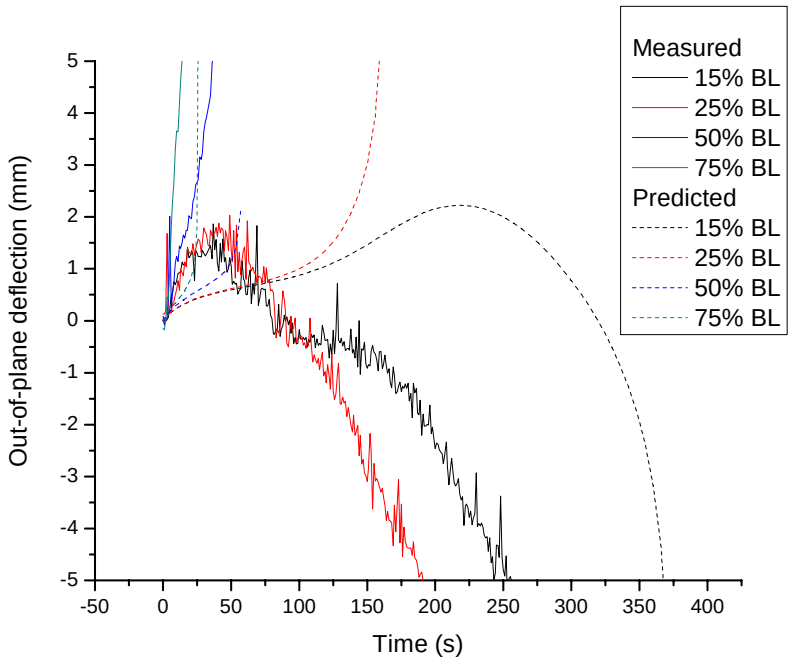

(a)

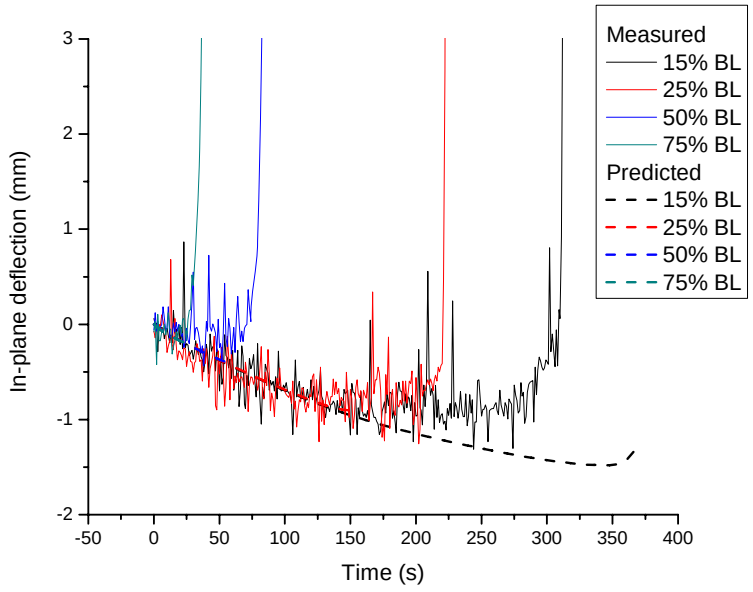

(b)

Figure 3.9: Comparison of (a) out-of-plane deflections at the center of unexposed surface and (b) in-plane deflections at the loading end of sample for the intermediate scale tests in which the 9 mm thick sample is subjected to compressive loads at different levels and the heat flux of 38 kW/m^2

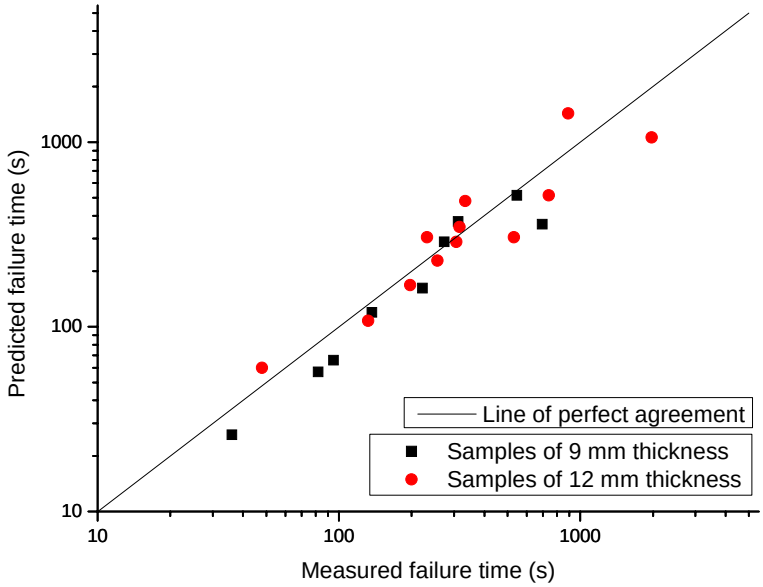

Figure 3.10: Comparison of failure time for intermediate scale one-sided heating tests conducted on laminate composites

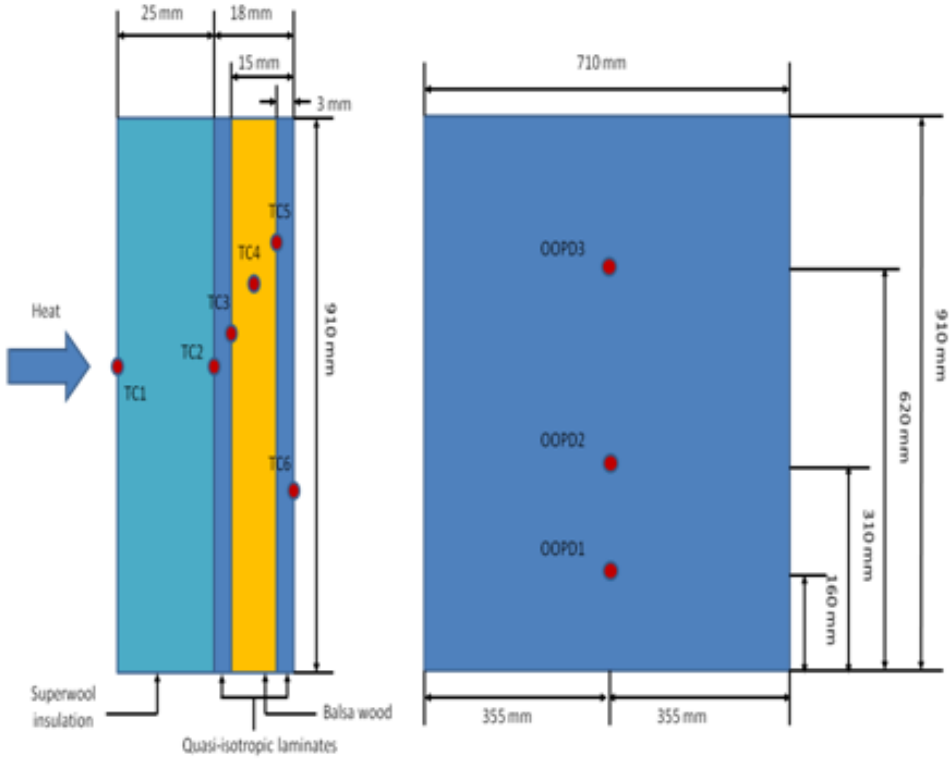

(a) (b)

Figure 3.11: The sensor locations of (a) measured temperature through the thickness and (b) out-of-plane deflection on the unexposed surface for intermediate scale tests conducted on laminate composites

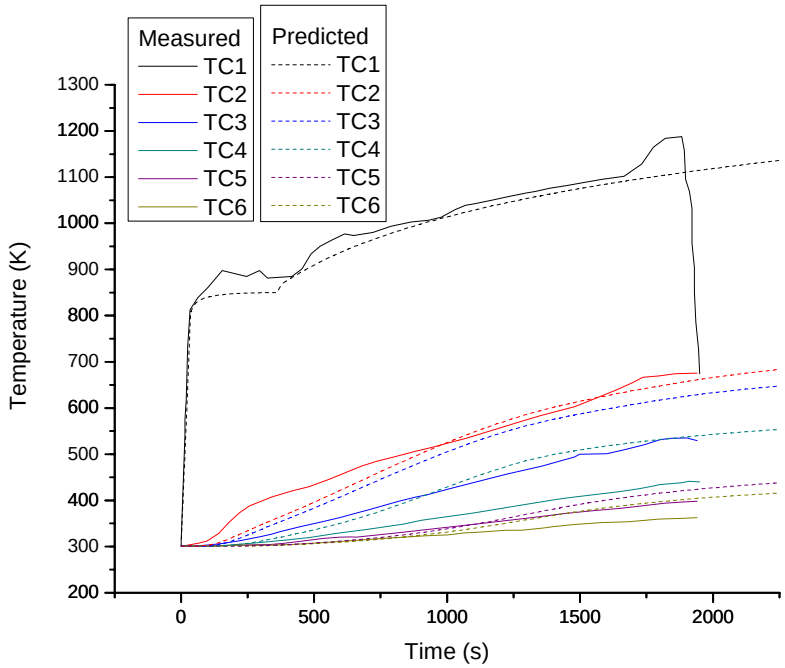

(a)

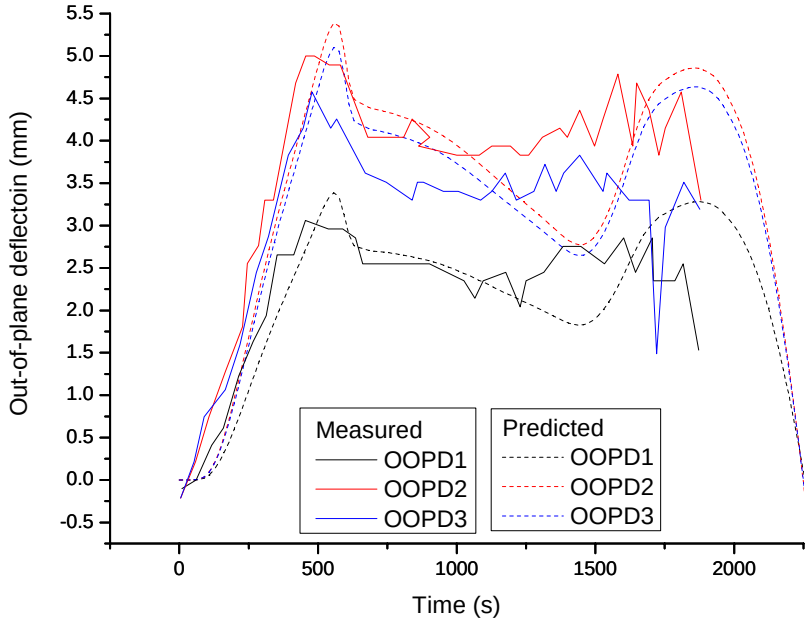

(b)

Figure 3.12: Comparison of (a) temperatures through the thickness and (b) out-of-plane deflections through the length on the unexposed surface for sandwich sample subjected to the compressive load of 10 kN and the fire scenario of ISO 834

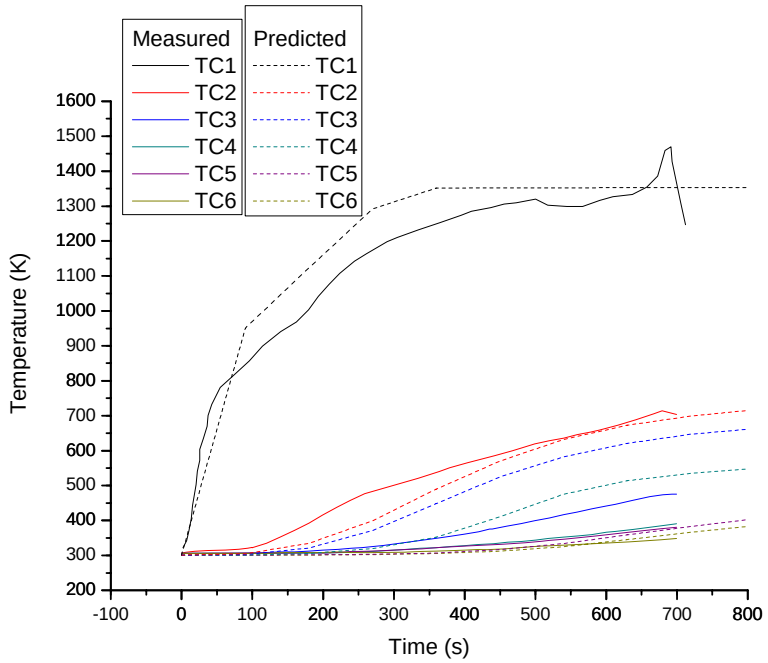

(a)

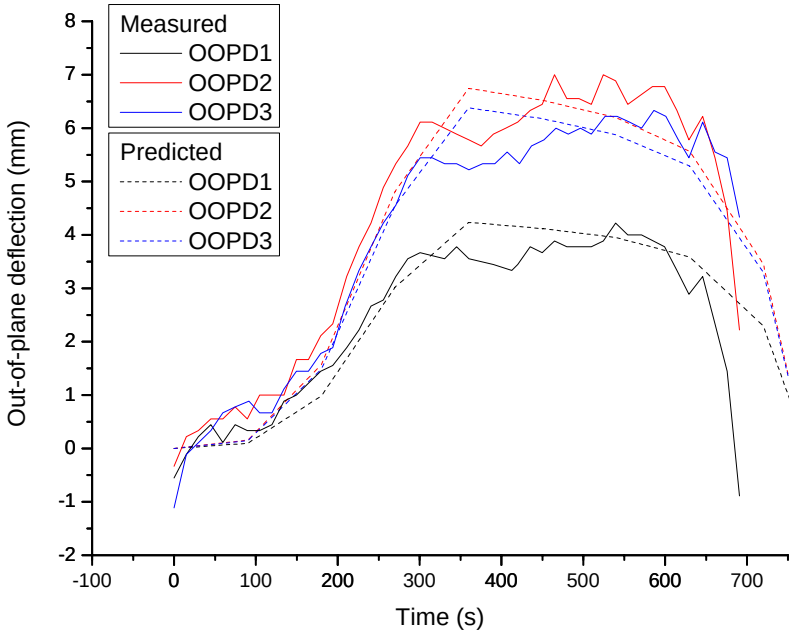

(b)

Figure 3.13: Comparison of (a) temperatures through the thickness and (b) out-of-plane deflections through the length on the unexposed surface for sandwich sample subjected to the compressive load of 22.2 kN and the fire scenario of UL 1709

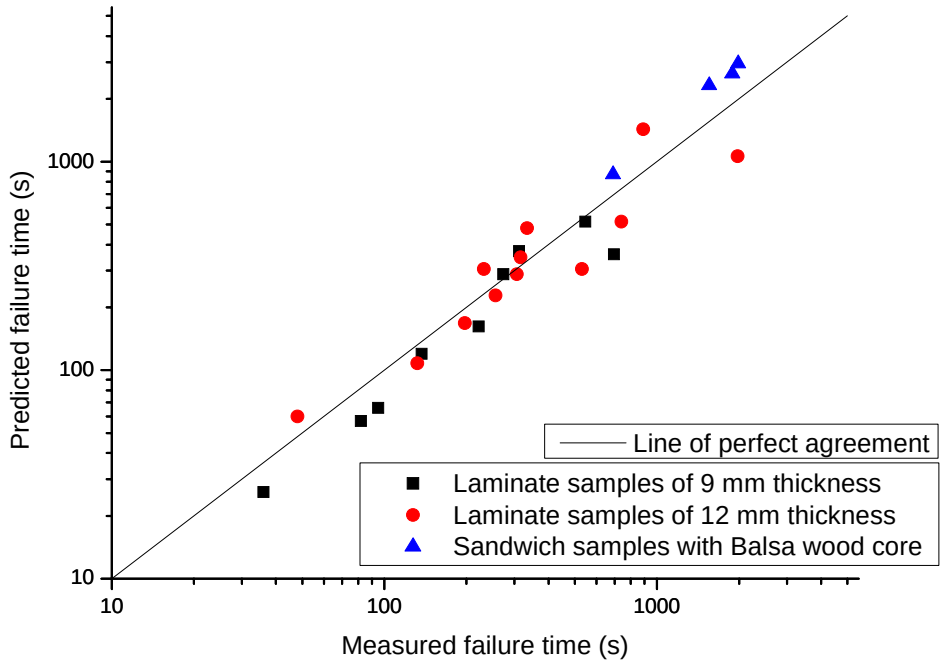

Figure 3.14: Comparison of failure time for intermediate scale one-sided heating tests conducted on both laminate and sandwich composites

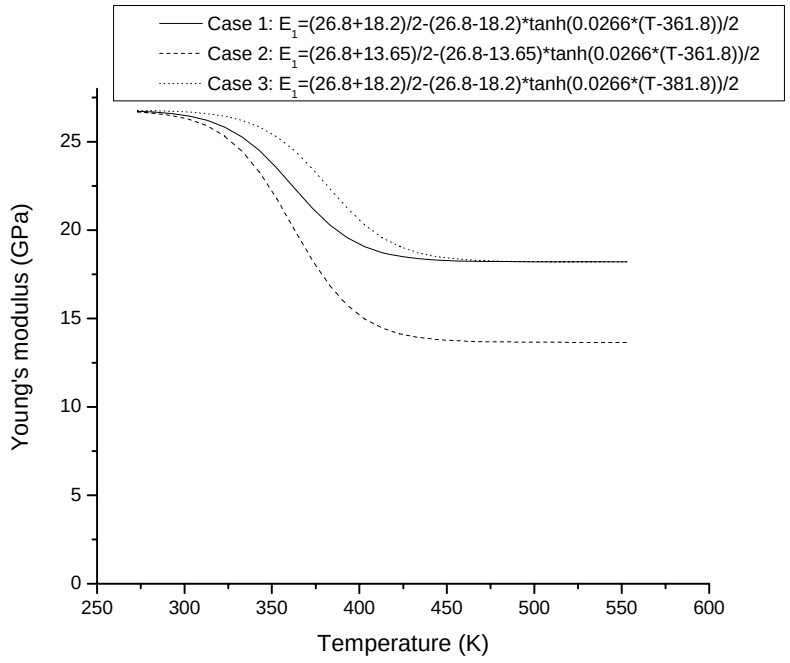

Figure 3.15: Three sets of Young's modulus to investigate the influence of property variability on predicted material behavior of composites

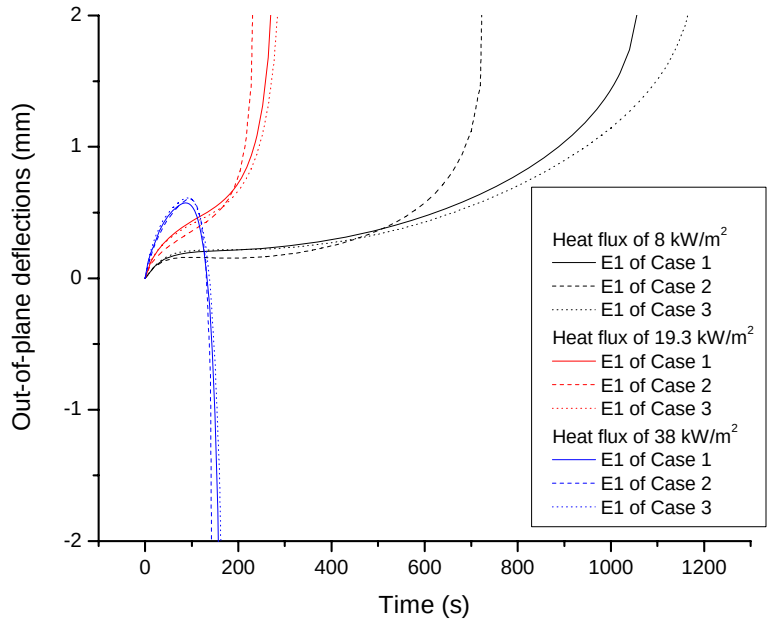

(a)

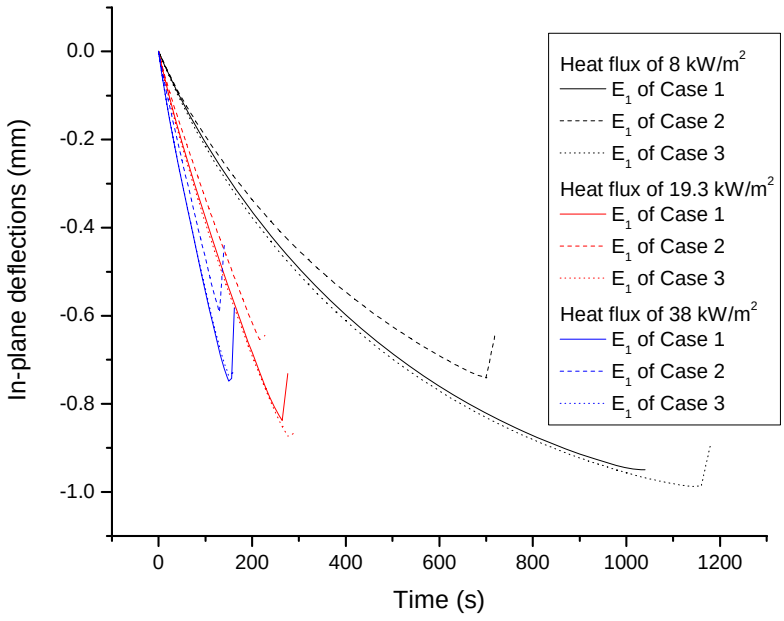

(b)

Figure 3.16: Comparison of (a) out-of-plane deflections at the center of the unexposed surface and (b) in-plane deflections at the loading end of the sample for the simulation of intermediate scale tests conducted on laminate composites subjected to the compressive load of 25% of buckling load and different heat fluxes with different inputs of stiffness

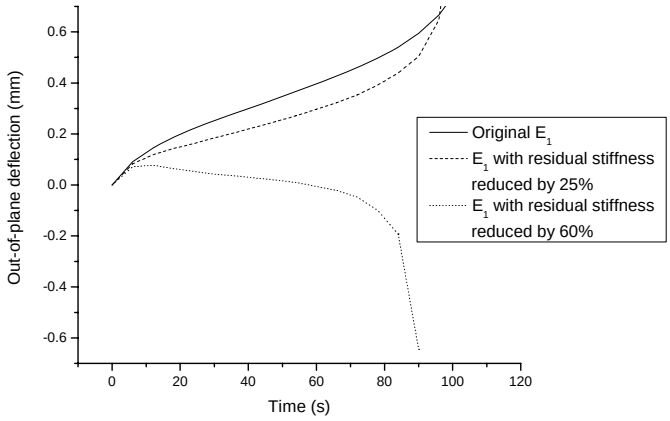

Figure 3.17: Out-of-plane deflection comparison for the simulation of intermediate scale tests conducted on laminate composites subjected to the compressive load of 50% of buckling load and heat flux of 19.3 kW/m^2 with different inputs of Young's modulus

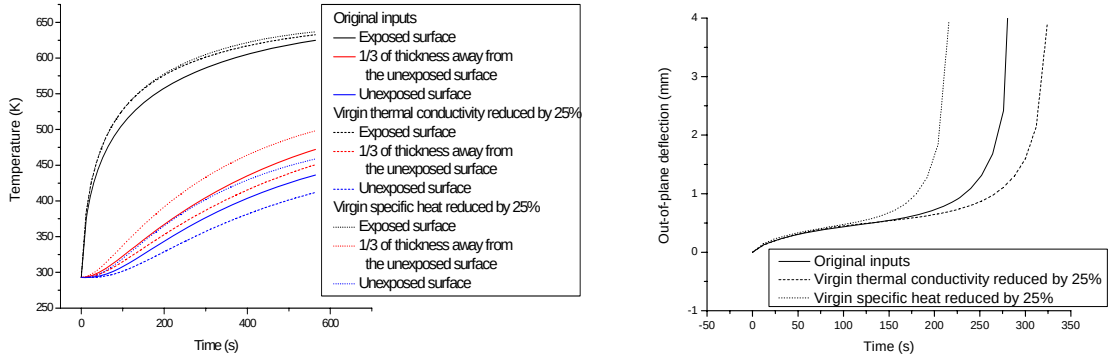

(a) (b)

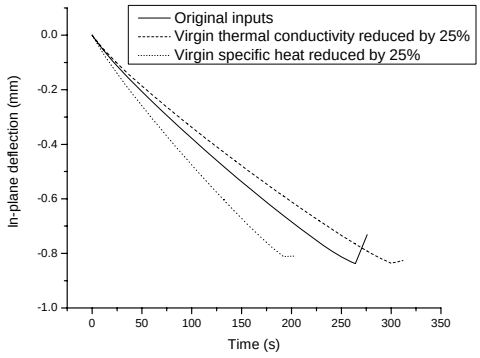

(c)

Figure 3.18: Comparison of (a) temperature through thickness, (b) out-of-plane deflections at the center of the unexposed surface, and (c) in-plane deflections at the loading end of the sample for the simulation of intermediate scale tests conducted on laminate composites subjected to the compressive load of 25% of buckling load and heat flux of 19.3 kW/m^2 with different thermal property inputs

Chapter 4: Investigation of Internal Pressure in Decomposing Polymer Matrix Composites at High Temperature

4.1 Abstract

A three-dimensional model to describe the thermal behavior of polymer matrix composites (PMCs) in fire is developed and implemented into commercial finite element package ABAQUS. The model is employed to predict the temperature and the internal pressure in one-sided heating tests for glass-talc/phenolic composites and it is validated by comparing the predicted results with the measured data. The effect of porosity and permeability on the temperature and the internal pressure is examined. In addition, an experimental technique based on Vacuum Assisted Resin Transfer Molding (VARTM) is developed to manufacture PMCs with inserted hypodermic needle for internal pressure measurement. One-sided heating tests are conducted on the glass/vinyl ester composites to measure the pressure at different locations through thickness during the decomposition process. The model is explored to simulate the heating process. Both predicted and measured results indicate that the range of the internal pressure peak in the designed test is around 1.1-1.3 atmosphere pressure.

Keywords: Polymer-matrix composites (PMCs); Thermal analysis; Decomposition; Internal pressure; Finite element analysis; Resin transfer molding (RTM)

4.2 Introduction

Polymer matrix composites (PMCs) are widely used in a number of industrial and military areas, such as bridges, wind turbine blades, industrial vessels, and submarine

structures. Advantages of PMCs include their high specific strength, long fatigue life, and excellent corrosion resistance. On the other hand, there are challenging issues for PMC application, including low rigidity, poor impact resistance, high cost, and difficulties in joining. In addition, one of the continuing concerns is the fire performance of PMCs. When the composites are exposed to fire, there is thermal conduction for heat transfer inside the composites at the beginning of the heating. As the temperature increases, the polymer matrix starts to decompose and gases are generated by the decomposition reaction. A porous network in the heated composites is formed with the continuing decomposition. Some gases carrying heat flow out of the composites and affect the temperature distribution by heat convection. Others are trapped inside the pores and impede the heat conduction because of their low thermal conductivity. Meanwhile, the gases held in the solid accumulate and build up the internal pressure which may contribute to the eventual failure through processes such as delamination. A description of this internal pressure is necessary for a better understanding of thermo-mechanical behavior of composites at high temperature. In addition, the experimental measurements of this pressure are needed to validate the existing models.

Some models have been developed to consider the pressure effect on thermo-mechanical response of composites in fire. Henderson et al. [72-73] presented a one-dimensional transient thermal model including the combined effects of thermo-chemical expansion and storage of the decomposition gases. The model was further developed in [74] by relaxing the assumption of local thermal equilibrium existing between the solid matrix and decomposition gases within the porous network of the composites. As described in Henderson's models, the internal pressure is mainly attributed to gas storage

and expansion. Sullivan and Salamon [35, 121] proposed a three-dimensional coupled thermo-mechanical model in which the internal pressure is not only influenced by the stored gases, but also by the mechanical deformation via the effect stress expression introduced from [112]. Later, the model was reduced to solve a two-dimensional plane strain problem for validation in [120]. This model was also adopted by Looyeh et al. [118] with some modifications and used to analyze the pyrolysis process of a glass fiber/polyester resin composite panel. Another model considering the contribution of moisture vapors, besides decomposed volatiles, to pressure in pores was developed by McManus and Springer [122-123] to describe the high temperature behavior of composites.

In order to examine the fire process, people developed and explored the experimental techniques to measure the internal pressure and thermal properties of composites. One important property directly related to the internal pressure is permeability of decomposed composites. A small value of permeability at the start of decomposition can hold gases in pores building up pressure. More gases are generated by the continuous heating and contribute to the increasing pressure; however, the permeability also becomes larger with more material decomposition leading more gases to flow out of the solid and release the pressure eventually. Lattimer et al. [24-25] measured the thermal properties and permeability of balsa wood and glass/vinyl ester composites at different levels of degradation. Furthermore, Goodrich [26] devised a gas infusion technique to measure the porosity and used a standard pressure differential gas flow technique to measure the permeability of composites and wood as functions of decomposition factor. Wiecek [29], Ramamurthy et al. [30-31], and Doherty [32]

examined the permeability of glass/phenolic composites, while Ahn et al. [33] used embedded fiber optic sensors to measure the permeability of glass fiber chopped strand mat. In order to predict the internal pressure accurately, Dimitrienko [34] determined the permeability by an expression in terms of porosity and Sullivan [35] defined permeability as a logarithmic function of the degree of char, based on the measured virgin and char values. Ramamurthy [36] measured the internal pressure of glass/phenolic composites at different locations by drilling holes and inserting the hypodermic tubes into the sample to carry gases to the pressure transducers. The range of measured pressure peaks falls between 1 to 10 atmosphere pressure corresponding to a permeability of 6.18×10^{-18} m^2 for virgin material and 4.85×10^{-15} m^2 for char. The internal pressure history of wood in fire was record in tests conducted by Tinney [38] and Lee [37] and the measured pressure peak is about 1.1-1.3 atmosphere pressure because of a large permeability resulting from the natural porous structure of wood.

In this work, a model based on Henderson's model [72] is extended to three-dimension with some simplifying assumptions and implemented into commercial finite element package ABAQUS by user subroutines UMATHT which allow users to define peculiar heat transfer and gas diffusion equations. The model and the code can be used to simulate the heating process of PMCs and predict the distribution and history profiles of temperature and pressure. The numerical method provides a framework for the implementation of more complicated models in further development, such as models considering multi-phase decomposition and mechanical behavior of composites. One of previous experimental techniques to measure the internal pressure of PMCs is to drill holes and insert tubes or probes into samples using cement to seal the tubes in the sample,

however, the poor bonding and the difference of thermal expansion coefficient between the cement and the sample cause cracking and leakage resulting in low measured pressure and experimental oscillation. A new experimental technique for the PMC pressure measurement is developed by using Vacuum Assisted Resin Transfer Molding (VARTM) to manufacture composites with the hypodermic needled inserted during the manufacture process to overcome the leakage issue in the previous experimental technique.

This study explores the three-dimensional model to simulate the one-sided heating tests conducted in [74] for glass-talc/phenolic composites and compared the predicted temperature and pressure with the measured data for model validation. Because the possibility of employing glass/vinyl ester composites to the construction of ship structures is being investigated by the Navy, the one-sided heating tests are set up for the internal pressure measurement of glass/vinyl ester composites using the developed experimental technique. Again, the model is used to predict the thermal behavior and pressure build up by the decomposed gases with the property inputs collected from [24-26] and the predicted pressures at different locations through the thickness of sample are compared with the measured data. Both predicted and measured results indicate that the range of the internal pressure peak in the designed test is around 1.1-1.3 atmosphere pressure.

4.3 Finite Element Implementation of Three-dimensional Thermal Model

The three-dimensional thermal model is extended from the one-dimensional model presented in [72] and composed of three governing equations: the heat transfer

equation Eq. (2.1), the decomposition equation Eq. (2.2), and the gas diffusion equation Eq. (2.3). The heat transfer equation deduced from the energy conservation equation assumes the thermal equilibrium between the gas and the solid, including the heat conduction, the heat convection, the heat generated or absorbed by the decomposition reaction, and the change of energy storage in the gas and solid components. The decomposition degree is determined by the n^{th} order Arrhenius equation and the kinetic parameters in the equation are obtained by the fitting of experimental data. The gas diffusion equation is derived from the mass conservation equation regarding that the decomposition gases are equal to the sum of the gases stored inside the solid and the gases flowing out of the solid. The gases in the solid are assumed behavior like the ideal gases and the mass flux of flowing gases is calculated by Darcy's law.

For the convenience of engineering application, the model is implemented into the commercial finite element software ABAQUS by the user subroutine called UMATHT. UMATHT can be used to define the thermal constitutive behavior of the material and the internal heat generation during heat transfer processes, which is suitable for the implementation of the heat transfer equation and the decomposition equation in the model. It is observed that the gas diffusion equation belongs to the same class of partial differential equation as the heat transfer equation. So the behavior of gas diffusion and pressure accumulation can also be described by UMATHT. However, ABAQUS only permits one UMATHT user subroutine to be assigned to one layer of elements to define the thermal behavior of one material. In order to implement all equations into ABAQUS, the technique of two overlaid layers of elements is employed. The UMATHT to define the heat transfer equation and the decomposition equation is applied to the first layer of

elements for the calculation of temperature and remaining solid mass, while the UMATHT to define the gas diffusion equation is applied to the second layer of elements for the calculation of pressure.

In practice, the three equations are not solved simultaneously in each time increment. First of all, the heat transfer equation and the decomposition equation are solved for one layer of elements. Then the calculated temperature and remaining solid mass are transferred to the other layer of elements for solving the gas diffusion equation. The pressure obtained at the end of the increment is used as known inputs to the heat transfer equation and the decomposition equation in the next time increment. The equations are solved in this order until the end of analysis. Variables in this solution procedure, such as temperature, decomposition fact, and pressure, are exchanged between user subroutines by common blocks in the code.

4.4 Investigation of Internal Pressure for Glass-Talc/Phenolic Composites

4.4.1 Model Validation

In order to validate the model and the code, the one-sided heating tests conducted by Ramamurthy [36] are simulated by employing two overlaid layers of elements and the predicted results from the model are compared to the measured data. The tested material system is glass-talc/phenolic and the size of the sample is a cylinder 1 cm in diameter and 3 cm in length with a supporting stem 0.32 cm in diameter and 2.5 cm in length. The thermocouples and hypodermic tubes connected to the pressure transducers were embedded into sample to measure the temperature and pressure at different locations

though the length. The sample was protected by alumina insulation except of one end exposed to the heat flux of 279.7 kW/m^2 applied by a heating element.

Since the test conditions in [36] are designed for the one-dimensional heat transfer process and the results from the three-dimensional model are anticipated to be compared to the numerical results from the one-dimensional model in [74], the geometry in ABAQUS simulation is set up to have only one element across the surface perpendicular to the length for modelling a one-dimensional problem. There are two columns of elements in geometry model as shown in Figure 4.1. One UMATHT is applied to one column of elements to calculate the temperature, while the other UMATHT for solving the gas diffusion equation is applied to the other column of elements in which the thermal degree of freedom is no longer interpreted as temperature but pressure. The thermal properties of glass-talc/phenolic composites used as inputs to the code, such as thermal conductivity, specific heat, and kinetic parameters in Arrhenius equation, are collected from [74]. Both the porosity and permeability are calculated using the rule of mixtures as a function of decomposition factor, given by

$$\phi = 0.113F + 0.274(1-F) \tag{4.1}$$

$$\gamma = 6.18\times10^{-18}F + 4.85\times10^{-15}(1-F) \tag{4.2}$$

The thermal boundary condition on the exposed surface is set to be

$$q''_{s,o} = \left(q''_{rad} - \varepsilon_s \sigma T_s^4\right) + h_{conv}\left(T_{\infty,o} - T_s\right) \tag{4.3}$$

where q"$_{rad}$ is the radiant heat flux of 279.7 kW/m^2, the emissivity of the exposed surface weighted by the decomposition factor $\varepsilon_s=\varepsilon_{sv}F+\varepsilon_{sc}(1-F)$ in which $\varepsilon_{sv}=0.84$ and $\varepsilon_{sc}=0.88$, the Stefan-Boltzman constant $\sigma=5.67\times10^{-11}$ kW/m^2-K^4, the convection heat flux coefficient $h_{conv}=0.01$ kW/m^2-K, and $T_{\infty,0}=313$K. The pressure boundary condition on the

exposed and unexposed surfaces is $P=P_{atm}$. The boundary conditions on the other surfaces are the thermal insulation and the pressure insulation defined as zero gradients with respect to the corresponding coordinates.

The contours of the thermal degree of freedom at 800 seconds taken directly from ABAQUS are shown in Figure 4.1. The pressure distribution is indicated on the colourful column of elements, while the temperature contour is displayed on the other column. Since the temperature values are very small compared to the pressure values in the SI unit system, the column for temperature appears to have the uniform colour although the temperature actually varies through the length. Figure 4.2 compares the measured and predicted temperatures from [74] with the predicted temperatures from the model at three different locations whose distances from the exposed surface are 0.1 cm, 1.0 cm, and 2.9 cm. The good agreement demonstrates that the model can predict the temperature well. Figure 4.3 shows the comparison of pressure history curves at two locations through the length. The model under-predicts the peak of pressure at the location x=0.6 cm. For the location x=2.25 cm, the predicted pressure peak from the model is closer to the measured data than the numerical results from [74]. The difference of the calculated pressure between two numerical results is caused by differences in the model formulation, such as the permeability expression and the assumption of thermo-chemical expansion. It is found that the model can capture the main feature of the pressure history curves and both predicted and measured results indicate a pressure peak in the range around 10 atmosphere pressures corresponding to a measured permeability of 6.18×10^{-18} m^2 for virgin material and 4.85×10^{-15} m^2 for char.

Although the internal pressure at different locations through the length was determined experimentally in [36], it was found that there is an oscillation of the pressure profile and the measured pressure at some locations is much lower than the predicted results. Cracking in the sample resulting from the difference of thermal expansion coefficient between the sample and the ceramic cement was observed, causing the poor bonding and leakage between the hypodermic tube and the sample. This leakage was the primary explanation offered for the experimental oscillation and low measured pressure. Also, the extent of cracking development is undetermined and can facilitate or influence the break of seal at other locations making the measured results potentially unreliable. It is the reason for the lack of consistency of pressure profiles measured from two one-sided heating tests with the same test conditions. It is necessary to improve the experimental technique for a more accurate pressure measurement.

4.4.2 Parametric Studies of Porosity and Permeability

The sensitivity of composite thermal response to the porosity and permeability is examined by comparing the temperature, pressure, decomposition factor, and mass flux with different setting cases for property inputs as listed in Table 4.1. The inputs of porosity and permeability in the first case are the measured data. The permeability is increased by an order of magnitude in the second case and decreased by an order of magnitude in the third case. The porosity is set to be two times of measured data in the fourth case and one half of measured data in the fifth case. The porosity in the sixth case is set to be zero and the model in the seventh case assumes that there is no accumulation of decomposition gases in the solid material.

Table 4.1: Different setting cases of porosity and permeability for parametric studies

Case Number	Initial porosity	Final porosity	Initial permeability (m^2)	Final permeability (m^2)
1	0.113	0.274	6.18×10^{-18}	4.85×10^{-15}
2	0.113	0.274	6.18×10^{-17}	4.85×10^{-14}
3	0.113	0.274	6.18×10^{-19}	4.85×10^{-16}
4	0.226	0.548	6.18×10^{-18}	4.85×10^{-15}
5	0.0565	0.137	6.18×10^{-18}	4.85×10^{-15}
6	0	0	6.18×10^{-18}	4.85×10^{-15}
7	One-dimensional model assuming no accumulation of gases in the solid [71]			

Figure 4.4 (a) and (b) compares the temperature history curves at different locations through thickness and the pressure distribution at different moments for the first three cases with different sets of permeability. It is found that the temperatures in the three cases are the same and the permeability has little influence on the temperature. However, the pressure is very sensitive to permeability. The maximum pressure at 400 seconds is 9.5 P_{atm} in the first case; the maximum pressure at 400 seconds in the second case is 3.2 P_{atm}; and the maximum pressure at the same moment in the third case is 29.9 P_{atm}. The location of the maximum pressure in three cases is the same, which is 0.017 m from the exposed surface. From the observation, the peak of pressure increases by about three times with permeability reduced by one order of magnitude. The decrease of permeability means that it becomes harder for the decomposition gases to flow through the material and more gases are trapped inside the solid building up higher internal pressure. Regarding the permeability effect on temperature, the permeability is incorporated into the mass flux term in the heat transfer equation which is the third term in Eq. (2.1). However, the mass flux is determined by a combined effect of permeability, pressure, and pressure gradient with respect to spacial coordinates. Figure 4.4 (c) shows the distribution of mass flux in the thickness direction at different moments. The positive

value represents the gas flow towards the exposed surface, while the negative value reflects the opposite direction of gas flow. It is found that the mass flux is insensitive to the permeability, which is the reason why the permeability has little influence on the temperature.

The porosity effect is examined by comparing the temperature, decomposition factor, and pressure for case 1, 4, and 5 with different sets of porosity. Figure 4.5 (a) shows the temperature history curves at different locations through thickness for these three cases. The temperature gradient through thickness becomes larger with increasing porosity. Since the gas thermal conductivity is smaller than the solid thermal conductivity and the porosity represents the volume ratio of gas to composites, the thermal conductivity of composites is decreased with increase of porosity. As a result, it becomes harder for the heat to transfer the composites and the temperature gradient through thickness becomes larger. Furthermore, the temperature influences the decomposition factor as shown in Figure 4.5 (b). The difference of decomposition factor resulting from the porosity difference becomes larger with the heating time. Since the permeability is a function of decomposition factor and the internal pressure is sensitive to permeability, the porosity also has apparent influence on the pressure. Figure 4.5 (c) shows the pressure distribution at different moments for different sets of porosity. It is observed that the variability of pressure distribution at the same moment among different cases becomes larger with the heating time. In addition, the maximum pressure at 800 seconds in case 4 is larger than the maximum pressure at 400 seconds because of the relative large decomposition factor and small permeability compared to the other two cases. The maximum pressure at 800 seconds in the other two cases is smaller than the maximum

pressure at 400 seconds because of large permeability facilitating the gas flow and impeding the accumulation of gases in solid. The same trend of pressure distribution in three cases is that the location of maximum pressure moves towards the unexposed surface with increasing time. From the above analysis, it is concluded that the effect of porosity on temperature in decomposed polymer composites is apparent and the temperature is insensitive to permeability. Both porosity and permeability have obvious influence on the internal pressure.

Figure 4.6 compares the calculated temperature using measured porosity, zero porosity, and one-dimensional model assuming there is no accumulation of gases in the solid. Again, the smaller porosity causes smaller temperature gradient through thickness. The temperature calculated from the three-dimensional model with zero porosity matches well the temperature calculated from the one-dimensional model except of a little difference at the end of curves. The mass flux in the one-dimensional model is calculated by integrating time rate of mass change through thickness and the direction of mass flux is assumed always towards the heater. The one-dimensional model cannot be applied to three-dimensional problem because of the issue of determining the direction of gas flow. However, the three-dimensional model can solve the issue by using Darcy's equation and the direction of gas flow can be towards the unexposed surface in the one-dimensional problem. The different assumptions and formulas to calculate mass flux in two models lead to the little difference at the end of temperature history curves.

4.5 Investigation of Internal Pressure for Glass/Vinyl Ester Composites

4.5.1 Sample Preparation and Experimental Set-up

Since glass/vinyl ester laminate is commonly used in ship structures and civil infrastructure, the internal pressure of glass/vinyl ester composites in fire is investigated for a further understanding of pressure effect on thermo-structural response of composites. In addition, the measured pressure of glass/vinyl ester can be used to validate the generality of the model for different material systems. In this study, the glass/vinyl ester samples were manufactured by a modified Vacuum Assisted Resin Transfer Molding (VARTM) and the one-sided heating flux tests were conducted on the samples in a heating chamber for measuring the internal pressure in the decomposing composites.

The composite panel with inserted hypodermic needle for pressure measurement was manufactured by VARTM as shown in Figure 4.7. In order to overcome the cracking and leakage issue coming from the measurement method shown in [36], the hypodermic needle was laid inside the panel before the resin transfer process instead of being inserted into panel through drilled holes after the manufacture. A 22-gauge hypodermic needle with inside diameter 0.4064 mm (0.016”) and outside diameter 0.7112 mm (0.028”) was attached to a hub fitting with 1/8 NPT external thread by 3M DP-420 epoxy adhesive. To confirm the good sealant between the needle and the hub fitting, the hub fitting was connected to a gas cylinder which can provide a constant pressure. The end of needle though which the gas can be released to the outside environment was blocked and the inside constant pressure read by a pressure regulator proved that there was no leakage at the connection between the needle and the hub fitting. Thereafter, a wire with outside diameter 0.3556 mm (0.014”), coated with vacuum grease, was inserted into the

hypodermic needle. The function of vacuum grease is to prevent the resin flowing into the space between the needle and the wire. The E-glass fiber sheets were laid up warp-aligned and the needle was placed between the fiber layers where the pressure will be measured. One end of needle was inside the layers, while the other end attaching to the hub fitting was enclosed by the sealant tape and vacuum bag for protecting the connection part from resin during the manufacture process. The wire was pulled out of the needle after the resin cured. Since the epoxy seal between the needle and the hub fitting is possible to be broken in the manufacturing process, the connection part was sealed again by the epoxy adhesive after manufacture.

The sample size is 240 mm in length and 230 mm in width with 20 layers of warp-aligned fibers. The material system is Vetrotex 324 E-glass fiber and Dekarane 411-350 vinyl ester resin and the cure package consists of 0.06% per resin weight of 2,4 Pentanedione (retarder), 1.5% of MEKP-925H (peroxide initiator), and 0.2% of Cobalt Naphthenate (catalyst). There are four samples prepared for the pressure measurement. The needles of the first 3 samples were laid on the 10^{th} fiber layer to measure the gas pressure on the mid-surface. The needle of the last sample was laid on the 15^{th} fiber layer to measure the pressure at the location of one quarter thickness from the exposed surface. Two K-type thermocouples were attached on the top and bottom surfaces of each sample using DP-420 epoxy adhesive for temperature measurement. At last, all samples were post cured at 80 °C for 2 hours.

Before the one-sided heating test, the hub fitting of the sample was connected to a gauge pressure transducer OMEGA PX209 whose measure range is from 0 to 4 atm. The sample was placed between two ceramic boards in a heating chamber where a cone heater

can apply heat flux on the top surface of the sample as shown in Figure 4.8. A 75 mm × 75 mm window was cut in the top ceramic board to expose a rectangular region on the top surface of the sample to the cone heater. The edges of the sample were still covered by the ceramic board for thermal insulation to ensure that there is no decomposition on the edges and the decomposed gases can only flow through the thickness. Under this situation, the test can be simulated as a one-dimensional problem. The heater temperature was ramped up to 750°C and the pressure transducer was protected by ceramic wool from high temperature. The exposed window in the top ceramic board was covered by another ceramic board till the heater temperature reached the set point, so that a constant heat flux can be applied to the exposed surface of sample immediately at the start of the test. The pressure and temperature signals were collected by a data acquisition system during the heating process.

4.5.2 Results and Discussion

Four one-sided heating tests for pressure measurement were conducted with the experimental process mentioned above. The pressure was measured on the mid-surface of samples in test 1-3, while the pressure was measured at the location of one quarter thickness from the exposed surface in test 4. Figure 4.9 summarizes the measured temperature and pressure history curves from the four tests. The temperature on the exposed surface in test 1 has a sudden drop around 1600 seconds. Since the thermocouple was observed to be broken after the test, one possible reason for the sudden drop is that the thermocouple was malfunctioning at that moment. Although there is good repeatability of temperatures on the unexposed surface, the temperatures on the exposed surface in test 3 and 4 increase faster than the temperatures in test 1 and 2, causing the

sharp peak of the measured pressure in test 3 and 4, as well as a relative flat trend of pressure history curves in test 1 and 2. The temperatures in test 1 and 2 have only a little difference in the first 750 seconds, there is, however, apparent difference of peak and trend for corresponding pressure curves. It is deduced that the internal pressure is very sensitive to the heating condition for glass/vinyl ester composites.

The model developed before is also used to analyze the heating procedure by the technique of overlaid elements. Since the simulated procedure is one-dimensional, the geometry model for the test is still two columns of elements and the thickness is 12 mm. The thermal properties of E-glass/vinyl ester are collected from [24-25].

The porosity and permeability at different levels of decomposition have been measured by Goodrich [26]. As property inputs to the code for numerical analysis, the porosity is defined as a linear function of decomposition factor by fitting the measured data, given by

$$\phi = 0.668189 - 0.627953 \times F \tag{4.4}$$

Since the measured permeability increases by four orders of magnitude from 5.72×10^{-15} m^2 to 6.36×10^{-11} m^2 with decreasing decomposition factor from 0.39 to 0.26, the permeability expression is divided into two segments. When the decomposition factor is larger than 0.39, the permeability is assumed as a small constant of 5.72×10^{-15} m^2. After the decomposition factor decreases to 0.39, the permeability is described as a linear function of decomposition factor based on the measured data. The permeability expression in the unit of m^2 is given by

$$\gamma = \begin{cases} 1.56\times10^{-10} - 3.9998533\times10^{-10}\times F, F \le 0.39 \\ 5.72\times10^{-15}, F > 0.39 \end{cases} \tag{4.5}$$

Considering the measured pressure is sensitive to the heating condition, the measured temperatures on the exposed and unexposed surfaces from each test are used as thermal boundary condition for an accurate analysis. The atmosphere pressure is applied on both surfaces of the sample.

The measured and predicted pressure history profiles for four tests are shown in Figure 4.10. It is found that the predicted results from the model can capture well the features of the measured pressure at different locations. Peaks of both measured and predicted results fall in the range of 1.1-1.3 atmosphere pressure. Once again, the variability of the pressure curves for four tests predicted by the model using measured temperatures as boundary condition for each test indicate that the pressure is sensitive to the temperature for glass/vinyl ester composites. Since the permeability has significant influence on the pressure, the pressure is very liable to the temperature. It is observed that there is difference between the measured and predicted pressure, especially in test 1 and 3. The possible reason is that the measured pressure is actually an average value for the region in the vicinity of the end of the needle and may be influenced by the placement of the needle with respect to the local weave architecture.

4.6 Conclusion

A three-dimensional model to describe the thermal behavior of composites in fire was developed and implemented into the finite element commercial software ABAQUS by user subroutine UMATHT. The model was used to simulate the one-sided heating tests conducted in [36] for glass-talc/phenolic composites by the overlaid element technique. The predicted temperatures and pressures at different locations were compared

to the calculated results and measured data from [74] and it is found they have good agreement. The effect of porosity and permeability on thermal response of composites was studied by comparing the temperature, pressure, decomposition factor, and mass flux calculated from the model using different sets of property inputs. Temperature is insensitive to permeability; however, permeability has a strong influence on pressure. The peak of pressure increases by about three times with permeability reduced by one order of magnitude. The influence of porosity on both temperature and pressure is apparent. Smaller porosity facilitates the heat transfer through composites. In order to investigate the internal pressure of glass/vinyl ester composites and overcome the leakage issue of previous experimental technique for pressure measurement, a manufacturing procedure based on VARTM was proposed and executed to make the glass/vinyl ester composite panel with inserted hypodermic needle. The one-sided heating tests for the sample with inserted needle were set up to measure the internal pressure at mid-surface and the location of one quarter thickness from the exposed surface. In addition, the three-dimensional model was employed to analyze the heating tests for glass/vinyl ester composites with measured temperatures on the exposed and unexposed surfaces as thermal boundary condition. The predicted pressures can capture the trend of the measured pressure history curves and both the measured and predicted results indicate a pressure peak in the range of 1.1-1.3 atmosphere pressure for glass/vinyl ester systems in the conducted heating tests. The good match between the predicted results and measured data for two different material systems validates the generality of the model.

4.7 Acknowledgements

The authors would like to acknowledge the financial support of the Office of Naval Research under the Naval International Cooperative Opportunities in Science and Technology Program (N00014-07-1-0514) and through the Small Business Innovation Research Program (N00014-08-C-0591). The authors also acknowledge ABAQUS technique support from Global Engineering and Materials Inc.

4.8 Figures

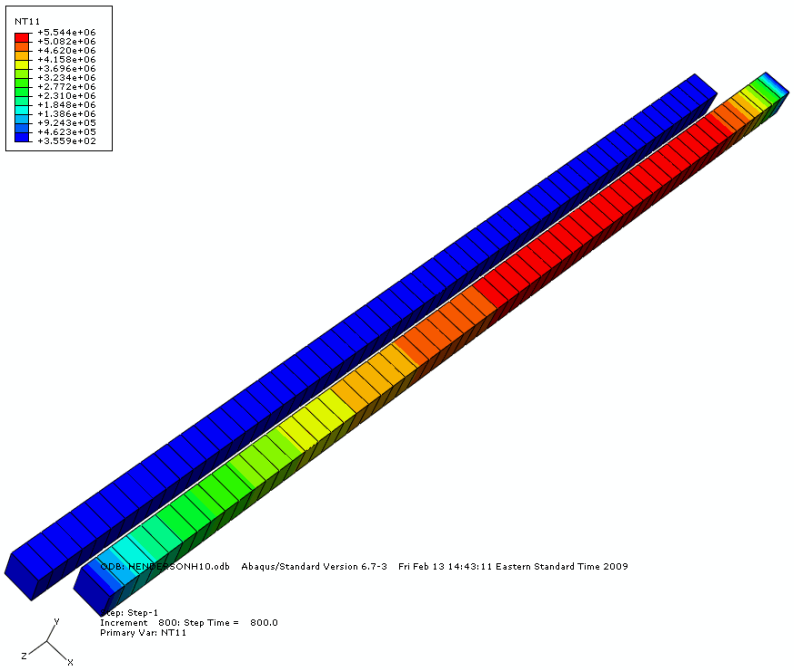

Figure 4.1: Geometric model and contour of thermal degree of freedom for the validation of one-sided heating tests for glass-talc/phenolic composites

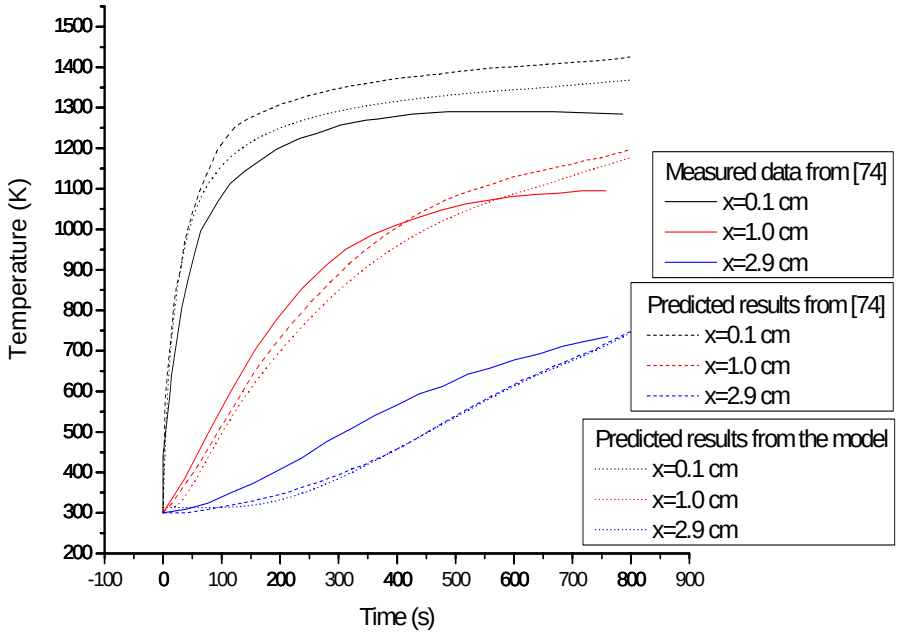

Figure 4.2: Comparison of temperature history curves at three different locations through length of glass-talc/phenolic composite sample

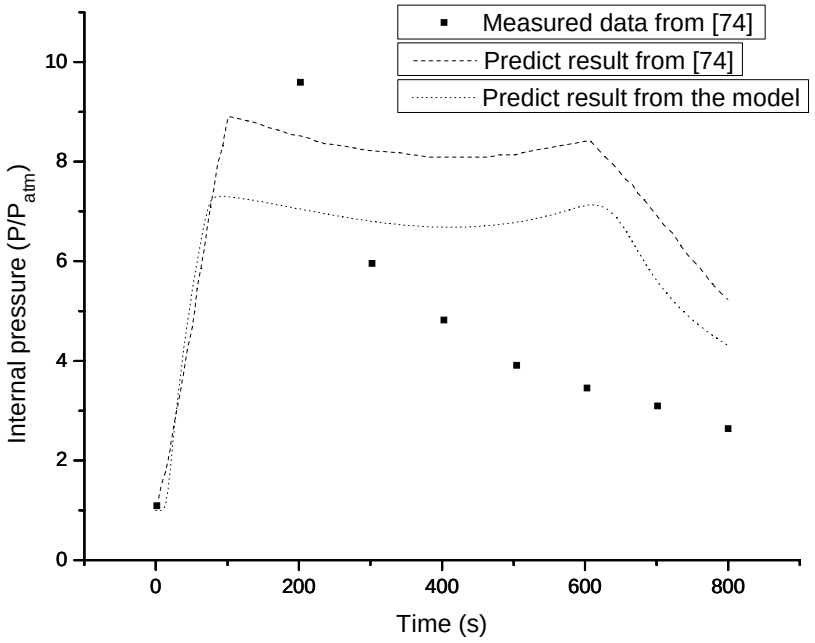

(a)

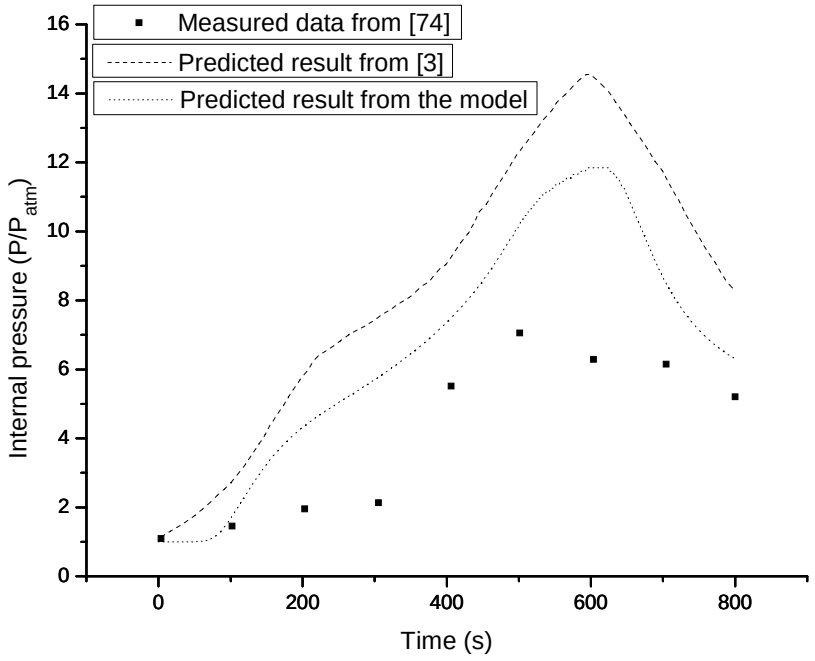

(b)

Figure 4.3: Comparison of pressure history curves at (a) 0.6 cm and (b) 2.25 cm away from the exposed surface of glass-talc/phenolic composite sample

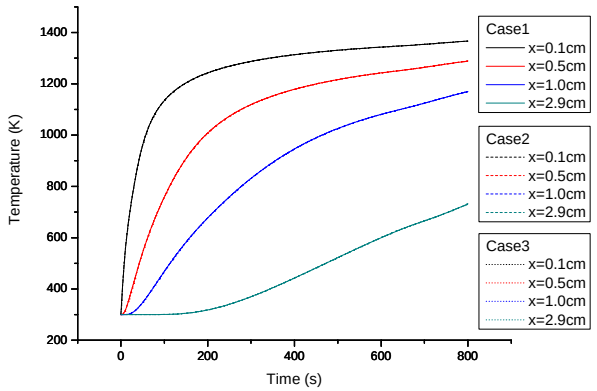

(a)

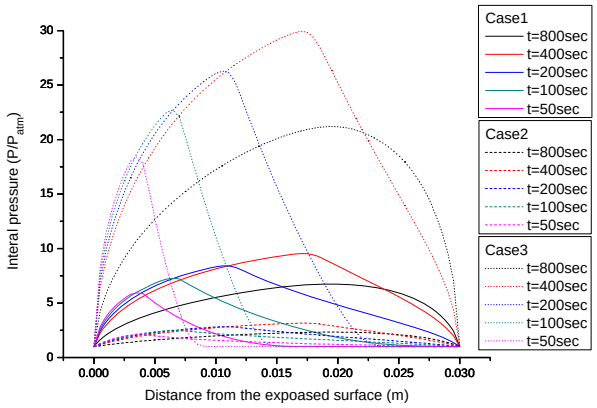

(b)

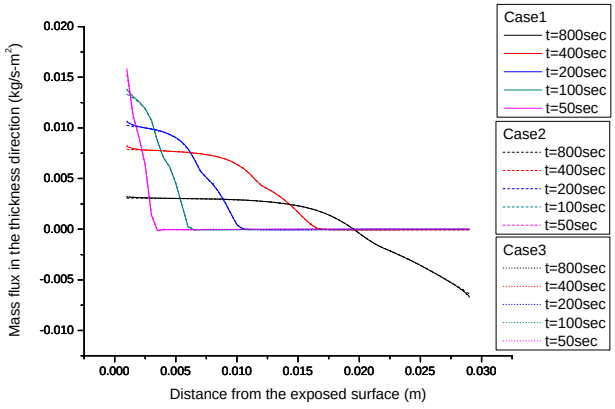

(c)

Figure 4.4: Comparison of (a) temperature versus time at different locations through thickness, (b) pressure versus thickness at different moments, and (c) mass flux versus thickness at different moments for investigating the sensitivity of thermal response to permeability

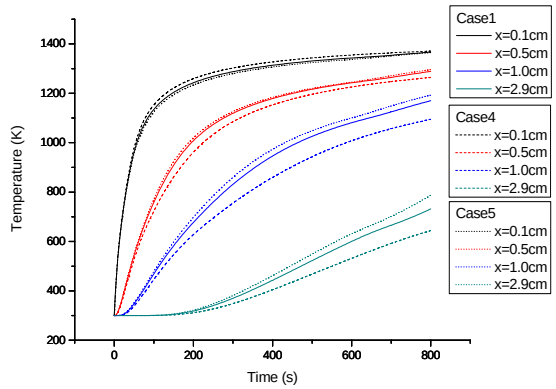

(a)

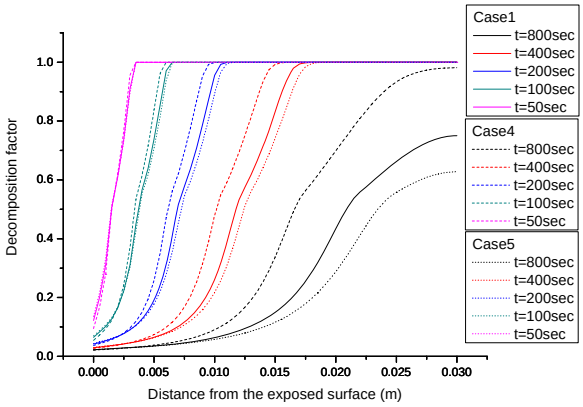

(b)

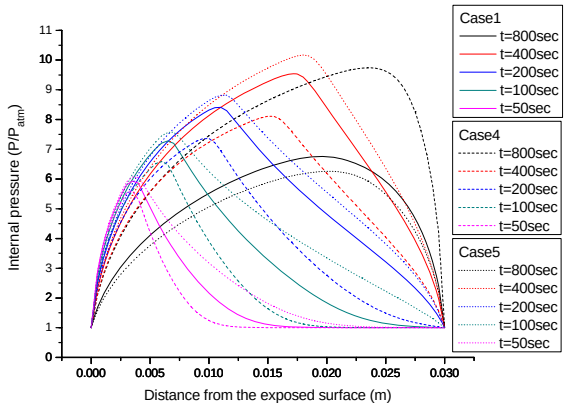

(c)

Figure 4.5: Comparison of (a) temperature versus time at different locations through thickness, (b) decomposition factor versus thickness at different moments, and (c) pressure versus thickness at different moments for investigating the sensitivity of thermal response to porosity

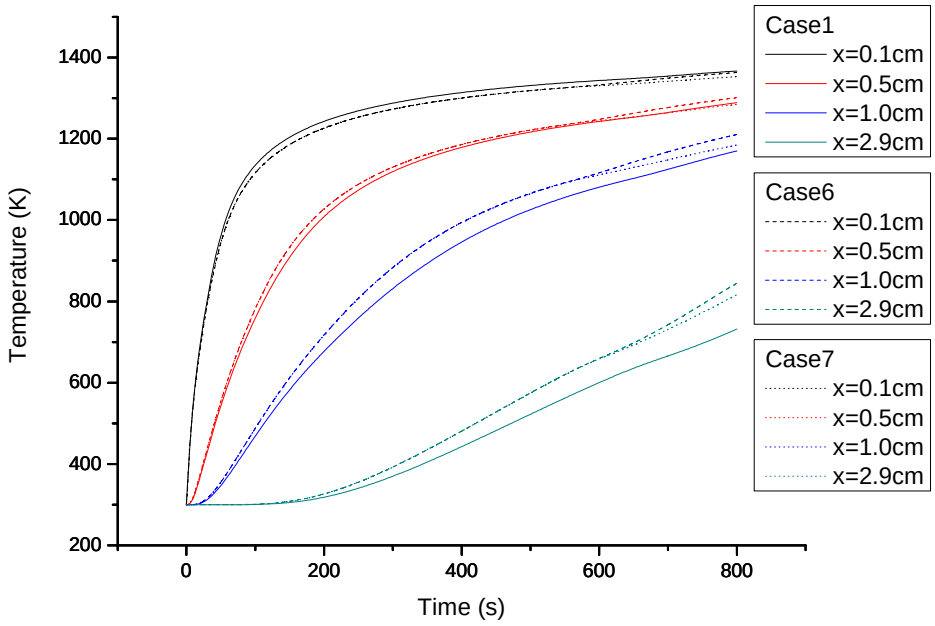

Figure 4.6: Comparison of temperature versus time at different locations through thickness for different models

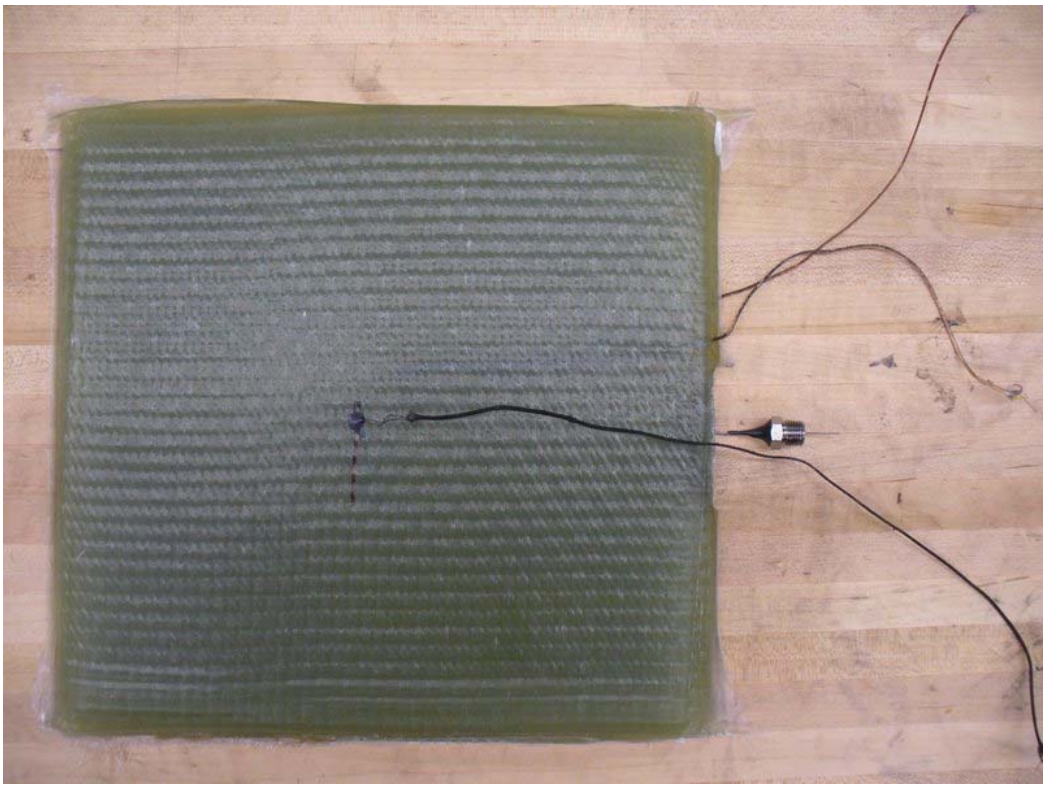

Figure 4.7: The testing sample with inserted hypodermic needle for pressure measurement

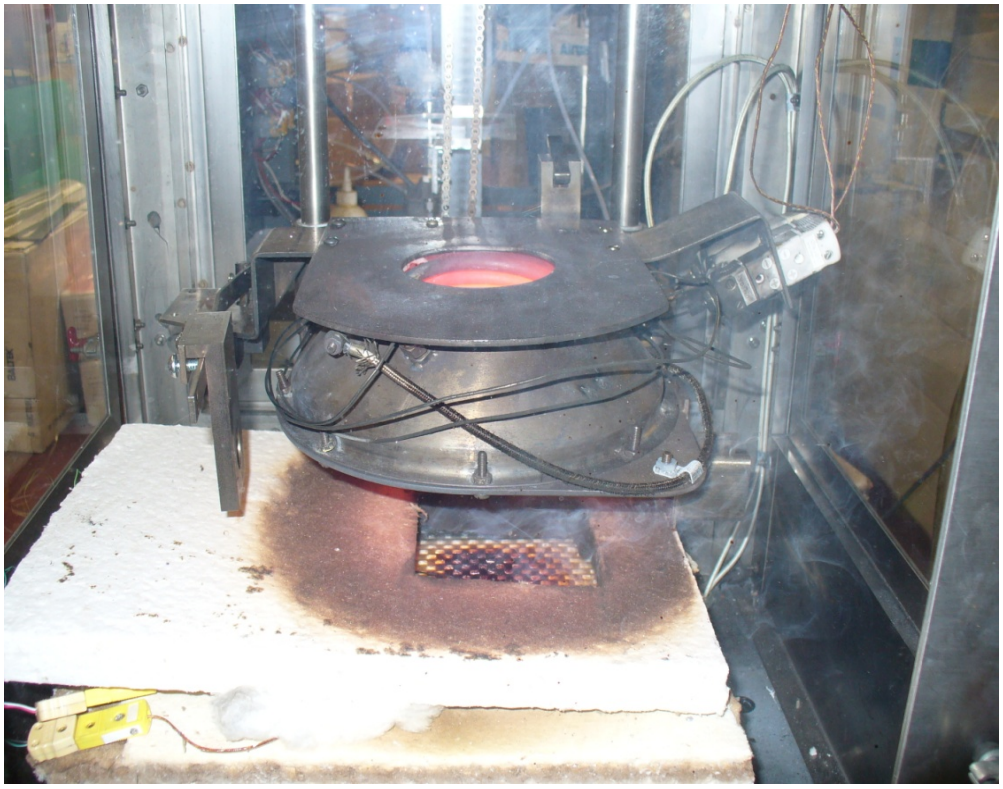

Figure 4.8: The experimental set-up for pressure measurement

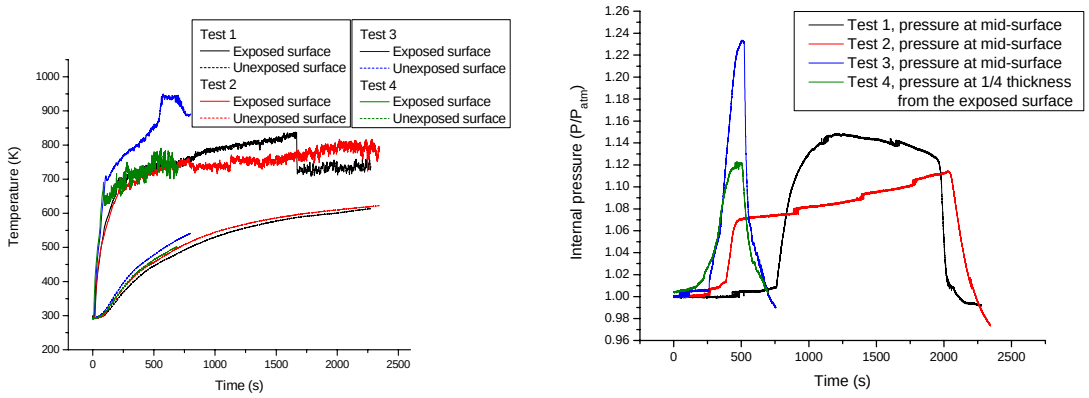

(a) (b)

Figure 4.9: Measured (a) temperature and (b) pressure of four one-sided heating tests

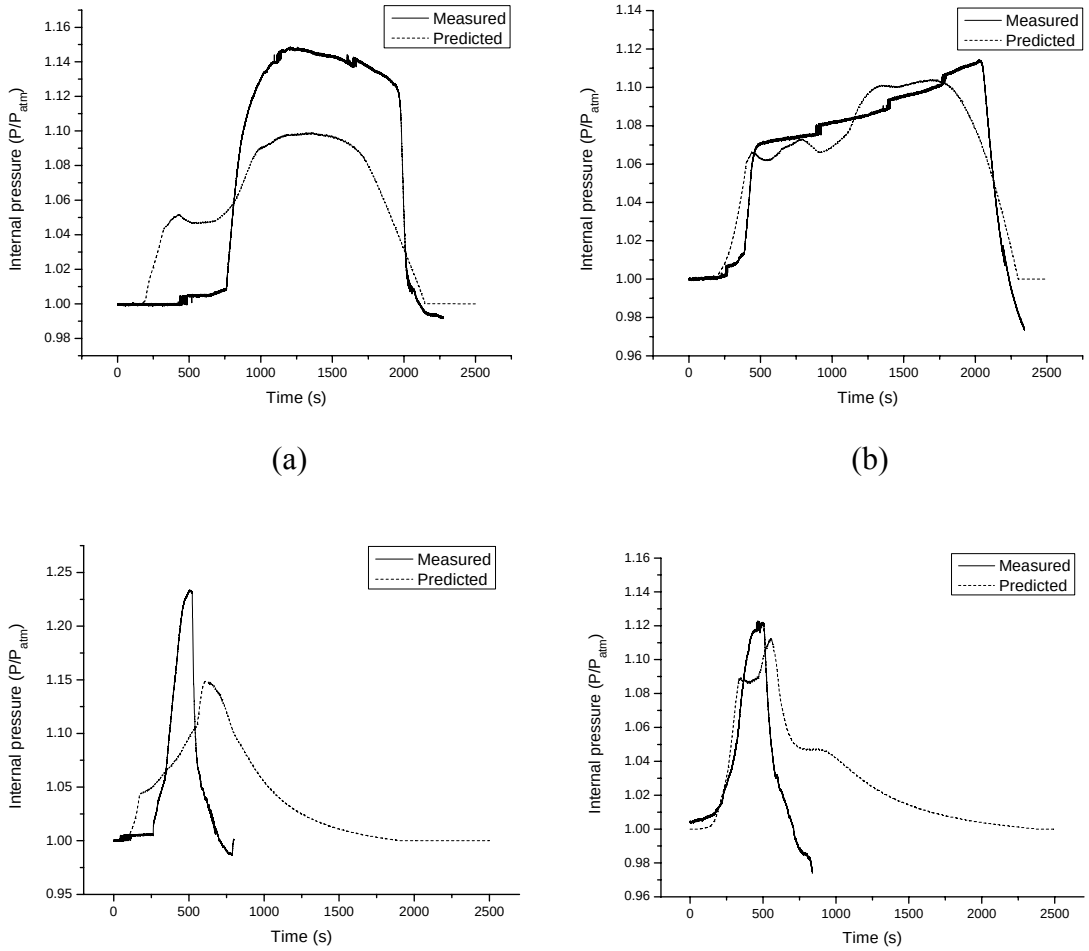

Figure 4.10: Comparison of measured and predicted pressure of (a) test 1 with measured pressure at mid-surface, (b) test 2 with measured pressure at mid-surface, (c) test 3 with measured pressure at mid-surface, and (d) test 4 with measured pressure at one quarter thickness from the exposed surface

Chapter 5: Conclusions and Recommendations

5.1 Conclusions

The main goal of the work is to develop a three-dimensional thermo-mechanical model to predict the material behavior of polymer matrix composites at high temperature and to implement the model into commercial finite element software to provide the practicing engineers a convenient tool to perform analysis and design studies.

The model is composed of four governing equations and a compression failure criterion. The heat transfer equation considers thermal conduction, thermal convection from the flow of decomposition gases, heat generated by the decomposition reaction, and temperature-dependent thermal properties. The decomposition equation is fitted by the n^{th} order Arrhenius expression. The gas diffusion equation considers the pores inside the composites, the internal pressure accumulated in the pores, and the mass flux of gas driven by the pressure difference. The material constitutive equation considers orthotropic viscoelasticity and decomposition. The temperature, remaining solid mass, internal pressure, deflection, and stress are determined by the four governing equations. The compression failure criterion corresponds to the kinking failure mode. A calculated time- and temperature-dependent compression strength is used to compare with the compression stress at each material point to decide if the point fails. The strength model incorporates local shear yielding and fiber misalignment. These governing equations can capture the major chemical and physical phenomena occurring in composites exposed to fire, such as thermal softening, decomposition, pores and compression kinking failure. The model can predict temperature, deflection, and time-to-failure over a wide

temperature range from temperatures below the glass transition temperature to temperatures above the decomposition temperature.

The model is incorporated into commercial finite element software ABAQUS for the convenience of engineering application. Since ABAQUS has not provided a particular type of element for PMCs with temperature, pressure, and displacements degrees of freedom, the overlaid element technique is developed and employed with UMAT and UMATHT subroutines to implement the three-dimensional thermo-mechanical model into ABAQUS. The heat transfer equation and the decomposition equation are defined in one UMATHT applied on the first layer of elements and the gas diffusion equation is solved in the other UMATHT applied on the second layer of elements. The material constitutive equation is solved in the UMAT for the first layer of elements. The stiffness of the second layer is set to be very small compared to the actual stiffness and the displacement degrees of freedom of two layers are tied together, so that the UMAT of the first layer determines the mechanical behavior of the system. The overlaid element technique and the solution strategy provides a practical numerical method for engineering application and allows further implementation of more complicated models. The resulting code can be explored to predict the composite thermo-mechanical behavior and compression failure for different material systems with different stack sequences of fiber orientation, different sample sizes, and different combined thermo-mechanical loadings.

In order to validate the model and the code, four sets of one-sided heating tests conducted at different labs are simulated and the predicted results are compared with the collected measured data. The material system in the first set of tests is Vetrotex 324 E-glass/Derakane 510A-40 vinyl ester resin with warp-aligned or quasi-isotropic fiber stack

sequence. The material system in the second set of tests is Colan A105 E-glass/Derakane 411-350 vinyl ester resin. The samples in these two sets of tests are small scale. The material system in the third set of tests is also Colan A105 E-glass/Derakane 411-350 vinyl ester resin, however, the samples are intermediate scale laminates with different numbers of fiber plies and different thickness. The material system in the fourth set of tests is sandwich composites with Balsa wood core and laminate facesheets. The sample is intermediate scale and insulated with Superwool on the exposed side. The range of the applied heat flux in these four sets of tests is from 5 kW/m^2 to 75 kW/m^2 and there are other particular fire scenarios applied in some tests. The range of compressive load is from 10% to 90% of compression strength at room temperature. Several failure modes, such as kinking, buckling/forced-response deflection, delamination, and debonding between the facesheet and wood core, are observed in these tests. Failure time is from tens of seconds to a few hours. In the one-sided heating tests, the sample expands first and the out-of-plane deflection moves towards the heater because of the thermal moment at the beginning of the heating. After some point when more and more damages, such as material degradation and progressive failure, occur inside the sample, the in-plane deflection turns to the compression direction. The eccentric moment caused by the material degradation counteracts the thermal moment as the heating continues and the direction of out-of-plane deflection depends on the balance between the eccentric moment and thermal moment. Although there is some discrepancy between the predicted and measured data in some tests, the model can predict the temperature, in-plane and out-of-plane deflections, and failure time very well for most of tests. It is found that the

accurate measurement and inputs of material properties and test conditions are significant to a good prediction of the model.

Another part of the work is to investigate the internal pressure of decomposing PMCs. A manufacturing procedure based on VARTM is proposed and executed to make the glass/vinyl ester composite panel with inserted hypodermic needle. The one-sided heating tests for the sample with inserted needle are set up to measure the internal pressure at different locations through the thickness. The manufacture and measurement approach overcome the leakage issue of previous experimental technique for pressure measurement. The developed thermo-mechanical model and code are employed to analyze the heating and decomposing process. The trend of the measured pressure history curves can be captured by the model and both the measured and predicted results indicate a pressure peak in the range of 1.1-1.3 atmosphere pressure for glass/vinyl ester systems in the conducted heating tests. Another set of heating tests for glass-talc/phenolic composites is also simulated and the effect of porosity and permeability on thermal response of composites is studied by comparing the temperature, pressure, decomposition factor, and mass flux calculated from the model using different sets of property inputs. The influence of porosity on both temperature and pressure is apparent. Temperature is insensitive to permeability; however, permeability has a strong influence on pressure. The peak of pressure increases by about three times with permeability reduced by one order of magnitude.

5.2 Recommendations for Future Work

Various experimental conditions and many measured parameters are involved into the inputs to the analysis using the model. The influence of the error between the actual experimental conditions and the simulated ideal conditions on the predicted results, such as mechanical boundary condition and initial geometry imperfection of sample, needs to be examined. Further characterization of material property for some composite material systems and sensitivity investigation of time impact in stiffness are necessary to improve the prediction accuracy. For example, viscoelasticity probably has a strong influence on mechanical behavior of samples for the tests with temperature around the glass transition temperature.

Other material systems, such as carbon fiber reinforced composites, and large scale tests should be analyzed by the model for further validation. Delamination failure should be included for a more comprehensive analysis of composites subjected to combined thermo-mechanical loadings. Since the execution of the resulting code would be computationally intensive for a large problem, a relatively simple numerical tool is needed to provide a rough estimate before the final execution of complicated analysis.

Regarding to the technique of internal pressure measurement, the pressure transducer with smaller volume should be used for a more precise measurement or an approach for correcting the error induced by the volume difference is needed. More than one hypodermic needle inserted at the same thickness should be used to assure the test repeatability.

References

1. Greene, E., *Marine Composites*. Second ed, ed. E. Greene. 1999, Annapolis, MD: Eric Green Assocate, Inc.

2. Mouritz, A.P., et al., *Review of Fire Structural Modelling of Polymer Composites.* Composites Part A: Applied Science and Manufacturing, 2009. **40**(12): p. 1800-1814.

3. Sorathia, U., T. Dapp, and J. Kerr, *Flammability Characteristics of Composites for Shipboard and Submarine Internal Applications*, in *36th International SAMPE Symposium and Exhibition* 1991, SAMPE, Covina, CA, United States: San Diego, CA, USA. p. 1868-1878.

4. Sorathia, U. and C. Beck, *Fire-Screening Results of Polymers and Composites*, in *Improved Fire- and Smoke-Resistant Materials for Commercial Aircraft Interiors*. 1995: Naval Surface Warfare Center, Annapolis, MD. p. 93-114.

5. Sevart, J.L., et al., *Flammability and Toxicity of Composite Materials for Marine Vehicles.* Naval Engineers Journal, 1990. **102**(5): p. 45-53.

6. Scudamore, M.J., *Fire Performance Studies on Glass-Reinforced Plastic Laminates.* Fire and Materials, 1994. **18**(5): p. 313-325.

7. Egglestone, G.T. and D.M. Turley, *Flammability of GRP for Use in Ship Superstructures.* Fire and Materials, 1994. **18**(4): p. 255-260.

8. Brown, J.R. and Z. Mathys, *Reinforcement and Matrix Effects on the Combustion Properties of Glass Reinforced Polymer Composites.* Composites Part A: Applied Science and Manufacturing, 1997. **28**(7): p. 675-681.

9. Sorathia, U., et al., *Fire Safety of Marine Composites*, in *45th International SAMPE Symposium and Exhibition*. 2000, SAMPE, Covina, CA, United States: Long Beach, CA, USA. p. II/-.

10. Sorathia, U., J. Ness, and M. Blum, *Fire Safety of Composites in the US Navy.* Composites Part A: Applied Science and Manufacturing, 1999. **30**(5): p. 707-713.

11. Sorathia, U. and I. Perez, *Improving the Fire Safety of Composite Materials for Naval Applications*, in *49th International SAMPE Symposium and Exhibition*. 2004, SAMPE: Long Beach, CA, United states. p. 1257-1270.

12. Lyon, R.E., et al., *Fire-Resistant Aluminosilicate Composites.* Fire and Materials, 1997. **21**(2): p. 67-73.

13. Koo, J.H., et al., *Flammability Properties of Polymer Matrix Composites for Marine Applications*, in *32nd International SAMPE Technical Conference*. 2000, SAMPE: Boston, MA, United states. p. 523-534.

14. Sastri, S.B., et al., *Flammability Characteristics of Phthalonitrile Composites*, in *42nd International SAMPE Symposium and Exhibition*. 1997, SAMPE, Covina, CA, United States: Anaheim, CA, USA. p. 1032-1038.

15. Sastri, S.B., J.P. Armistead, and T.M. Keller, *Phthalonitrile-Carbon Fiber Composites.* Polymer Composites, 1996. **17**(6): p. 816-822.

16. Sorathia, U. and C. Beck, *Fire Protection of Glass/Vinyl Ester Composites for Structural Applications*, in *41st International SAMPE Symposium and Exhibition*. 1996, SAMPE, Covina, CA, United States: Anaheim, CA, USA. p. 687-697.

17. Brown, J.R., et al., *Fire-Retardant Performance of Some Surface Coatings for Naval Ship Interior Applications.* Fire and Materials, 1995. **19**(3): p. 109-118.

18. Ohlemiller, T., T. Cleary, and J. Shields, *Effect of Ignition Conditions on Upward Flame Spread on a Composite Material in a Corner Configuration*, in *41st International SAMPE Symposium and Exhibition*. 1996, SAMPE, Covina, CA, United States: Anaheim, CA, USA. p. 734-747.

19. Henderson, J.B., et al., *Characterization of the High-Temperature Behaviour of a Glass-Filled Polymer Composite.* Composites, 1987. **18**(3): p. 205-215.

20. Henderson, J.B. and M.R. Tant, *Measurement of Thermal and Kinetic Properties of a Glass-filled Polymer Composite to High Temperatures*, in *9th European Conference on Thermophysical Properties*. 1986: Manchester, UK. p. 17-28.

21. Henderson, J.B. and M.P. Dohert, *Measurement of Selected Properties of a Glass-filled Polymer Composite.* High Temperatures - High Pressures, 1987. **19**(1): p. 95-102.

22. Florio, J.J., J.B. Henderson, and F.L. Test, *Measurement of the Thermochemical Expansion of Porous Composite Materials.* High Temperatures - High Pressures, 1989. **21**(2): p. 157-165.

23. Florio, J.J., et al., *Experimental Determination of Volumetric Heat Transfer Coefficients in Decomposing Polymer Composites*, in *Porous Media, Mixture, and Multiphase Heat Transfer*. 1989, ASME, New York, NY, United States: San Francisco, CA, USA.

24. Lattimer, B.Y. and J. Ouellette, *Properties of Composite Materials for Thermal Analysis Involving Fires.* Composites Part A: Applied Science and Manufacturing, 2006. **37**(7): p. 1068-1081.

25. Lattimer, B.Y., J. Ouellette, and J. Trelles, *Thermal Response of Composite Materials to Elevated Temperatures*, in *Modeling of Naval Composite Structures in Fire*, L. Couchman and A.P. Mouritz, Editors. 2006, Cooperative Research Centre for Advanced Composite Structures: Melbourne, Australia. p. 1-49.

26. Goodrich, T.W., *Thermophysical Properties and Microstructural Changes of Composite Materials at Elevated Temperature*, in *Mechanical Engineering*. 2009, Virginia Polytechnic Institute and State University: Blacksburg, VA, USA.

27. Lua, J., et al., *A Temperature and Mass Dependent Thermal Model for Fire Response Prediction of Marine Composites.* Composites Part A: Applied Science and Manufacturing, 2006. **37**(7): p. 1024-1039.

28. Welch, S., et al., *BRE Large Compartment Fire Tests-Characterising Post-Flashover Fires for Model Validation.* Fire Safety Journal, 2007. **42**(8): p. 548-567.

29. Wiecek, T.E., *A Study of the High Temperature Thermal Response of Decomposing and Expanding Polymer Composites*, in *Mechanical Engineering and Applied Mechanics*. 1986, University of Rhode Island: Kingston, RI, USA. p. 184.

30. Ramamurthy, H., *An experimental investigation into the thermophysical properties of decomposing polymer composites*, in *Mechanical Engineering and Applied Mechanics*. 1988, University of Rhode Island: Kingston, Rhode Island, USA.

31. Ramamurthy, H., F.L. Test, and J.B. Henderson, *Experimental Determination of the Permeability of Porous Composite Materials.* High Temperatures - High Pressures, 1989. **21**(2): p. 167-176.

32. Doherty, M.P., *Characterization of the porous microstructure of decomposing glass-filled polymer composites*, in *Mechanical Engineering and Applied Mechanics*. 1988, University of Rhode Island: Kingston, Rhode Island, USA.

33. Ahn, S.H., W.I. Lee, and G.S. Springer, *Measurement of the Three-Dimensional Permeability of Fiber Preforms Using Embedded Fiber Optic Sensors.* Journal of Composite Materials, 1995. **29**(6): p. 714-733.

34. Dimitrienko, Y.I., *Thermomechanical Behaviour of Composite Materials and Structures under High Temperatures. 1. Materials.* Composites Part A: Applied Science and Manufacturing, 1997. **28A**(5): p. 453-461.

35. Sullivan, R.M. and N.J. Salamon, *Finite Element Method for the Thermochemical Decomposition of Polymeric Materials - II. Carbon Phenolic Composites.* International Journal of Engineering Science, 1992. **30**(7): p. 939-951.

36. Ramamurthy, H., et al., *Internal Pressure and Temperature Distribution in Decomposing Polymer Composites.* Heat Transfer, Proceedings of the International Heat Transfer Conference, 1990: p. 335-340.

37. Lee, C.K., R.F. Chaiken, and J.M. Singer, *Charring Pyrolysis of Wood in Fires by Laser Simulation*, in *16th Symposium on Combustion*. 1976, Combust Inst, Pittsburgh, Pa: Cambridge, MA, USA. p. 1459-1470.

38. Tinney, E.R., *The Combustion of Wooden Dowels in Heated Air*, in *10th Symposium on Combustion*. 1965, Combustion Institute, Pittsburgh, Pa. p. 925-930.

39. Bausano, J.V., J.J. Lesko, and S.W. Case, *Composite Life under Sustained Compression and One Sided Simulated Fire Exposure: Characterization and Prediction.* Composites Part A: Applied Science and Manufacturing, 2006. **37**(7): p. 1092-1100.

40. Boyd, S.E., S.W. Case, and J.J. Lesko, *Compression Creep Rupture Behavior of a Glass/Vinyl Ester Composite Subject to Isothermal and One-Sided Heat Flux Conditions.* Composites Part A: Applied Science and Manufacturing, 2007. **38**(6): p. 1462-1472.

41. Boyd, S.E., J.J. Lesko, and S.W. Case, *Compression Creep Rupture Behavior of a Glass/Vinyl Ester Composite Laminate Subject to Fire Loading Conditions.* Composites Science and Technology, 2007. **67**(15-16): p. 3187-3195.

42. Boyd, S.E., J.J. Lesko, and S.W. Case, *The Thermo-Viscoelastic, Viscoplastic Characterization of Vetrotex 324/Derakane 510A-40 through Tg.* Journal of Engineering Materials and Technology, Transactions of the ASME, 2006. **128**(4): p. 586-594.

43. Ha, S.K. and G.S. Springer, *Time Dependent Behavior of Laminated Composites at Elevated Temperatures.* Journal of Composite Materials, 1989. **23**(11): p. 1159-1197.

44. Ha, S.K. and G.S. Springer, *Nonlinear Mechanical Properties of a Thermoset Matrix Composite at Elevated Temperatures.* Journal of Composite Materials, 1989. **23**(11): p. 1130-1158.

45. Pering, G.A., P.V. Farrell, and G.S. Springer, *Degradation of Tensile and Shear Properties of Composites Exposed to Fire or High Temperature.* Journal of Composite Materials, 1980. **14**: p. 54-68.

46. Shen, C.-H. and G.S. Springer, *Effects of Moisture and Temperature on the Tensile Strength of Composite Materials.* Journal of Composite Materials, 1977. **11**(1): p. 2-16.

47. Chowdhury, E.U., et al., *Mechanical Characterization of Fibre Reinforced Polymers Materials at High Temperature* Fire Technology, 2009.

48. Mouritz, A.P. and Z. Mathys, *Mechanical Properties of Fire-Damaged Glass-Reinforced Phenolic Composites.* Fire and Materials, 2000. **24**(2): p. 67-75.

49. Mouritz, A.P. and Z. Mathys, *Post-Fire Mechanical Properties of Glass-Reinforced Polyester Composites.* Composites Science and Technology, 2001. **61**(4): p. 475-490.

50. Mouritz, A.P. and Z. Mathys, *Post-Fire Mechanical Properties of Marine Polymer Composites*, in *10th International Conference on Composite Structures*. 1999, Elsevier Ltd: Melbourne, Aust. p. 643-653.

51. Mouritz, A.P., *Post-fire Flexural Properties of Fibre-reinforced Polyester, Epoxy and Phenolic Composites.* Journal of Materials Science, 2002. **37**(7): p. 1377-1386.

52. Gardiner, C.P., Z. Mathys, and A.P. Mouritz, *Post-fire Structural Properties of Burnt GRP Plates.* Marine Structures, 2004. **17**(1): p. 53-73.

53. Mouritz, A.P., *Fire Resistance of Aircraft Composite Laminates.* Journal of Materials Science Letters, 2003. **22**(21): p. 1507-1509.

54. Mouritz, A.P., Z. Mathys, and C.P. Gardiner, *Thermomechanical Modelling the Fire Properties of Fibre-polymer Composites.* Composites Part B: Engineering, 2004. **35B**(6-8): p. 467-474.

55. Gibson, A.G., et al., *Modelling Residual Mechanical Properties of Polymer Composites after Fire*, in *Plastics, Rubber and Composites*. 2003, IOM Communications Ltd. p. 81-90.

56. Springer, G.S. and M.H. Do, *Degradation of Mechanical Properties of Wood during Fire*. 1983. p. 133p.

57. Dastin, R.M., D.A. Stanke, and G.S. Springer, *Mechanical Properties of Southern Pine and Douglas Fir at Elevated Temperatures.* The Journal of Fire and Flammability, 1982. **13**(4): p. 237-249.

58. Lua, J., *Thermal-mechanical Cell Model for Unbalanced Plain Weave Woven Fabric Composites.* Composites Part A: Applied Science and Manufacturing, 2007. **38**(3): p. 1019-1037.

59. Deng, X. and N. Chawla, *Three-Dimensional (3D) Modeling of the Thermoelastic Behavior of Woven Glass Fiber-Reinforced Resin Matrix Composites.* Journal of Materials Science, 2008. **43**(19): p. 6468-6472.

60. Kucner, L.K. and H.L. Mcmanus, *Experimental Studies of Composite Laminates Damaged by Fire*, in *Proceedings of the 26th International SAMPE Technical Conference*. 1994, SAMPE, Covina, CA, United States: Atlanta, GA, USA. p. 341-353.

61. Lee, S.-Y. and G.S. Springer, *Effects of Cure on the Mechanical Properties of Composites.* Journal of Composite Materials, 1988. **22**(1): p. 15-29.

62. Springer, G.S., J.M. Tang, and W.I. Lee, *Effects of Cure Pressure on Resin Flow, Voids, and Mechanical Properties*. 1987. p. 84p.

63. Cain, J.J., et al., *Post-Curing Effects on Marine VARTM FRP Composite Material Properties for Test and Implementation.* Journal of Engineering Materials and Technology, Transactions of the ASME, 2006. **128**(1): p. 34-40.

64. Green, D.W., J.E. Winandy, and D.E. Kretschmann, *Mechanical Properties of Wood*, in *Wood Handbook : Wood as an Engineering Material*. 1999, USDA Forest Service, Forest Products Laboratory: Madison, WI p. 4.1-4.45.

65. Smith, S.A., et al., *Evaluation of Composite Sandwich Panels Fabricated Using Vacuum Assisted Resin Transfer Molding*, in *45th International SAMPE Symposium and Exhibition*. 2000. p. I/-.

66. Icten, B.M., B. Okutan, and R. Karakuzu, *Failure Strength of Woven Glass Fiber-Epoxy Composites Pinned Joints.* Journal of Composite Materials, 2003. **37**(15): p. 1337-1350.

67. Yang, T., et al., *Overall Moduli and Natural Frequencies of Composite Laminates Containing Multiple Interlaminar Transverse Cracks.* Composite Structures, 2004. **66**(1-4): p. 223-230.

68. Cicek, O. and M. Demirsoy, *Stress Analysis of Pin-Loaded Woven-Glass Fiber Reinforced Epoxy Laminate Conveying Chain Components.* Composite Structures, 2005. **69**(4): p. 470-481.

69. Smith, P., C.D. Rudd, and A.C. Long, *The Effect of Shear Deformation on the Processing and Mechanical Properties of Aligned Reinforcements.* Composites Science and Technology, 1997. **57**(3): p. 327-344.

70. Green, D.W., *Wood: Strength and Stiffness*, in *Encyclopedia of Materials - Science and Technology*, K.H.J. Buschow, et al., Editors. 2001, Elsevier. p. 9732-9736.

71. Henderson, J.B., J.A. Wiebelt, and M.R. Tant, *A Model for the Thermal Response of Polymer Composite Materials with Experimental Verification.* Journal of Composite Materials, 1985. **19**(6): p. 579-595.

72. Henderson, J.B. and T.E. Wiecek, *A Mathematical Model to Predict the Thermal Response of Decomposing, Expanding Polymer Composites.* Journal of Composite Materials, 1987. **21**(4): p. 373-393.

73. Henderson, J.B. and T.E. Wiecek, *A Numerical Study of the Thermally-Induced Response of Decomposing, Expanding Polymer Composites.* Waerme- und Stoffuebertragung, 1988. **22**(5): p. 275-284.

74. Florio, J.J., et al., *A Study of the Effects of the Assumption of Local-Thermal Equilibrium on the Overall Thermally-Induced Response of a Decomposing, Glass-Filled Polymer Composite.* International Journal of Heat and Mass Transfer, 1991. **34**(1): p. 135-147.

75. Miano, V.U. and A.G. Gibson, *FIRE Model for Fibre Reinforced Plastic Composites Using Apparent Thermal Diffusivity (ATD)*, in *13th European Conference on Composite Materials*. 2009, Maney Publishing, United Kingdom. p. 87-92.

76. Dodds, N., et al., *Fire Behaviour of Composite Laminates.* Composites Part A: Applied Science and Manufacturing, 2000. **31**(7): p. 689-702.

77. Gibson, A.G., et al., *Model for the Thermal Performance of Thick Composite Laminates in Hydrocarbon Fires.* Revue de l'Institute Francais du Petrole, 1995. **50**(1): p. 69-74.

78. Looyeh, M.R.E., P. Bettess, and A.G. Gibson, *A One-Dimensional Finite Element Simulation for the Fire-Performance of GRP Panels for Offshore Structures.* International Journal of Numerical Methods for Heat and Fluid Flow, 1997. **7**(6): p. 609-625.

79. Milke, J.A. and A.J. Vizzini, *Thermal Response of Fire-exposed Composites.* Journal of Composites Technology and Research, 1991. **13**(3): p. 145-151.

80. Looyeh, M.R.E., K. Rados, and P. Bettess, *Thermochemical Responses of Sandwich Panels to Fire.* Finite Elements in Analysis and Design, 2001. **37**(11): p. 913-927.

81. Jowsey, A., *Fire Imposed Heat Fluxes for Structural Analysis*. 2006, The University of Edinburgh: Edinburgh, UK.

82. Boyer, G.T. and W.C. Thomas, *Analytical Investigation of Charring Composite Undergoing Thermochemical Expansion*, in *1985 ASME National Heat Transfer Conference*. 1985, ASME, New York, NY, USA: Denver, CO, USA.

83. Xie, W. and P.E. Des Jardin, *A Level Set Embedded Interface Method for Conjugate Heat Transfer Simulations of Low Speed 2D Flows.* Computers and Fluids, 2008. **37**(10): p. 1262-1275.

84. Lin, K.Y. and I.H. Hwang, *Thermo-Viscoelastic Analysis of Composite Materials.* Journal of Composite Materials, 1989. **23**(6): p. 554-569.

85. Zocher, M.A., S.E. Groves, and D.H. Allen, *A Three-Dimensional Finite Element Formulation for Thermoviscoelastic Orthotropic Media.* International Journal for Numerical Methods in Engineering, 1997. **40**(12): p. 2267-2288.

86. Zienkiewicz, O.C., M. Watson, and I.P. King, *A Numerical Method of Visco-Elastic Stress Analysis.* International Journal of Mechanical Sciences, 1968. **10**(10): p. 807-827.

87. Gramoll, K.C., D.A. Dillard, and H.F. Brinson, *A Stable Numerical Solution Method for In-Plane Loading of Nonlinear Viscoelastic Laminated Orthotropic Materials.* Composite Structures, 1989. **13**(4): p. 251-274.

88. J.A. Czyz and W. Szyszkowski, *An Effective Method for Non-Linear Viscoelastic Structural Analysis.* Computers and Structures, 1990. **37**(5): p. 637-646.

89. Guedes, R.M., et al., *Prediction of Long-Term Behaviour of Composite Materials.* Computers and Structures, 2000. **76**(1-3): p. 183-194.

90. Burdette, J.A., *Fire Response of Loaded Composite Structures - Experiments and Modeling*, in *Engineering Mechanics*. 2001, Virginia Polytechnic Institute and State University: Blacksburg, VA, USA.

91. Gibson, A.G., et al., *The Integrity of Polymer Composites during and after Fire.* Journal of Composite Materials, 2004. **38**(15): p. 1283-1307.

92. Feih, S., et al., *Modelling the Compression Strength of Polymer Laminates in Fire.* Composites Part A: Applied Science and Manufacturing, 2007. **38**(11): p. 2354-2365.

93. Mouritz, A.P., et al., *Modelling the Tension and Compression Strengths of Polymer Laminates in Fire.* Composites Science and Technology, 2007. **67**(3-4): p. 551-564.

94. Feih, S., et al., *Tensile Strength Modeling of Glass Fiber-Polymer Composites in Fire.* Journal of Composite Materials, 2007. **41**(19): p. 2387-2410.

95. Mouritz, A.P., et al., *Mechanical Property Degradation of Naval Composite Materials in Fire*, in *Modeling of Naval Composite Structures in Fire*, L. Couchman and A.P. Mouritz, Editors. 2006, Cooperative Research Centre for Advanced Composite Structures: Melbourne, Australia. p. 51-107.

96. Gibson, A.G., et al., *Laminate Theory Analysis of Composites under Load in Fire.* Journal of Composite Materials, 2006. **40**(7): p. 639-658.

97. Easby, R.C., et al., *Failure Model for Phenolic and Polyester Pultrusions under Load in Fire.* Plastics, Rubber and Composites, 2007. **36**(9): p. 379-388.

98. Mouritz, A.P., et al., *Modeling Compressive Skin Failure of Sandwich Composites in Fire.* Journal of Sandwich Structures and Materials, 2008. **10**(3): p. 217-245.

99. Asaro, R.J., B.Y. Lattimer, and W. Ramroth, *Structural Response of FRP Composites during Fire.* Composite Structures, 2009. **87**(4): p. 382-393.

100. Liu, L., et al., *Thermal Buckling of a Heat-exposed, Axially Restrained Composite Column.* Composites Part A: Applied Science and Manufacturing, 2006. **37**(7): p. 972-980.

101. Bai, Y., T. Keller, and T. Vallee, *Modeling of Stiffness of FRP Composites under Elevated and High Temperatures.* Composites Science and Technology, 2008. **68**(15-16): p. 3099-3106.

102. Bai, Y., T. Vallee, and T. Keller, *Modeling of Thermal Responses for FRP Composites under Elevated and High temperatures.* Composites Science and Technology, 2008. **68**(1): p. 47-56.

103. Bai, Y. and T. Keller, *Modeling of Mechanical Response of FRP Composites in Fire.* Composites Part A: Applied Science and Manufacturing, 2009. **40**(6-7): p. 731-738.

104. Flanagan, G., et al., *Elevated Temperature Facesheet Debond Test and Analysis*, in *Modeling of Naval Composite Structures in Fire*, L. Couchman and A.P. Mouritz, Editors. 2006, Cooperative Research Centre for Advanced Composite Structures: Melbourne, Australia. p. 281-299.

105. Lua, J., C. Luo, and L. Chen, *Fire Integrity in Advanced Ship Structures*. 2009.

106. Gu, P. and R.J. Asaro, *Designing Polymer Matrix Composite Panels for Structural Integrity in Fire.* Composite Structures, 2008. **84**(4): p. 300-309.

107. Gu, P. and R.J. Asaro, *Designing Sandwich Polymer Matrix Composite Panels for Structural Integrity in Fire.* Composite Structures, 2009. **88**(3): p. 461-467.

108. Gu, P. and R.J. Asaro, *Distortion of Polymer Matrix Composite Panels under Transverse Thermal Gradients.* Composite Structures, 2008. **82**(3): p. 413-421.

109. Gu, P. and R.J. Asaro, *Wrinkling of Sandwich Polymer Matrix Composite Panels under Transverse Thermal Gradients.* Fire Safety Journal, 2008. **43**(2): p. 151-160.

110. Key, C.T. and J. Lua, *Constituent Based Analysis of Composite Materials Subjected to Fire Conditions.* Composites Part A: Applied Science and Manufacturing, 2006. **37**(7): p. 1005-1014.

111. Biot, M.A. and D.G. Willis, *The Elastic Coefficients of the Theory of Consolidation.* Journal of Applied Mechanics, 1957. **24**: p. 594-601.

112. Carroll, M.M., *An Effective Stress Law for Anisotropic Elastic Deformation.* Journal of Geophysical Research, 1979. **84**(B13): p. 7510-7512.

113. Dimitrienko, Y.I., *Mechanics of Porous Media with Phase Transformations and Periodical Structures. 1. Method of Asymptotic Averaging.* European Journal of Mechanics, A/Solids, 1998. **17**(2): p. 305-319.

114. Dimitrienko, Y.I., *Mechanics of Porous Media with Phase Transformations and Periodical Structures. 2. Solutions of Local and Global Problems.* European Journal of Mechanics, A/Solids, 1998. **17**(2): p. 321-337.

115. Dimitrienko, Y.I., *Thermomechanical Behaviour of Composite Materials and Structures under High Temperatures. 2. Structures.* Composites Part A: Applied Science and Manufacturing, 1997. **28A**(5): p. 463-471.

116. Dimitrienko, Y.I., *Thermomechanical Behaviour of Composites under Local Intense Heating by Irradiation.* Composites Part A: Applied Science and Manufacturing, 2000. **31**(6): p. 591-598.

117. Dimitrienko, Y.I., *Thermal Stresses and Heat-Mass Transfer in Ablating Composite Materials.* International Journal of Heat and Mass Transfer, 1995. **38**(1): p. 139-146.

118. Looyeh, M.R.E., et al., *Modelling of Reinforced Polymer Composites Subject to Thermo-Mechanical Loading.* International Journal for Numerical Methods in Engineering, 2005. **63**(6): p. 898-925.

119. Lee, S., N.J. Salamon, and R.M. Sullivan, *Finite Element Analysis of Poroelastic Composites Undergoing Thermal and Gas Diffusion.* Journal of thermophysics and heat transfer, 1996. **10**(4): p. 672-680.

120. Sullivan, R.M., *A Coupled Solution Method for Predicting the Thermostructural Response of Decomposing, Expanding Polymeric Composites.* Journal of Composite Materials, 1993. **27**(4): p. 408-434.

121. Sullivan, R.M. and N.J. Salamon, *Finite Element Method for the Thermochemical Decomposition of Polymeric Materials - I. Theory.* International Journal of Engineering Science, 1992. **30**(4): p. 431-441.

122. McManus, H.L.N. and G.S. Springer, *High Temperature Thermomechanical Behavior of Carbon-Phenolic and Carbon-Carbon Composites. I. Analysis.* Journal of Composite Materials, 1992. **26**(2): p. 206-229.

123. McManus, H.L.N. and G.S. Springer, *High Temperature Thermomechanical Behavior of Carbon-Phenolic and Carbon-Carbon Composites. II. Results.* Journal of Composite Materials, 1992. **26**(2): p. 230-255.

124. Wu, Y. and N. Katsube, *A Constitutive Model for Thermomechanical Response of Decomposing Composites under High Heating Rates.* Mechanics of Materials, 1996. **22**(3): p. 189-201.

125. Luo, C. and P.E. Des Jardin, *Thermo-Mechanical Damage Modeling of a Glass-Phenolic Composite Material.* Composites Science and Technology, 2007. **67**(7-8): p. 1475-1488.

126. Luo, C., W. Xie, and P.E. Des Jardin, *Numerical Simulation of Composite Structure Response from a Fire Plume*, in *50th International SAMPE Symposium and Exhibition*. 2005, Society for the Advancement of Material and Process Engineering: Long Beach, CA, United states. p. 2665-2676.

127. Luo, C., W. Xie, and P.E. Des Jardin, *Fluid-Structure Simulations of Composite Material Response for Fire Environments*, in *Modeling of Naval Composite Structures in Fire*, L. Couchman and A.P. Mouritz, Editors. 2006, Cooperative Research Centre for Advanced Composite Structures: Melbourne, Australia. p. 255-279.

128. Budiansky, B. and N.A. Fleck, *Compressive Failure of Fibre Composites.* Journal of the Mechanics and Physics of Solids, 1993. **41**(1): p. 183-211.

129. Jensen, H.M. and J. Christoffersen, *Kink Band Formation in Fiber Reinforced Materials.* Journal of the Mechanics and Physics of Solids, 1997. **45**(7): p. 1121-1136.

130. Bausano, J.V., *Structural Integrity of Polymer Matrix Composites Exposed to Fire Conditions*, in *Engineering Mechanics*. 2003, Virginia Polytechnic Institute and State University: Blacksburg, VA, USA.

131. Boyd, S.E., *Compression Creep Rupture of an E-glass/Vinyl Ester Composite Subjected to Combined Mechanical and Fire Loading Conditions*, in *Engineering Mechanics*. 2006, Virginia Polytechnic Institute and State University: Blacksburg, VA, USA.

132. *UMAT*, in *Abaqus User Subroutines Reference Manual, Version 6.7*. 2007, ABAQUS, Inc.

133. *UMATHT*, in *Abaqus User Subroutines Reference Manual, Version 6.7*. 2007, ABAQUS, Inc.

134. Summers, P., *Predicting Compression Failure of Fiber-reinforced Polymer Laminates during Fire*, in *Mechanical Engineering*. 2010, Virginia Polytechnic Institute and State University: Blacksburg.

135. Feih, S., *Temperature Dependent Bending and Tensile Stiffness*. 2010: Blacksburg, VA.

Appendix A: UMATHT Implementation of Three-dimensional Thermal Model for PMCs in Fire

From the energy perspective, the one-dimensional heat transfer equation for decomposing polymer composites developed by Henderson and Wiecek [72] is given by

$$\frac{\partial}{\partial t}\left(m_g h_g + m h_s\right) = \frac{\partial}{\partial x}\left(k_g \phi \frac{\partial T}{\partial x} + k_s (1-\phi)\frac{\partial T}{\partial x}\right)\Delta x \Delta A - \frac{\partial}{\partial x}\left(\dot{m}_g' h_g\right)\Delta x \Delta A - Q_i \frac{\partial m}{\partial t} \qquad \text{(A.1)}$$

where T is temperature, m is solid mass, m_g is mass of gases, $\dot{m}_g'$ is mass flux of gases, $h_s = \int_{T_0}^{T} C_p dT$ is solid enthalpy, C_p is solid specific heat, $h_g = \int_{T_0}^{T} C_{pg} dT$ is enthalpy of gases, C_{pg} is specific heat of gases, k_s is solid thermal conductivity, k_g is thermal conductivity of gases, ϕ is porosity, Δx is control volume thickness, ΔA is cross-sectional area of control volume, and Q_i is decomposition heat. Eq. (A.1) is extended to three-dimensional case and divided by the control volume V, yielding

$$\frac{1}{V}\frac{\partial}{\partial t}\left(m_g h_g + m h_s\right) - \nabla \bullet \left(k_1 \frac{\partial T}{\partial x}\mathbf{i} + k_2 \frac{\partial T}{\partial y}\mathbf{j} + k_3 \frac{\partial T}{\partial z}\mathbf{k}\right) + \nabla \bullet \left(\dot{\mathbf{m}}_\mathbf{g}' h_g\right) + \frac{1}{V} Q_i \frac{\partial m}{\partial t} = 0 \qquad \text{(A.2)}$$

where $k_i = k_g \phi + k_{si}(1-\phi)$ $(i = 1, 2, 3)$ are thermal conductivities of composites in three coordinate directions. The first term is the rate of composite internal energy with respect to time; the second term is the conduction heat flux of both solid and gas components; the third term is the convection energy because of the decomposition gases flowing through composites; the last term is time rate of energy absorbed or generated by decomposition reaction. The continuity equation is also extended to three-dimension.

$$\frac{1}{V}\frac{\partial m}{\partial t} + \frac{1}{V}\frac{\partial m_g}{\partial t} + \nabla \bullet \left(\dot{\mathbf{m}}_\mathbf{g}'\right) = 0 \qquad \text{(A.3)}$$

The first term is the time rate of solid mass; the second term is the time rate of gas mass; and the last term is sum of rates of gas mass flux with respect to special coordinates. Eq. (A.1) is recast by expanding the first term using differentiation rules and combining the heat convection term using Eq. (A.3).

$$\begin{aligned}&\frac{1}{V}\left(mC_p + m_g C_{pg}\right)\frac{\partial T}{\partial t} - \nabla \bullet \left(k_1 \frac{\partial T}{\partial x}\mathbf{i} + k_2 \frac{\partial T}{\partial y}\mathbf{j} + k_3 \frac{\partial T}{\partial z}\mathbf{k} \right) \\ &+ C_p \dot{\mathbf{m}}'_g \bullet \nabla T + \frac{1}{V}\left(h - h_g\right)\frac{\partial m}{\partial t} = 0\end{aligned} \tag{A.4}$$

where h is defined as $h = h_s + Q_i$. Three-dimensional Darcy's law in principal directions is given by

$$\dot{\mathbf{m}}'_{\mathbf{g}} = -\frac{\rho_g}{\mu}\gamma_i \nabla P \tag{A.5}$$

where P is gas pressure and ρ_g is gas density. Gas pressure is related to the mass of gases stored in the pores by using ideal gas state equation.

$$P = \frac{m_g RT}{MV\phi} \tag{A.6}$$

Substitute Eq. (A.5) and Eq. (A.6) into Eq. (A.4), yielding the final form of heat transfer equation for finite element implementation.

$$\begin{aligned}&\frac{1}{V}\left(mC_p + m_g C_{pg}\right)\frac{\partial T}{\partial t} - \nabla \bullet \left(k_1 \frac{\partial T}{\partial x}\mathbf{i} + k_2 \frac{\partial T}{\partial y}\mathbf{j} + k_3 \frac{\partial T}{\partial z}\mathbf{k} \right) \\ &- \frac{PM}{RT} C_{pg} \left(\frac{\gamma_1}{\mu}\frac{\partial P}{\partial x}\mathbf{i} + \frac{\gamma_2}{\mu}\frac{\partial P}{\partial y}\mathbf{j} + \frac{\gamma_3}{\mu}\frac{\partial P}{\partial z}\mathbf{k} \right) \bullet \nabla T + \frac{1}{V}\left(h - h_g\right)\frac{\partial m}{\partial t} = 0\end{aligned} \tag{A.7}$$

Substitute Eq. (A.5) into Eq. (A.3), yielding three-dimensional gas diffusion equation

$$-\nabla \bullet \left[\rho_g \left(\frac{\gamma_1}{\mu}\frac{\partial P}{\partial x}\mathbf{i} + \frac{\gamma_2}{\mu}\frac{\partial P}{\partial y}\mathbf{j} + \frac{\gamma_3}{\mu}\frac{\partial P}{\partial z}\mathbf{k} \right) \right] + \frac{1}{V}\left(\frac{\partial m}{\partial t} + \frac{\partial m_g}{\partial t} \right) = 0 \tag{A.8}$$

The basic energy balance for heat transfer analysis is given by

$$\int_V \rho \dot{U} dV = \int_S q dS + \int_V r dV \tag{A.9}$$

where V is the volume of the solid material with surface area S, ρ is the density, $\dot{U}$ is the time rate of the internal energy per unit mass, q is the heat flux per unit area flowing into the body, and r is the heat supplied externally into the body per unit volume. A heat flux vector $\mathbf{f}$ is defined so that

$$q = -\mathbf{f} \bullet \mathbf{n} \tag{A.10}$$

where $\mathbf{n}$ is the unit vector outward normal to the surface. Substituting Eq. (A.10) into Eq. (A.9) and using the divergence theorem, the energy balance equation can be recast as

$$\int_V \rho \dot{U} dV = -\int_V \frac{\partial}{\partial \mathbf{x}} \bullet \mathbf{f} dV + \int_V r dV \tag{A.11}$$

The internal energy $\dot{U}$, the heat flux vector $\mathbf{f}$, and their partial derivatives with respect to temperature and temperature spacial gradients are the interface variables provided by UMATHT for numerical implementation [133]. These variables must be updated to their values at the end of each time increment.

In order to relate Eq. (A.11) to Eq. (A.7), the density ρ is set to be one unit, and the time rate of the internal thermal energy per unit mass and the heat flux vector are defined as

$$\begin{aligned} \dot{U} = & \frac{1}{V}(mC_p + m_g C_{pg}) \frac{\partial T}{\partial t} + \frac{1}{V}(h - h_g) \frac{\partial m}{\partial t} \\ & - C_{pg} \frac{PM}{RT} \left(\frac{\gamma_1}{\mu} \frac{\partial P}{\partial x} \frac{\partial T}{\partial x} + \frac{\gamma_2}{\mu} \frac{\partial P}{\partial y} \frac{\partial T}{\partial y} + \frac{\gamma_3}{\mu} \frac{\partial P}{\partial z} \frac{\partial T}{\partial z} \right) \end{aligned} \tag{A.12}$$

$$\mathbf{f} = -k_1 \frac{\partial T}{\partial x} \mathbf{i} - k_2 \frac{\partial T}{\partial y} \mathbf{j} - k_3 \frac{\partial T}{\partial z} \mathbf{k} \tag{A.13}$$

Introducing the finite difference approximation, the incremental form of Eq. (A.12) is given by

$$\begin{aligned}\Delta U = & \frac{1}{V}(mC_p + m_g C_{pg})\Delta T + \frac{1}{V}(h - h_g)\Delta m \\ & - C_{pg}\frac{PM}{RT}\left(\frac{\gamma_1}{\mu}\frac{\partial P}{\partial x}\frac{\partial T}{\partial x} + \frac{\gamma_2}{\mu}\frac{\partial P}{\partial y}\frac{\partial T}{\partial y} + \frac{\gamma_3}{\mu}\frac{\partial P}{\partial z}\frac{\partial T}{\partial z}\right)\Delta t\end{aligned} \tag{A.14}$$

Eq. (A.14) is used to update the internal energy at the end of time increment $U(t+\Delta t)$ using the energy at the beginning of the time increment $U(t)$.

$$U(t+\Delta t) = U(t) + \Delta U \tag{A.15}$$

Provided that the internal energy is a function of time, temperature, remaining mass, pressure and their partial derivative with respect to spacial coordinates, the total derivative of the internal energy with respect to time is given by

$$\begin{aligned}\frac{dU}{dt} = & \frac{\partial U}{\partial t} + \frac{\partial U}{\partial T}\frac{dT}{dt} + \frac{\partial U}{\partial(\partial T/\partial x_i)}\frac{d(\frac{\partial T}{\partial x_i})}{dt} + \frac{\partial U}{\partial m}\frac{dm}{dt} + \frac{\partial U}{\partial(\partial m/\partial x_i)}\frac{d(\frac{\partial m}{\partial x_i})}{dt} \\ & + \frac{\partial U}{\partial P}\frac{dP}{dt} + \frac{\partial U}{\partial(\partial P/\partial x_i)}\frac{d(\frac{\partial P}{\partial x_i})}{dt}\end{aligned} \tag{A.16}$$

Compare terms in Eq. (A.16) and Eq. (A.12), yielding

$$\frac{\partial U}{\partial T} = \frac{1}{V}(mC_p + m_g C_{pg}) \tag{A.17}$$

$$\frac{\partial U}{\partial(\partial T/\partial x_i)} = 0\,,\ i = 1,2,3 \quad x_1 = x, x_2 = y, x_3 = z \tag{A.18}$$

Based on Eq. (A.13), the partial derivative of heat flux vector with respect to temperature and temperature spacial gradient can be expressed by

$$\frac{\partial \mathbf{f}}{\partial T} = -\frac{\partial T}{\partial x}\frac{\partial k_1}{\partial T}\mathbf{i} - \frac{\partial T}{\partial y}\frac{\partial k_2}{\partial T}\mathbf{j} - \frac{\partial T}{\partial z}\frac{\partial k_3}{\partial T}\mathbf{k} \tag{A.19}$$

$$\frac{\partial \mathbf{f}}{\partial(\partial T/\partial x_i)} = \begin{bmatrix} -k_1 & 0 & 0 \\ 0 & -k_2 & 0 \\ 0 & 0 & -k_3 \end{bmatrix},\ i = 1,2,3 \quad x_1 = x, x_2 = y, x_3 = z \tag{A.20}$$

In order to relate Eq. (A.11) to Eq. (A.8), the density ρ is set to be one unit, and corresponding $\dot{U}$ and $\mathbf{f}$ for gas diffusion equation are defined as

$$\dot{U} = \frac{1}{V}\left(\frac{\partial m}{\partial t} + \frac{\partial m_g}{\partial t}\right) \tag{A.21}$$

$$\mathbf{f} = -\frac{PM}{RT}\left(\frac{\gamma_1}{\mu}\frac{\partial P}{\partial x}\mathbf{i} + \frac{\gamma_2}{\mu}\frac{\partial P}{\partial y}\mathbf{j} + \frac{\gamma_3}{\mu}\frac{\partial P}{\partial z}\mathbf{k}\right) \tag{A.22}$$

Since the gas diffusion equation is solved by a separate UMATHT other than the routine for heat transfer equation, the pressure is interpreted as virtual temperature degree of freedom. The incremental form of Eq. (A.21) is given by

$$\Delta U = \frac{1}{V}\left(\Delta m + \Delta m_g\right) \tag{A.23}$$

The partial derivatives of the internal energy and the heat flux vector with respect to pressure and pressure spacial gradient are derived using the same procedure for the heat transfer equation.

$$\frac{\partial U}{\partial P} = \frac{M\phi}{RT} \tag{A.24}$$

$$\frac{\partial U}{\partial(\partial P/\partial x_i)} = 0\ ,\ i = 1,2,3 \quad x_1 = x, x_2 = y, x_3 = z \tag{A.25}$$

$$\frac{\partial \mathbf{f}}{\partial P} = -\frac{M}{RT}\left(\frac{\gamma_1}{\mu}\frac{\partial P}{\partial x}\mathbf{i} + \frac{\gamma_2}{\mu}\frac{\partial P}{\partial y}\mathbf{j} + \frac{\gamma_3}{\mu}\frac{\partial P}{\partial z}\mathbf{k}\right) \tag{A.26}$$

$$\frac{\partial \mathbf{f}}{\partial(\partial P/\partial x_i)} = -\frac{PM}{RT\mu}\begin{bmatrix}\gamma_1 & 0 & 0\\ 0 & \gamma_2 & 0\\ 0 & 0 & \gamma_3\end{bmatrix},\ i=1,2,3 \quad x_1 = x, x_2 = y, x_3 = z \tag{A.27}$$

Regarding the implementation of the decomposition equation, the explicit expression using forward finite difference is given by

$$m(t+\Delta t) = -A\left(\frac{m(t)-m_f}{m_0-m_f}\right)^n e^{(-E/RT)}\left(m_0-m_f\right)\Delta t + m(t) \tag{A.28}$$

where $m(t)$ and $m(t+\Delta t)$ are solid mass at the start and the end of the time increment respectively.

Appendix B: UMAT Implementation of Three-dimensional Mechanical Model for PMCs in Fire

The constitutive equation describing the orthotropic viscoelasticitic behavior of virgin material and including the decomposition effect for PMCs in fire is given by

$$\sigma_i(\xi) = F\int_0^{\xi} C_{ij}^{v}(\xi-\xi')\frac{\partial \varepsilon_j^m(\xi')}{\partial \xi'}d\xi' + \left(1-F\right)C_{ij}^{c}\varepsilon_j^m(\xi) \tag{B.1}$$

where

$$C_{ij}^{v}(\xi) = C_{ij\infty} + \sum_{m=1}^{M} C_{ijm}e^{-\xi/\tau_{ijm}} \tag{B.2}$$

Neglecting the second term on the right side of Eq. (B.1) based on the assumption that the stiffness of char material is very small compared to virgin material, the constitutive equation is reduced to

$$\sigma_i(\xi) = F\int_0^{\xi} C_{ij}^{v}(\xi-\xi')\frac{\partial \varepsilon_j^m(\xi')}{\partial \xi'}d\xi' \tag{B.3}$$

The stress at the moment of t_n and t_{n+1} can be expressed as

$$\sigma_i(\xi_n) = F_n\int_0^{\xi_n} C_{ij}^{v}(\xi_n-\xi')\frac{\partial \varepsilon_j^m(\xi')}{\partial \xi'}d\xi' \tag{B.4}$$

$$\sigma_i(\xi_{n+1}) = F_{n+1}\int_0^{\xi_{n+1}} C_{ij}^{v}(\xi_{n+1}-\xi')\frac{\partial \varepsilon_j^m(\xi')}{\partial \xi'}d\xi' \tag{B.5}$$

where $\xi_n = \int_0^{t_n}\frac{1}{a_T}d\tau$ and $\xi_{n+1} = \int_0^{t_{n+1}}\frac{1}{a_T}d\tau$. The increment of stress is obtained by subtracting Eq. (B.4) from Eq. (B.5).

$$\Delta\sigma_i = F_{n+1}\left(\int_0^{\xi_{n+1}} C_{ij}^v(\xi_{n+1}-\xi')\frac{\partial\varepsilon_j^m(\xi')}{\partial\xi'}d\xi' - \int_0^{\xi_n} C_{ij}^v(\xi_n-\xi')\frac{\partial\varepsilon_j^m(\xi')}{\partial\xi'}d\xi'\right) + \frac{F_{n+1}-F_n}{F_n}\sigma_i(t_n) \tag{B.6}$$

Eq. (B.6) can be also written as

$$\Delta\sigma_i = F_{n+1}\Delta\sigma_i^R + F_{n+1}\int_{\xi_n}^{\xi_{n+1}} C_{ij}^v(\xi_{n+1}-\xi')\frac{\partial\varepsilon_j^m(\xi')}{\partial\xi'}d\xi' + \frac{F_{n+1}-F_n}{F_n}\sigma_i(t_n) \tag{B.7}$$

where

$$\Delta\sigma_i^R = \int_0^{\xi_n} \Delta C_{ij}^v \frac{\partial\varepsilon_j^m(\xi')}{\partial\xi'}d\xi' \tag{B.8}$$

$$\Delta C_{ij}^v = C_{ij}^v(\xi_{n+1}-\xi') - C_{ij}^v(\xi_n-\xi') \tag{B.9}$$

The mechanical strain is assumed to be linear over the interval $[\xi_n, \xi_{n+1}]$, $\Delta\varepsilon_j^m / \Delta\xi = const.$, and Eq. (B.2) is substituted into Eq. (B.7), yielding

$$\Delta\sigma_i = F_{n+1}\left(C_{ij}'\Delta\varepsilon_j^m + \Delta\sigma_i^R\right) + \frac{F_{n+1}-F_n}{F_n}\sigma_i(t_n) \tag{B.10}$$

where

$$C_{ij}' = C_{ij\infty} + \frac{1}{\Delta\xi}\sum_{m=1}^{M} C_{ijm}\tau_{ijm}(1-e^{-\Delta\xi/\tau_{ijm}}) \tag{B.11}$$

In order to write $\Delta\sigma_i^R$ in a convenient form, Eq. (B.9) can also be expressed as

$$\Delta C_{ij}^v = -\sum_{m=1}^{M} C_{ijm}e^{-(\xi_n-\xi')/\tau_{ijm}}(1-e^{-\Delta\xi/\tau_{ijm}}) \tag{B.12}$$

Eq. (B.12) is substituted into Eq. (B.8), yielding

$$\Delta\sigma_i^R = -\sum_{j=1}^{J}\sum_{m=1}^{M}(1-e^{-\Delta\xi/\tau_{ijm}})S_{ijm}(\xi_n) \tag{B.13}$$

where

$$S_{ijm}(\xi_n) = \int_0^{\xi_n} C_{ijm}\left(e^{-(\xi_n-\xi')/\tau_{ijm}}\right)\frac{\partial \varepsilon_j^m(\xi')}{\partial \xi'}d\xi' \tag{B.14}$$

If the mechanical strain is assumed to be linear over the interval $[\xi_{n-1}, \xi_n]$, the recursive of Eq. (B.14) can be written as

$$S_{ijm}(\xi_n) = e^{-\Delta\xi/\tau_{ijm}} S_{ijm}(\xi_{n-1}) + C_{ijm}\tau_{ijm}(1-e^{-\Delta\xi/\tau_{ijm}})\frac{\Delta\varepsilon_j^m}{\Delta\xi} \tag{B.15}$$

where $\Delta\xi = \xi_n - \xi_{n-1}$.

The variables needed to be defined in UMAT are stress at the end of time increment and the stress/strain Jacobian matrix. Eq. (B.10) is used to update the stress status and the three-dimensional matrix form used in the routine is given by

$$\begin{Bmatrix} \Delta\sigma_1 \\ \Delta\sigma_2 \\ \Delta\sigma_3 \\ \Delta\tau_{12} \\ \Delta\tau_{13} \\ \Delta\tau_{23} \end{Bmatrix} = F_{n+1}\left(\begin{bmatrix} C_{11}' & C_{12}' & C_{13}' & 0 & 0 & 0 \\ C_{12}' & C_{22}' & C_{23}' & 0 & 0 & 0 \\ C_{13}' & C_{23}' & C_{33}' & 0 & 0 & 0 \\ 0 & 0 & 0 & C_{44}' & 0 & 0 \\ 0 & 0 & 0 & 0 & C_{55}' & 0 \\ 0 & 0 & 0 & 0 & 0 & C_{66}' \end{bmatrix}\begin{Bmatrix} \Delta\varepsilon_1 \\ \Delta\varepsilon_2 \\ \Delta\varepsilon_3 \\ \Delta\gamma_{12} \\ \Delta\gamma_{13} \\ \Delta\gamma_{23} \end{Bmatrix} + \begin{Bmatrix} \Delta\sigma_1^R \\ \Delta\sigma_2^R \\ \Delta\sigma_3^R \\ \Delta\tau_{12}^R \\ \Delta\tau_{13}^R \\ \Delta\tau_{23}^R \end{Bmatrix}\right) + \frac{F_{n+1}-F_n}{F_n}\begin{Bmatrix} \sigma_1(t_n) \\ \sigma_2(t_n) \\ \sigma_3(t_n) \\ \tau_{12}(t_n) \\ \tau_{13}(t_n) \\ \tau_{23}(t_n) \end{Bmatrix} \tag{B.16}$$

$S_{ijm}(\xi_n)$ in $\Delta\sigma_i^R$ are treated as state variables and updated for each time increment. The Jacobian matrix $\partial\boldsymbol{\sigma}/\partial\boldsymbol{\varepsilon}$ is the change in the ith stress component at the end of the time increment caused by an infinitesimal perturbation of the jth component of the strain increment array. In the principal orientation of orthotropic material, it is calculated by

$$\frac{\partial \Delta \boldsymbol{\sigma}}{\partial \Delta \boldsymbol{\varepsilon}} = F_{n+1} \begin{bmatrix} C_{11}' & C_{12}' & C_{13}' & 0 & 0 & 0 \\ C_{12}' & C_{22}' & C_{23}' & 0 & 0 & 0 \\ C_{13}' & C_{23}' & C_{33}' & 0 & 0 & 0 \\ 0 & 0 & 0 & C_{44}' & 0 & 0 \\ 0 & 0 & 0 & 0 & C_{55}' & 0 \\ 0 & 0 & 0 & 0 & 0 & C_{66}' \end{bmatrix} \tag{B.17}$$

If the mechanical behavior of PMCs in fire is described using the temperature dependent stiffness of virgin material and the decomposition factor, the constitutive equation can be written as

$$\sigma_i = FC_{ij}(T)\varepsilon_j^m \tag{B.18}$$

The stress at the moment of t_n and t_{n+1} is given by

$$\sigma_i(t_n) = F_n C_{ij}(T(t_n))\varepsilon_j^m(t_n) \tag{B.19}$$

$$\sigma_i(t_{n+1}) = F_{n+1} C_{ij}(T(t_{n+1}))\varepsilon_j^m(t_{n+1}) \tag{B.20}$$

The incremental stress is obtained by subtracting Eq. (B.19) from Eq. (B.20).

$$\Delta\sigma_i = F_{n+1}C_{ij}(T_{n+1})\Delta\varepsilon_j^m + F_{n+1}\left(C_{ij}(T_{n+1}) - C_{ij}(T_n)\right)\varepsilon_j^m(t_n) + \frac{F_{n+1}-F_n}{F_n}\sigma_i(t_n) \tag{B.21}$$

Eq. (B.21) is used to update stress at the end of time increment in UMAT. Since stress and strain at the beginning of time increment are passed in the routine for each time increment, the second and the third terms on the right hand side of Eq. (B.21) are considered as known terms and the Jacobian matrix is calculated by

$$\frac{\partial \Delta \boldsymbol{\sigma}}{\partial \Delta \boldsymbol{\varepsilon}} = F_{n+1}C_{ij}(T_{n+1}) \tag{B.22}$$